NTNU

Norwegian University of
Science and Technology

# Foam Materials used for Energy Absorption and Damage Prevention during Blast Loading

Bjarki Sigurdsson

Master of Science in Civil and Environmental Engineering
Submission date: June 2016
Supervisor: Aase Gavina Roberg Reyes, KT
Co-supervisor: Tore Børvik, KT

Norwegian University of Science and Technology
Department of Structural Engineering

*Department of Structural Engineering*

Faculty of Engineering Science and Technology

**NTNU- Norwegian University of Science and Technology**

ACCESSIBILITY

Open

# MASTER THESIS 2016

| SUBJECT AREA: | DATE: | NO. OF PAGES: |
|---|---|---|
| Computational Mechanics | June 10th 2016 | 92 |

TITLE:

**Foam materials used for energy absorption and damage prevention during blast loading**

Skum materialer brukt til energiabsorbering og skade forebygging ved eksplosjonslaster

BY:

Bjarki Sigurdsson

SUMMARY:

Following several high profile bomb attacks in the western hemisphere in recent years, e.g. Brussels 2016 and Norwegian government quarter 2011, the protection of structures against blast loading has received a lot of attention. Blast loading (due to an accident or a terrorist attack) to important structures in our society can be extremely critical, and it is important to verify that the structure is able to withstand a realistic blast load, or at least minimize the damage to avoid disastrous consequences.

The main objective of the present work was to investigate how a polymer foam (XPS) behaves under dynamic impact and blast loading, and evaluate the performance of this type of foam, when used in structural protection, under these load conditions. Several laboratory experiments and numerical analyses were performed in order to document the polymer foams behavior, and investigate the predictive capabilities of numerical methods.

Considering the complexity of the problems analyzed, the overall observation is that the numerical simulation is in many cases able to predict the test results with reasonable accuracy. Based on the results found both experimentally and numerically, XPS foam is believed to perform well as an energy absorbent in a flexible sandwich configuration, for both low-velocity dynamic impacts and blast loads. Further findings indicate that the blast protection performance of the studied sandwich panels greatly depend on the design parameters, e.g. foam core density. Trends indicate a higher energy absorption for lower foam densities, which suggests that for optimal energy absorption, it is beneficial to use a foam with as low density as possible. However in order to obtain a sound design, the strength of the foam needs to be addressed.

| | |
|---|---|
| RESPONSIBLE TEACHER: | Professor Aase Reyes |
| SUPERVISOR(S): | Professor Aase Reyes & Professor Tore Børvik |
| CARRIED OUT AT: | SIMLab, The department of Structural Engineering, NTNU |

*Institutt for konstruksjonsteknikk*

Fakultet for ingeniørvitenskap og teknologi

**NTNU- Norges teknisk- naturvitenskapelige universitet**

TILGJENGELIGHET

Åpen

# MASTEROPPGAVE 2015

| FAGOMRÅDE: | DATO: | ANTALL SIDER: |
|---|---|---|
| Beregningsmekanikk | 10. Juni 2016 | 92 |

TITTEL:

**Skum materialer brukt til energiabsorbering og skade forebygging ved eksplosjonslaster**

Foam materials used for energy absorption and damage prevention during blast loading

UTFØRT AV:

Bjarki Sigurdsson

SAMMENDRAG:

Etter flere omfattende bombeangrep i den vestlige verden de siste årene, f.eks. Brussel 2016 og det norske regjeringskvartalet 2011, har eksplosjons beskyttelse av konstruksjoner fått mye oppmerksomhet. Eksplosjons belastning (på grunn av en ulykke eller et terrorangrep) på viktige konstruksjoner kan være svært kritisk, og det er viktig å kontrollere at konstruksjonen er i stand til å tåle en eksplosjons last, eller i det minste minimere skaden for å unngå katastrofale konsekvenser.

Hovedmålet med arbeidet i denne masteroppgaven var å undersøke hvordan et polymerskum (XPS) oppfører seg under dynamiske støtlaster og eksplosjonstrykk, og evaluere ytelsen av denne typen skum, når det brukes i beskyttelsen av konstruksjoner, utsatt for denne typen belastninger. Flere laboratorieforsøk og numeriske simuleringer ble utført for å dokumentere oppførselen til polymerskummet og undersøke numeriske metoders evne til å predikere responsen.

Men tanke på kompleksiteten av de analyserte problemstillingene, har vi sett at de numeriske simuleringene i mange tilfeller er i stand til å beskrive og forutse de eksperimentelle testresultatene med akseptabel nøyaktighet. Basert på både de eksperimentelle og numeriske resultatene, ser det ut til at XPS skum fungerer godt som energi absorbent i de fleksible «sandwich» konfigurasjonene vi har undersøkt, for både støt laster og eksplosjonslaster. Videre observasjoner viser at effektiviteten til «sandwich» konfigurasjonen, med hensyn på eksplosjonsdemping, er avhengig av flere parametere, særlig skummets densitet. Det ser ut til at være en trend mot at lavere skum densiteter absorberer mer energi for de samme last trykkene, dette indikerer at det er gunstig å bruke skum med så lav densitet som mulig. Men for å oppnå et godt design er det viktig at man tar høyde for at summet har tilstrekkelig styrke.

FAGLÆRER: Professor Aase Reyes

VEILEDER(E): Professor Aase Reyes og Professor Tore Børvik

UTFØRT VED: SIMLab, Institutt for konstruksjonsteknikk, NTNU

**Department of Structural Engineering**
FACULTY OF ENGINEERING SCIENCE AND TECHNOLOGY
NTNU – Norwegian University of Science and Technology

# MASTER'S THESIS 2016

for

*Bjarki Sigurdsson*

# Foam materials used for energy absorption and damage prevention during blast loading

## 1. INTRODUCTION

Protection of engineering structures against blast loading has received a lot of attention in recent years. Blast loading (due to e.g. an accident or a terrorist attack) to important structures in our society can be extremely critical, and it is important to verify that the structure is able to withstand a realistic blast load, or at least minimise the damage to avoid disastrous consequences. Polymer foams could be used as blast protection to absorb energy and thereby protect structures against blast loads. Computational methods are now available to predict both the loading and structural response in these extreme loading situations, and experimental validation of such methods is necessary in the development of safe and cost-effective structures. In this study impact and blast experiments will be performed, and the results will be used for validation and verification of computational methods for structural response analysis of blast loading.

## 2. OBJECTIVES

The main objective of the research project is to investigate how polymer foam behaves under dynamic impact and blast loading, and to validate to which extent this can be predicted using computational tools.

## 3. A SHORT DESCRIPTION OF THE RESEARCH PROJECT

The main topics in the research project will be as follows:

1. A comprehensive literature review should be conducted to understand the blast load phenomenon, blast load design, the characteristics of polymer foam, constitutive modelling of polymer foam exposed to extreme loadings, and explicit finite element methods.
2. Foams with various densities should be considered.
3. Proper constitutive relations are chosen and calibrated based on material tests.
4. Non-linear FE numerical simulations will be carried out in order to study the effect of different design parameters on the energy absorption.
5. Sandwich structures will be tested in a drop tower in order to verify the FE model and study the effect of foam density, thickness and other design parameters on the energy absorption.
6. The SIMLab Shock Tube Facility will be used to validate the numerical model of sandwich structures to blast loading, as an alternative to explosive detonations.

*Supervisors:* Aase Reyes (NTNU), Torodd Berstad (NTNU), Tore Børvik (NTNU)

The thesis must be written according to current requirements and submitted to the Department of Structural Engineering, NTNU, no later than June 10th, 2016.

NTNU, January 15th, 2016

Aase Reyes
Professor

# ABSTRACT

Following several high profile bomb attacks in the western hemisphere in recent years, e.g. Brussels 2016 and Norwegian government quarter 2011, the protection of structures against blast loading has received a lot of attention. Blast loading (due to an accident or a terrorist attack) to important structures in our society can be extremely critical, and it is important to verify that the structure is able to withstand a realistic blast load, or at least minimize the damage to avoid disastrous consequences.

The main objective of the present work was to investigate how a polymer foam (XPS) behaves under dynamic impact and blast loading, and evaluate the performance of this type of foam, when used in structural protection, under these load conditions. Several laboratory experiments and numerical analyses were performed in order to document the polymer foams behavior, and investigate the predictive capabilities of numerical methods.

Considering the complexity of the problems analyzed, the overall observation is that the numerical simulation is in many cases able to predict the test results with reasonable accuracy. Based on the results found both experimentally and numerically, XPS foam is believed to perform well as an energy absorbent in a flexible sandwich configuration, for both low-velocity dynamic impacts and blast loads. Further findings indicate that the blast protection performance of the studied sandwich panels greatly depend on the design parameters, e.g. foam core density. Trends indicate a higher energy absorption for lower foam densities, which suggests that for optimal energy absorption, it is beneficial to use a foam with as low density as possible. However in order to obtain a sound design, the strength of the foam needs to be addressed.

# ACKNOWLEDGEMENTS

This thesis is written for the Structural Impact Laboratory (SIMLab) at the Norwegian University of Science and Technology in the spring of 2016. During the work on this thesis I have been supervised by Professors Aase Reyes and Tore Børvik.

I would like to thank my supervisors Professor Aase Reyes and Professor Tore Børvik for weekly guidance during the work. They are thanked for their insight, comments and discussions which have been deeply appreciated.

I would also like to thank Technical Engineer Trond Auestad for his assistance when performing the drop tower and shock tube experiments, and Senior Engineer Tore Wisth for preparing the test specimens. Further thanks go to Torodd Berstad for invaluable help with creating the numerical LS-DYNA analyses models.

I would further like to express special thanks to Dr. Gudfinnur Sigurdsson for his great support at feedback, which have been invaluable for my work.

Trondheim, June 10th 2016

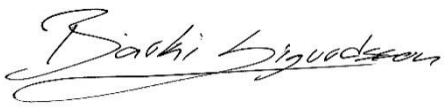

Bjarki Sigurdsson

# CONTENTS

# NOMENCLATURE

| | |
|---|---|
| $A_0$ | Initial cross sectional area |
| $\alpha$ | Linear thermal expansion coefficient |
| $\alpha_2$ | Non-linear scale factor |
| $b$ | Exponential decay coefficient |
| $\beta$ | Non-linear shape factor |
| $C_0$, $C_1$, $n$ | Power-law function constants |
| $C_p$ | Specific heat capacity |
| $DIC$ | Digital Image Correlation |
| $e$ | Engineering strain |
| $\varepsilon$ | True strain |
| $\varepsilon_D$ | Densification strain |
| $f$ | Yield function |
| $F$ | Actual impactor force on specimen |
| $FE$ | Finite Element |
| $F_n$ | Previous force |
| $F_{n+1}$ | Current force |
| $FSI$ | Fluid Structure Interaction |
| $g$ | Gravitational acceleration |
| $\gamma$ | Linear strain hardening coefficient |
| $I$ | Impulse |
| $i_{r+}$ | Specific impulse of positive phase of blast wave |
| $\chi$ | Taylor-Quinney coefficient |
| $L_0$ | Initail length |
| $m$ | Impacting mass |
| $m_1$ | Mass of striker |
| $m_2$ | Mass im impactor |
| $m_p$ | Impacting mass |
| $NTNU$ | Norwegian University of Science and Technology |
| $P$ | pressure |
| $P$ | Measured impactor force |
| $\dot{p}^*$ | Normalized plastic strain rate |
| $\dot{p}_0$ | Reference stain rate |
| $P_a$ | Atmospheric pressure |
| $\dot{p}$ | Equivalent plastic strain rate |
| $p_f$ | Foam density |
| $p_{f0}$ | Density of the foams base material |
| $\Phi$ | Yield function |
| $P_r$ | Peak reflected pressure |
| $P_{so}$ | Peak incident overpressure |
| $Q_i$, $C_i$ | Voce hardenng parameters |
| $R$ | Isotropic hardening |
| $\rho$ | Material density |
| $s$ | Engineering stress |

| | |
|---|---|
| $\hat{\sigma}$ | Equivalent stress |
| $\sigma_e$ | von Mises effective strain |
| $\sigma_m$ | Mean stress |
| $\sigma_p$ | Plateau stress |
| *SIMLab* | Structural Impact Laboratory |
| $T$ | Absolute temperature |
| $T^*$ | Normalized temperature |
| $t_+$ | Duration of the positive phase of a blast wave |
| $t_a$ | Time after an explosion |
| $T_m$ | Melting temperature of the material |
| $T_r$ | Room temperature |
| $t_w$ | Time of shockwave impact |
| $u_n$ | Previous displacement |
| $u_{n+1}$ | Current displacement |
| $v_0$ | Impact velocity |
| $v_n$ | Previous velocity |
| $v_{n+1}$ | Current velocity |
| $\nu^p$ | Plastic coefficient of contraction |
| $v_r$ | Residual velocity |
| $W$ | Work |
| *XPS* | Extruded polystyrene |
| $Y$ | Yield stress |
| $\sigma_0$ | Yield stress |
| $\sigma_{eq}$ | Equivalent stress |

# 1 INTRODUCTION

Following several high profile bomb attacks in the western hemisphere in recent years, e.g. Brussels 2016 and Norwegian government quarter 2011 (Figure 1.1), the protection of structures against blast loading has received a lot of attention. Blast loading (due to an accident or a terrorist attack) to important structures in our society can be extremely critical, and it is important to verify that the structure is able to withstand a realistic blast load, or at least minimize the damage to avoid disastrous consequences.

*Figure 1.1: A high rise building in the Norwegian government quarter after the bombing on July 22. 2011, Photo by: Fartein Rudfjord [1]*

A way of protecting structures from blast loads is to use some form of sacrificial protective cladding on the façade of the structure. However, to get the desired strength from traditional building materials, such cladding can get very heavy. The feasible way of reducing the weight is to reduce the density of the material. As indicated by Figure 1.2 (Ashby plot of strength vs density for engineering materials), foamed materials deliver significant strength for very low densities, which shows great promise for use in protection.

Both esthetics and cost efficiency are important when designing structures in today's society. It is therefore important to create efficient protective designs without compromising the safety of the structure. A proposed way of doing this, is to use the protective cladding as thermal insulation of the building. Many polymeric foams are relatively strong and exhibit good

energy absorbing qualities, as well as low thermal conductivity. This makes them suitable to use in thermally insulating protective cladding. It was therefore decided to study the response of a sandwich configuration with a rigid polymer foam core made from a typical insulation material. Sundolitt XPS [2] (extruded polystyrene) was chosen for this purpose.

In this study, impact and blast experiments were performed on sandwich panels with polymer foam cores, made from extruded polystyrene, and steel skins. The experiments were used to investigate the response of such a sandwich configurations. Focus was on the energy absorption of the sandwich panels.

Further, the performance of the foam sandwich panels where investigated using numerical modelling in LS-DYNA. Compressive tests were performed on the polymer foam in order to derive a numerical material model. The numerical models of the experiments were not calibrated to the experimental data but were based on rough assumptions and engineering judgment. Thus, the numerical results serve more as a proof of concept with regard to the numerical modelling. Nevertheless, the numerical results were compared to the experiments in order to validate to which extent the response could be predicted numerically using a basic model.

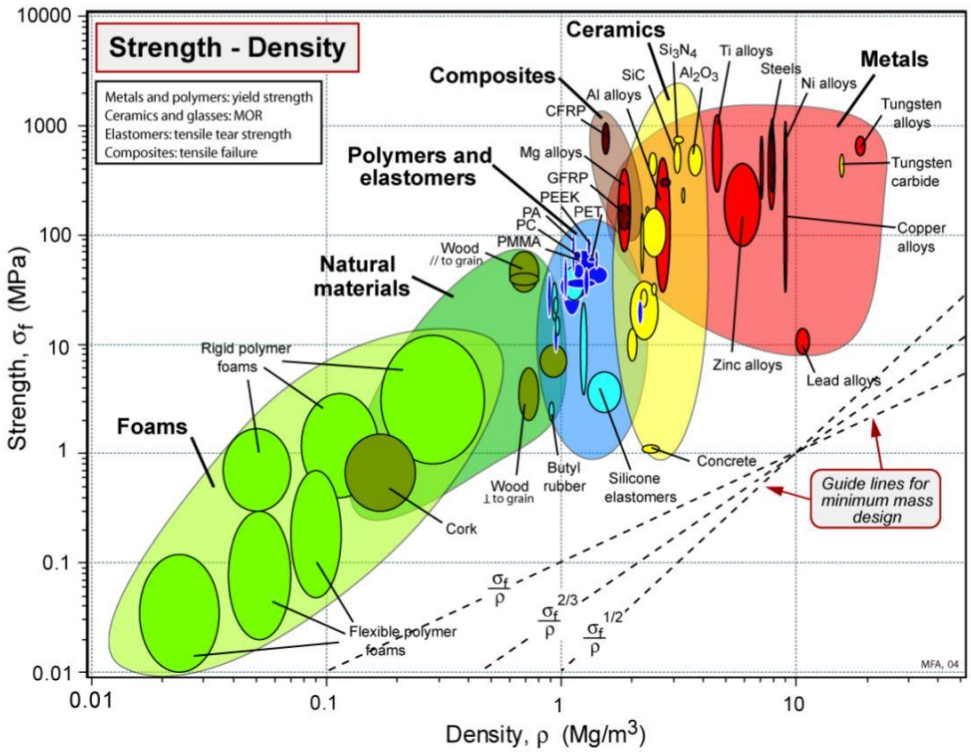


*Figure 1.2: Ashby chart of strength vs. density for typical engineering materials [3]*

# 2 BACKGROUND

## 2.1 STATE OF THE ART

The protection of critical infrastructure against blast loads, has received a lot of attention the last couple of years [4] [5] [6] [7] [8]. Loading during such events often involve complex interaction between the structural geometry and the blast wave. To be able to predict the structural response under blast loads, it is important to have a good understating of the material behavior and the structure-blast wave interaction. As full scale testing often is not a feasible approach, blast resistant design rely on numerical modeling and small scale testing. The classical approach to protective design assumes rigid reflections of the shockwave. Although this assumption generally is on the safe side, the predicted deformations and internal forces are usually significantly overestimated, resulting in overly conservative design.

The most obvious and effective way to mitigate the blast wave, is to increase the distance between the source and the target. However, the limited space of urban areas creates the need for innovative and optimized protective designs. Research into fluid-structure interaction has shown that flexible structural response can have a positive effect on mitigating the blast load on the structure [9] [10]. This implies that energy absorption through the deformation of structural members can be favorable with respect to the structural response, as part of the blast wave is absorbed. With this in mind, the design can be optimized and cost effective, without compromising safety.

Adding sacrificial cladding to the surface of a structure is a way to protect against blast loads. The idea behind such protection is to let non loadbearing parts deform and absorb the energy, reducing the loading on important structural components. Such protection is proposed in many different forms, and the materials used vary greatly. However, using a sandwich configuration with a energy absorbing core and structural skins appears to be a widespread solution. Some researchers propose complex geometric designs such as a honeycomb structure [11] , or a sandwich with corrugated steel plates [12]. Solutions based on a sandwich configuration are usually easy to manufacture and mount. Typically, cellular metallic foams has been a popular choice to use as a core material, due to their ability to sustain large plastic deformations at nearly constant stress, which allows for significant energy absorption and relatively low force transfers. But several other cellular materials, such as polymer foams, exhibits similar behavior and might be well suited as core materials as well. The sandwich

panels are effective in blast protection since the progressive collapse of the core material absorbs energy, while the skins maintain the structural integrity of the panels. The performance of protective cladding of various designs has been investigated by numerous researchers [13] [14] [15] [12] [16], and there appears to be a general consensus that foam-cored sandwich panels performs well.

Radford et al. [16] compared the shock resistance of monolithic plates to sandwich constructions with a metallic foam core of equal area mass. The shock resistance was measured by loading the mid-span of clamped plates with metallic foam projectiles. It was found that the sandwich structures outperformed the monolithic plates at sufficiently high projectile momentum.

Mazurkiewicz et al. [13] investigated the blast resistance of supporting elements when a metallic foam protective cover was used. It was found that the protective cover was very effective in blast protection, but the performance was sensitive to various design parameters such as panel thickness and stiffness and strength of the materials. The researchers managed to obtain very satisfying results by optimizing these parameters. This suggests that a case by case optimization of the design parameters could yield very effective blast resistant design.

An advantage of protecting structures with sacrificial cladding, is that it can be designed either to be retrofitted onto existing structures, or it can be incorporated into the initial design. By incorporating the protection into the façade of a structure, the components can be designed to serve multiple purposes, such as doubling as thermal insulation.

The use of polymer foams as energy absorbents under blast loads has been studied by several authors [17] [18] [19], but nowhere near as much as the metallic counterparts. However, various research on the mechanical behavior of polymeric foams exist [20] [21] [22] [23] [24] [25]. Among these, an interesting study was performed by Daniel et al. [21], who investigated strain rate effects on the material behavior of a closed-cell polymeric foam (PVC foam). They found that the plastic material response, i.e. yielding, the plateau stress and strain hardening, varied linearly with the logarithm of the strain rate, while the initial (elastic) response was strain rate independent.

At the given time, the research on the behavior of extruded polystyrene (XPS) foam is rather limited [26] [27].

## 2.2 PROTECTIVE CLADDING AND POLYMER FOAM

Adding protective cladding to the surface of a structure is a way of protecting the structure from dynamic loads such as explosions. However, the cladding can be heavy and might not be very appealing to hang on the façade of a building. It is therefore proposed to incorporate the thermal insulation used in the façade, into a sandwich panel that will double as protective cladding. Sandwich structures consist of layered structures of different materials and/or geometry. The type of sandwich structure considered in this study is a simple configuration with a closed-cell polymer foam core (Sundolitt XPS [2]), surrounded by two relatively stiff steel skins (Docol600DL [28]). The performance of such panels is highly influenced by the core material and geometry. The foam core controls the energy absorption and the transfer of forces through the structure.

### 2.2.1 Extruded Poly Styrene (XPS)

Sundolitt XPS is a rigid closed-cell polymer foam based on the monomer styrene ($C_8H_8$). It has high relative strength, low weigh, low thermal conductivity, and a long life span. It is produced as continuous foam sheets by extrusion machines. Molten polystyrene is mixed with a blowing agent (typically HCFCs or $CO_2$) and other additives before it is extruded through a flat nozzle which gives the boards their desired profile and thickness. After cooling down the sheet is cut down to the desired lengths.

It should be noted that XPS is highly flammable. For this reason, not all XPS products might be suitable to use as thermal insulators due to building regulations. It is however possible to add flame retardants to the foam, such that it meets building and fire codes. A commonly used flame retardant in XPS foam is HBCD (HexaBromoClodoDecane). The fire safety of Sundolitt XPS has not been further addressed in this study, as the main object has been the structural response to blast loading.

***Polymer foam***

Polymer foams have several appealing qualities that makes them attractive to use for a wide range of applications in various parts of the industry. They are lightweight, have low thermal conductivity, high strength to weight ratio, high acoustic damping and high energy absorption.

The constitutive behavior of closed-cell cellular materials, such as XPS, have been extensively investigated and explained in many publications [29]. The subject is therefore only briefly explained here.

The response of closed-cell cellular materials under compressive loads, are generally characterized by three distinct stages of the stress strain curve (see Figure 2.1). The initial response occur for low strains, and is nearly linear elastic. The stresses in this stage are caused by elastic stretching, contraction and bending of the cell walls and edges. The linear elastic stage is followed by a long plastic plateau where compaction of the material results in only a small stress increase over a wide range of strains. The stress plateau is a result of successive buckling, fracture and plastic collapse of the cells. The small stress increase over this stage is caused by the cell faces capacity to carry membrane stresses. The third stage is a region of densification, in which the stress rises rapidly. When the strain reaches a critical level (densification strain), almost all the cells collapses. As a result, the collapsed cell walls contact each other causing the stiffening of the material response.

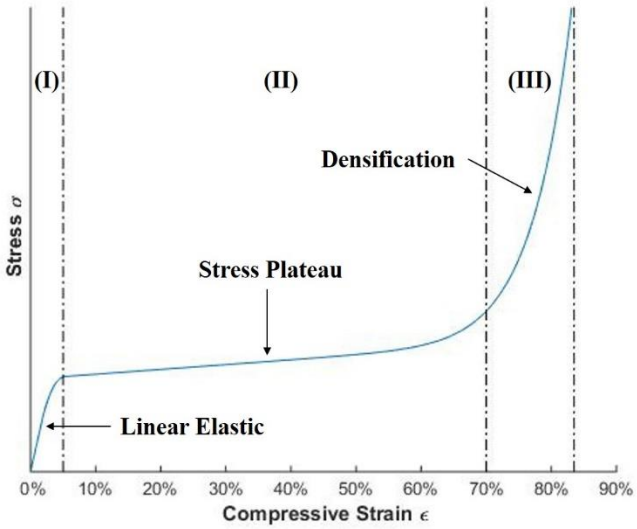


*Figure 2.1: Typical stress-strain curve for closed-cell cellular materials*

For protective cladding to perform satisfyingly, it is vital that a large amount of energy is absorbed while keeping the force transfer through the cladding as low as possible. The energy that is absorbed by the material is related to the area under the stress-strain curve. A stress plateau, such as exhibited by polymeric foam, allows for a great amount of energy to be absorbed, while the low stress level keeps the force transfer low. Thus, polymeric foams show great promise as energy absorbents in protective cladding.

## 2.3 DYNAMIC LOADING

### 2.3.1 Blast loading

The protection of structures against blast loading has gained a lot of attention over the last couple of years. As a result, the need to be able to design structures that are blast-resistant has become more relevant. In order to develop efficient and accurate blast-resistant designs, it is important to understand the blast load phenomenon.

***The blast phenomenon***

An explosion can be defined as a large-scale, rapid and sudden release of energy [30]. Explosions are often categorized according to the system that the released energy was originally stored in, i.e.:

- Physical - Physical explosions are caused by mechanical forces. E.g., the fracture of a pressure vessel.
- Nuclear – Nuclear explosions occur as energy is released from a high-speed nuclear reaction.
- Chemical - Chemical explosions occurs as a result of a rapid exothermic chemical reaction.

Chemical explosions are the main concern in design as such explosions are the most common source of both accidental and intentional blast loading. They are usually categorized based on the way the explosive energy propagates, i.e. if it deflagrate or detonate. Low explosives deflagrates, and are characterized by a subsonic gradual increase in overpressures. High explosives on the other hand, detonates, and are characterized by a supersonic high intensity

shock wave. Figure 2.2 illustrates the difference between a typical deflagration wave and a typical detonation wave.

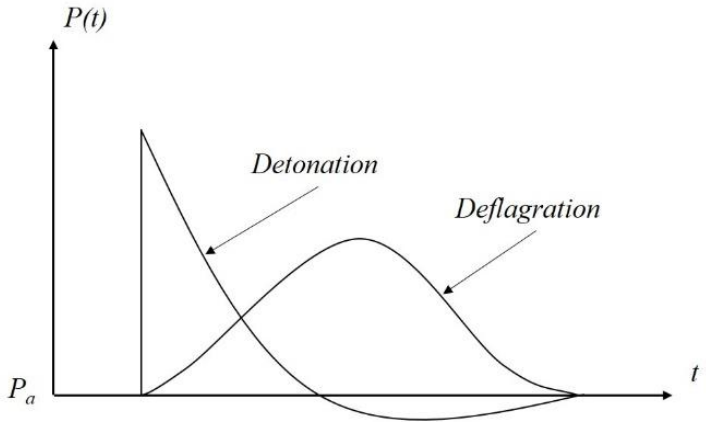


*Figure 2.2: Typical deflagration and detonation wave*

The typical demand for blast-resistant designs, is protection against the blast pressure caused by the detonation of high explosives. When an explosive detonates, a very rapid and stable chemical reaction propagates through the explosive material, at what is called the detonation velocity. This chemical reaction converts the explosive into a very hot and dense gas. The gas expands to occupy lower pressure space in the surrounding air, forming a high intensity pressure wave that is transmitted spherically (in free air) away from the center of the explosion. As a result, the air surrounding the blast also expands causing a layer of compressed air, called a shock front, in front of the blast wave. As the blast wave expands, the strength and wave velocity decreases, and the duration lengthens.

The following theory can be found in Aune et al. [31].

***Idealization of the blast wave***

Generally, blast loading is a complex phenomenon which needs to be investigated using a coupled fluid dynamics model, or to be simplified for design analysis purposes. Figure 2.3 show the idealized pressure-time history of a blast wave caused by an explosive detonation. It is characterized by a near instantaneous increase in pressure, from the ambient atmospheric pressure $P_a$, to a peak incident overpressure $P_{so}$. As the shock front expands, the pressure decays exponentially until it reaches the ambient pressure $P_a$. This constitutes the positive phase of the blast wave. Following the positive phase, a phase of suction (negative pressure)

is initiated. The negative phase is a result of an overexpansion caused by the momentum of the expanding gas.

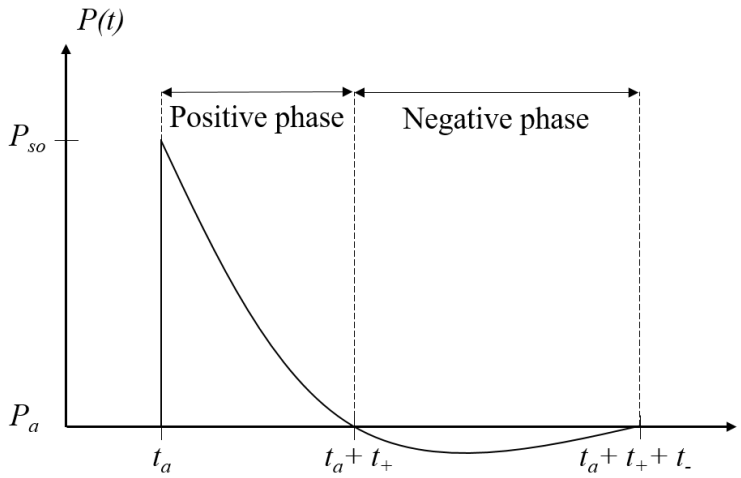


*Figure 2.3: Idealized pressure time history of a blast wave*

When a structure interacts with a blast wave, the structural geometry, properties and relative orientation between the structure and the wave direction is important. When a blast wave interacts with a structure with complex geometry and/or the orientation is not parallel to the wave direction, the wave may be reflected and reinforced. The reflected pressure might be significantly greater than the peak pressure of the blast wave. Therefore, the reflected peak pressure should be used for design purposes.

For design purposes, the negative phase is usually neglected, as the positive phase is associated with the most significant structural damages. It should however, be considered when the total structural response is investigated, and not only the structural integrity. The positive pressure-time history is often represented by the Friedlander equation:

$$P(t) = P_a + P_r\left(1 - \frac{t}{t_+}\right)e^{-\frac{bt}{t_+}}, \tag{2.1}$$

where $P_a$ is the ambient pressure, $P_r$ is the peak reflected pressure, $b$ is the exponential decay coefficient, and $t_+$ is the duration of the positive phase.

The specific impulse of the blast wave is given as the area under the pressure-time history curve, which may be expressed as:

$$i_{r+} = \int_{t_a}^{t_a+t_+} P_r(t)dt \tag{2.2}$$

For the Friedlander equation, the analytical solution is given by:

$$i_{r+} = \frac{P_r t_+}{b^2}[b - 1 + e^{-b}] \tag{2.3}$$

### 2.3.2 The Shock-Tube facility at SIMLab

To investigate the effects of blast loading on the proposed sandwich structures, the shock tube facility at SIMLab was used. The shock tube is a good alternative to detonating high explosives since it can produce a repeatable uniform shock wave under controlled conditions. The shock tube has been thoroughly studied by several researchers at the department of structural engineering at NTNU. They found it to produce similar pressure-time characteristics as actual far field explosive detonations [32].

The shock tube facility at SIMLab is made from P355NH stainless steel, and it is designed according to ISO 2768-1. It consists of a long tube ending in a dump tank. The overall length of the tube is 18.275 m. The tube is divided into the following sections;

- The driver section
- The firing section
- The driven section
- The window section
- Expansion 1
- Expansion 2
- The dump tank

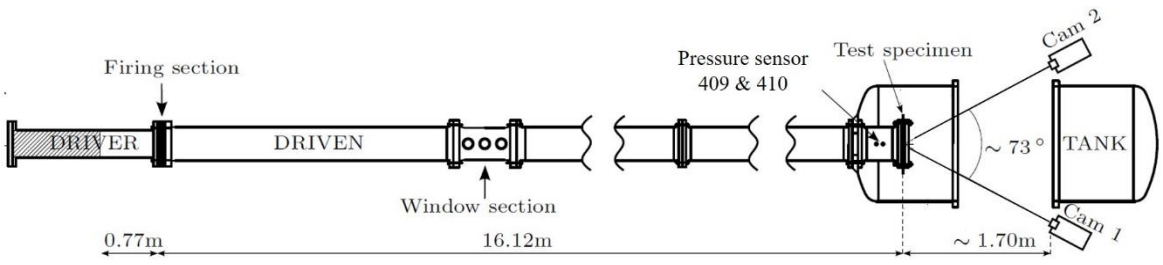


*Figure 2.4: Illustration of shock tube setup [32]*

*Figure 2.5: The shock tube facility at SIMLab*

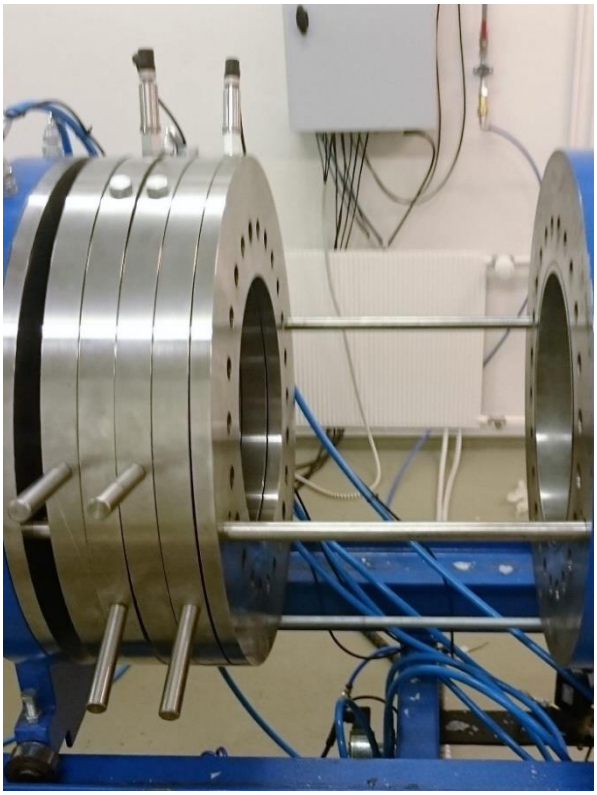

*Figure 2.6: Firing section without membranes*

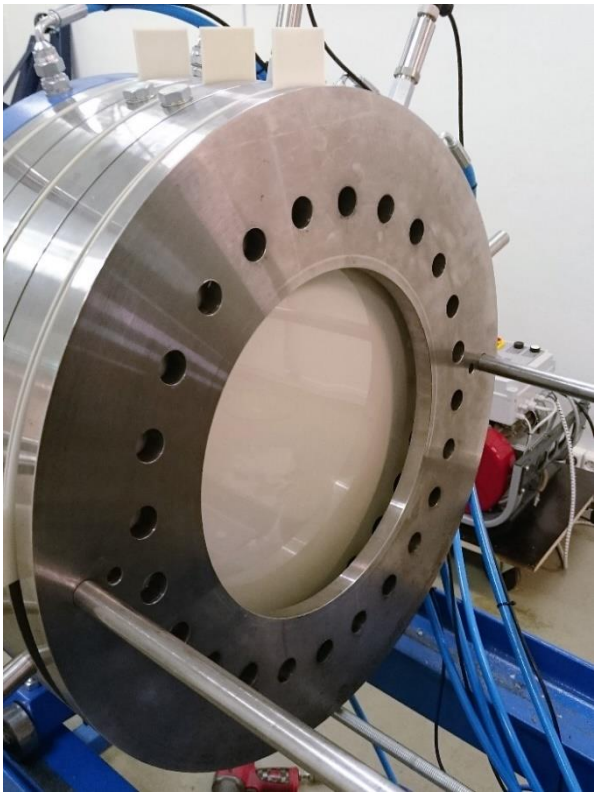

*Figure 2.7: Firing section with membranes*

The driver section is a 2.02 m long tube with a circular cross section. The inner diameter of the tube is 0.331 m. The volume of the driver section can be adjusted with inserts that limit the inner length of the tube. Different loading conditions can be achieved by adjusting the volume of the driver section.

The firing section that follows the driver section consists of two intermediate pressure chambers that are separated by membranes. These membranes are designed to rupture in order to trigger the shockwave. The membranes can be made of different materials, but SIMLab currently uses membranes made from the polyester Melinex. A combination of different membrane thicknesses are chosen based on the desired firing pressure. The two intermediate chambers are pressurized in sync with the driver section at approximately 2/3 and 1/3 of the driver pressure. Thus, the pressure differential is achieved stepwise. When the driver section reaches the desired pressure the membranes are ruptured to release the shockwave. The membranes are ruptured by venting the intermediate pressure chamber closest to the driver section. When this chamber is vented, the pressure differential loads the membranes past their capacity resulting in the rupture of the membranes. However, venting the intermediate chamber causes a slight expansion of the volume in the driver section prior to membrane rupture, and subsequently a slight drop in driver pressure. It is therefore necessary to pressurize the driver section slightly higher than the desired firing pressure.

The driver section gradually changes the cross section from circular to 0.3 m x 0.3 m square. The driven section is followed by the window section. This section has windows on three sides of the square tube, and is used to investigate the interaction and flow around objects. The driven section is extended past the window section by extension 1 and 2.

The tube ends with a clamping rig for test specimens, encased in a dump tank. The volume expansion of the tank serves to lower the pressure after the experiment, while it contains the blast wave and protect the surrounding structure and test equipment such as high-speed cameras.

When the membrane ruptures the sudden release of the pressurized section causes a uniform shockwave to propagate down the low-pressure driven section. This can be illustrated by the simple shock tube showed in Figure 2.9 and the 4 different stages of the shock wave as it propagates through the tube showed in Figure 2.10. Figure 2.10 a) shows the pressure state in the tube just as the membrane ruptures. The driver section is at constant pressure $p_4$, and the driven section at constant pressure $p_1$. In Figure 2.10 b) the membrane has ruptured, and the

incident shock wave is propagating into the driven section with the constant pressure $p_2$ behind the shock front. The contact surface between the driven gases and the driver gases moves in the same direction, but at a lower velocity. At the same time a rarefaction wave travels back into the driver section. This rarefaction wave reflects of the end of the driver section and propagates towards the end of the shock tube as shown in Figure 2.10 c). The pressure behind the wave is now $p_3$. Figure 2.10 d) shows how the incident shock wave is reflected by the end of the shock tube, and the reflected pressure rises to $p_5$. It should be noted that interaction between reflected waves and wave fronts will cause pressure peaks throughout the experiment. However, the time window of interest is limited to the duration of the positive phase and thus such peaks is often of no concern. However, at high driver pressures, they might result in secondary and tertiary peaks during the positive phase (see Figure 2.8).

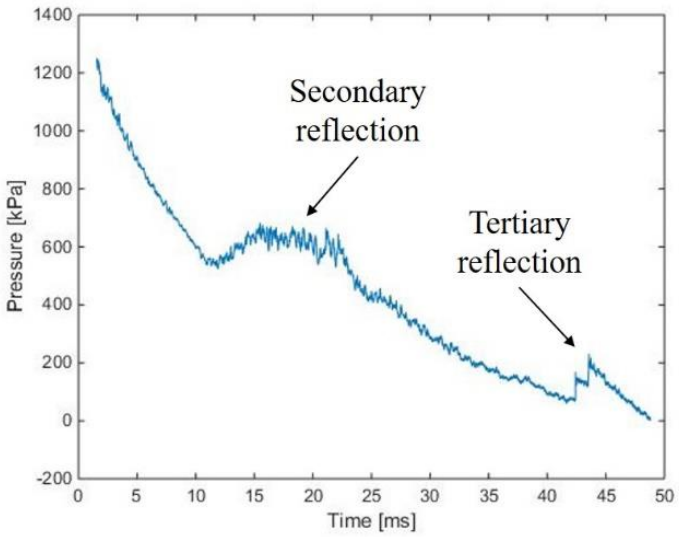


*Figure 2.8 Secondary and tertiary reflections in the shock tube*

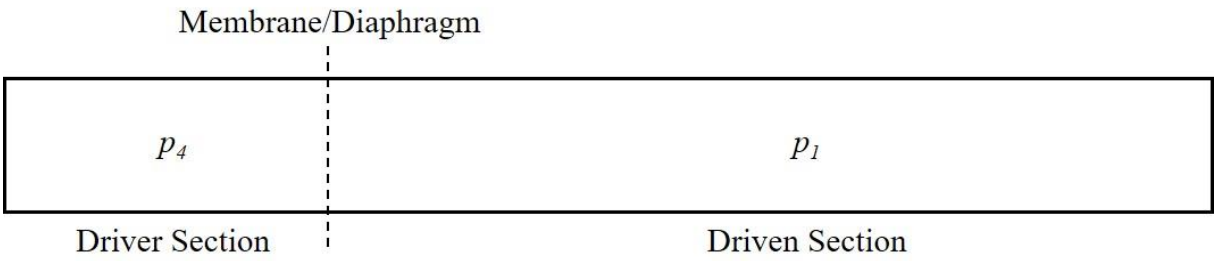


*Figure 2.9: Illustration of a simple shock tube*

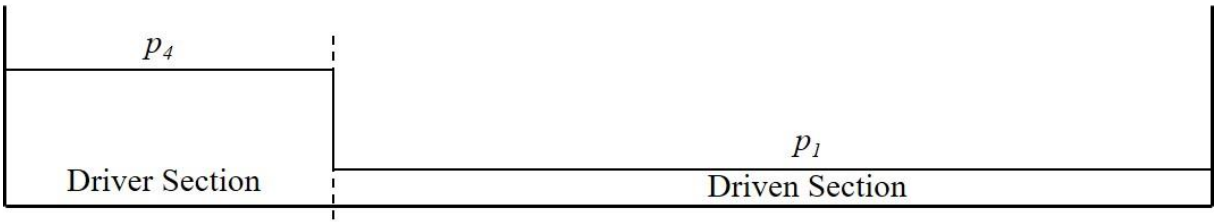


*a)*

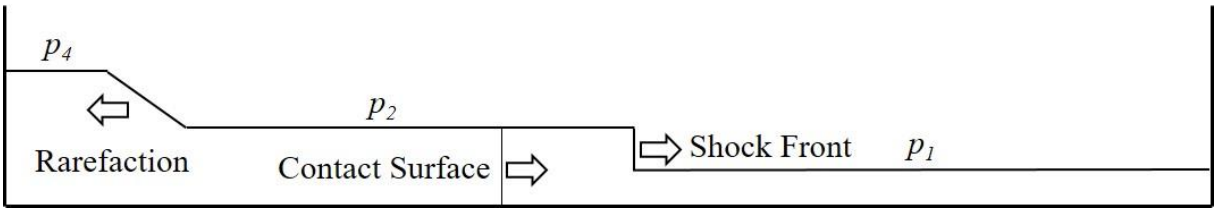


*b)*

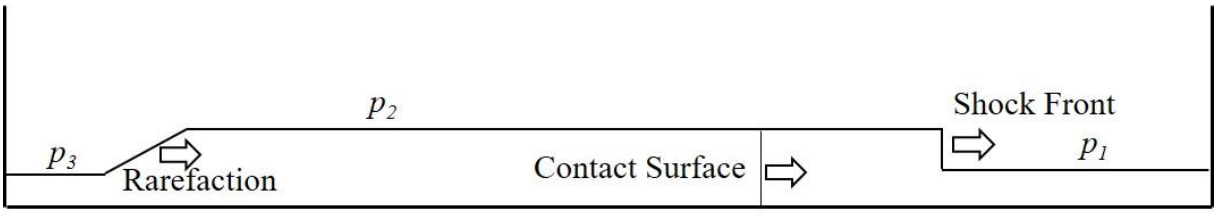


*c)*

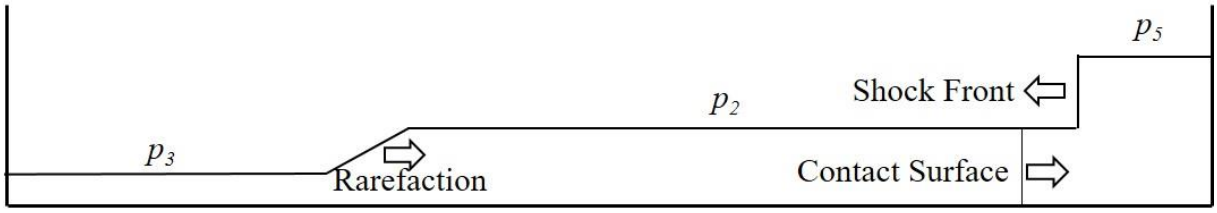


*d)*

*Figure 2.10: Shock wave propagation in a shock tube [33]*

### 2.3.3 Drop tower impact system

The Instron CEAST 9350 is a floor standing impact system. The rig contains a striker that is dropped on a test specimen. The striker is given the desired impactor shape and mass prior to

the test. The rig incorporates a spring system that allows the falling mass to achieve velocities higher than the terminal velocity. It is designed to deliver impacts at up to 24 m/s, with a maximum kinetic energy of 1800 J [34].

There are several advantages of using a drop tower impact system to investigate specimens behaviour under impact loads. The rig takes accurate force measurements at a high frequency, and the experiments are easy to control and repeatable, which gives a good basis for comparing experimental results.

## 2.4 DIGITAL IMAGE CORRELATION (DIC)

Digital Image Correlation (DIC) is a non-contact optical measuring technique used to track displacement fields in mechanical experiments. Rapid development in computer hardware and high-resolution digital imaging over the last decade has made DIC a viable measuring technique, which is widely used today. High image resolution makes the technique accurate, and since it does not rely on contact with the specimen, the technique is often preferable to other measuring methods such as extensometers. DIC is primarily used as a post processing technique, but it can also be applied as a way to track points in real time during experiments. 3D deformation patterns, like out-of-plane deformation, can be tracked by using more than one camera. For such an application, a proper calibration of the camera positions need to be performed in advance. To calibrate the camera model i.e. the relationship between image coordinates and 3D target coordinates, a set of image pairs are taken of a calibration target with known geometry. In this study, a cylinder with 80 mm diameter were used as a calibration target. The cylinder was covered in a checkerboard pattern with 6.527 mm squares. A camera model optimization is then performed to extract the corresponding image and target coordinates.

To prepare specimens for a DIC analysis, the surface of the specimen is coated with a random pattern of unique points prior to the experiments. The pattern is photographed with short intervals during the test. The image series is then post processed with special DIC software. First, a surface mesh is generated on the patterned surface in the undeformed configuration, the mesh is related to the position of individual unique points, and grayscale values in the pattern. Then the software uses a tracking algorithm to track the movement these points from

image to image, and the mesh is deformed accordingly. The mesh deformation can then be used to get the desired output. DIC is however limited to tracing surface deformations.

In the present work, the 3D DIC software ECorr [35] developed at SIMLab, is used as a tool to measure the response of the test specimens in the experiments performed in the shock tube and the drop tower. DIC is also used to track the displacement in the material compression tests.

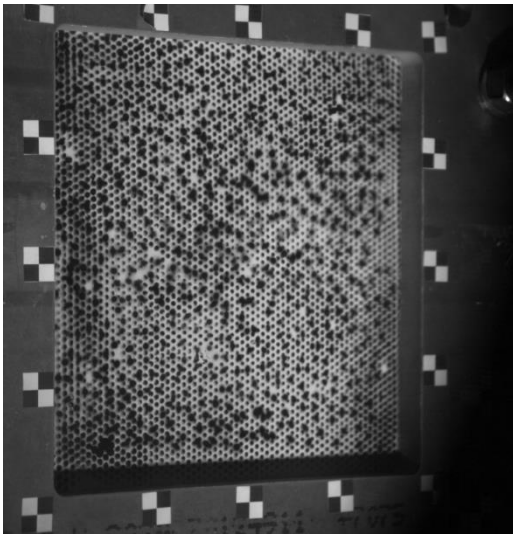

*Figure 2.11: Typical DIC pattern*

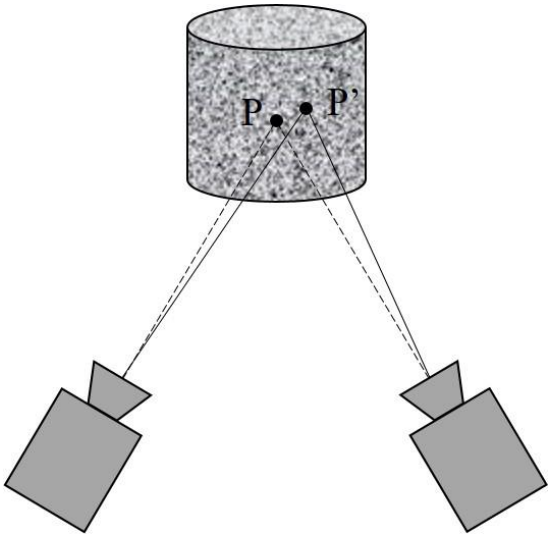


*Figure 2.12: Illustration of stereovision setup*

# 3 MATERIAL MODEL & IDENTIFICATION OF PARAMETERS

## 3.1 STEEL MODEL

The steel skins used in the current study are made from 0.8 mm thick plates of Docol600DL steel. Docol600DL is a dual-phase, cool-rolled steel manufactured by Swedish Steel Ltd (SSAB). It has medium strength with high hardening. During production, the steel receives a heat treatment that results in a two-phase structure with ferrite and martensite. The ferrite gives the steel good formability, while the martensite gives high strength properties. Table 3.1 gives the chemical composition of the material, as reported by the manufacturer [28].

*Table 3.1: Chemical composition of Docol600DL [28]*

| C [%] | Si [%] | Mn [%] | P [%] | S[%] | $Al_{tot}$ [%] |
|---|---|---|---|---|---|
| 0.10 | 0.40 | 1.50 | 0.010 | 0.002 | 0.040 |

### 3.1.1 Constitutive model

Due to the high strain rates associated with blast loading, a thermoelastic-thermoviscoplastic material model suggested by Børvik et al. [36], was chosen to describe the steel material. This model is based on a slightly modified version of the constitutive relation proposed by Johnson and Cook [37], and continuum damage mechanics as proposed by Lemaitre [38]. This model is implemented in LS-DYNA as *MAT_107, and is well suited for large plastic strains, high strain rates and temperature softening of an isotropic material. Fracture is described using the Cockcroft-Latham fracture criterion [39]. The theory behind application of the constitutive material model can be found in [36], but is summarized briefly in the following.

The yield function is defined by:

$$f = \sigma_{eq} - (\sigma_0 + R) \leq 0, \tag{3.1}$$

where $\sigma_0$ is the yield stress and $R$ is the isotropic hardening, while the equivalent stresses can be expressed by the constitutive equation:

$$\sigma_{eq} = \left[\sigma_0 + \sum_{i=1}^{2} Q_i(1 - e^{-C_i p})\right][1 + \dot{p}^*]^c[1 - T^{*m}] \tag{3.2}$$

Where $\sigma_{eq}$ is the equivalent stress and $p$ is the equivalent plastic strain. $\sigma_0$ represents the initial yield strength and $Q_i$, $C_i$, $c$ and $m$ is material constants. While $\dot{p}^*$ is a dimensionless strain rate given by:

$$\dot{p^*} = \frac{\dot{p}}{\dot{p}_0} \tag{3.3}$$

Where $\dot{p}_0$ is a user defined reference strain rate. $T^*$ is a normalized temperature, defined by:

$$T^* = \frac{T - T_r}{T_m - T_r} \tag{3.4}$$

Where T is the absolute temperature, $T_r$ is the room temperature and $T_m$ is the melting temperature of the material.

The first term of the constitutive equation can be recognized as the two-term Voce hardening rule. The following two terms represent a strain rate correction term, and a temperature correction term respectively. If it is necessary, temperature change due to adiabatic heating effects can be expressed as:

$$\Delta T = \int_0^p \chi \frac{\sigma_{eq}}{\rho C_p} dp \tag{3.5}$$

Where $\rho$ is the material density, $C_p$ is the specific heat and $\chi$ is the Taylor-Quinney coefficient representing the proportion of plastic work converted into heat.

### 3.1.2 Material tests & numerical model

The material parameters $\sigma_0$, $Q_i$ and $C_i$ may be obtained by inverse modeling material tensile test using FE. No material tests were performed on Docol600DL in this study, as the material has been thoroughly studied in previous work at SIMLab. All the necessary material parameters are therefore taken from previous work [40]. The applied material parameters, and physical constants are given in Table 3.2 and Table 3.3. Figure 2.1 is taken from [40], and shows the nominal (engineering) stress-strain curves for representative uniaxial tension tests and the optimized Voce hardening rule corresponding to the parameters given in Table 3.2. It

can be seen that the material exhibits the same properties in all directions (isotropic) and the FE model is capable to predict the material test really well.

*Table 3.2: Material parameters for the modified Johnson-Cook constitutive relation for Docol600DL [40]*

| $\sigma_0$ [MPa] | $Q_1$ [MPa] | $C_1$ [-] | $Q_2$ [MPa] | $C_2$ [-] | c [-] | m [-] | $\dot{\boldsymbol{p}}_{\boldsymbol{0}}$ [$s^{-1}$] |
|---|---|---|---|---|---|---|---|
| 370 | 236.4 | 39.3 | 408.1 | 4.5 | 0.001 | 1.0 | $5 \times 10^{-4}$ |

*Table 3.3 Physical material constants for Docol600DL [40]*

| E [GPa] | $\nu$ [-] | $\rho$ [$kg/m^3$] | $\alpha$ [$K^{-1}$] | $C_p$ [J/kgK] | $\chi$ [-] | $T_r$ [K] | $T_m$ [K] |
|---|---|---|---|---|---|---|---|
| 210.0 | 0.33 | 7850 | $1.2 \times 10^{-5}$ | 452 | 0.9 | 293 | 1800 |

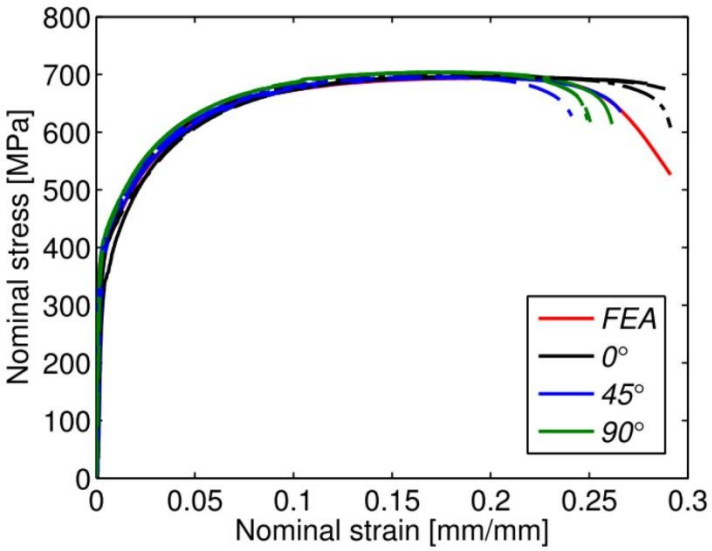


*Figure 3.1: Nominal (engineering) stress-strain curves for uniaxial tension test on Docol600DL and FE solution corresponding to the material parameters in Table 3.2 [40]*

## 3.2 FOAM MODEL

Commercially available extruded polystyrene (XPS) foam sheets, produced by Sundolitt [2], were used as the core material in the current study. Foams with three different average densities was investigated; XPS250 with a producer specified density of approximately 33 kg/m$^3$, XPS400 with a producer specified density of approximately 37 kg/m$^3$ and XPS700 with a producer specified density of approximately 50 kg/m$^3$ [41].

### 3.2.1 Constitutive foam model

As stated by Reyes et al. [42], several constitutive models for foam exist in the literature [43] [44]. However, not all of these models are suited for the current study. The numerical analyses used in the current study are quite computational demanding, and therefore it was decided to use a relatively simple, but accurate model to represent the foam material. For this reason, the constitutive model suggested by Deshpande and Fleck [45] was chosen. This model was implemented in LS-DYNA as *MAT_154 by Reyes et al. [42]. The applied model an theory is based on their work and is briefly summarized in the following.

The so-called Deshpande-Fleck model [45] can be regarded as an extension to the von Mises yield criterion where hydrostatic stresses are incorporated. This incorporation is important due to the change in volume when foam cells collapse. The yield function is defined by:

$$\phi = \hat{\sigma} - Y \leq 0, \tag{3.6}$$

where the yield stress $Y$ can be expressed as:

$$Y = \sigma_p + R(\hat{\varepsilon}) \tag{3.7}$$

$R(\hat{\varepsilon})$ represents the strain hardening, $\sigma_p$ represents the plateau stress and $\hat{\varepsilon}$ the equivalent strain. The equivalent stress,$\hat{\sigma}$, is given by:

$$\hat{\sigma} = \frac{1}{\left[1 + \left(\alpha/3\right)^2\right]}\left[\sigma_e^2 + \alpha^2\sigma_m^2\right], \tag{3.8}$$

where $\sigma_e$ is the von Mises effective strain, and $\sigma_m$ the mean stress. The parameter $\alpha$ is a function of the plastic coefficient of contraction $\nu^p$, and describes the shape of the yield surface. $\alpha$ is defined as follows:

$$\alpha^2 = \frac{9}{2}\frac{(1-2\nu^p)}{(1+\nu^p)} \tag{3.9}$$

The material properties of foam are greatly dependent on the foam density. In order to easier let the hardening be density dependent, Reyes et al. introduced a slightly modified version of a hardening model suggested by Hanssen et al. [46]:

$$\sigma = \sigma_p + \gamma\frac{\varepsilon}{\varepsilon_D} + \alpha_2 \ln\left[\frac{1}{1-(\varepsilon/\varepsilon_D)^\beta}\right], \tag{3.10}$$

where γ is a linear strain-hardening coefficient, $\alpha_2$ is a non-linear scale factor, and β is a non-linear shape factor. Further, ε is the true strain, and $\varepsilon_D$ is defined as the densification strain. If the plastic coefficient of contraction is assumed to be zero, the densification strain can be expressed as:

$$\varepsilon_D = -\ln\left[\frac{p_f}{p_{f0}}\right] \tag{3.11}$$

Where $p_f$ and $p_{f0}$ represents the density of the foam and the density of the base material respectively. Furthermore, the material parameters $\sigma_p$, γ, $\alpha_2$ and β, can all be expressed as a power law function of the relative foam density:

$$\{\sigma_p, \alpha_2, \gamma, \beta\} = C_0 + C_1\left(\frac{p_f}{p_{f0}}\right)^n \tag{3.12}$$

Where $C_0$, $C_1$ and $n$ are calibrated constants for each material parameter.

### 3.2.2 Material tests

To obtain the necessary material data to create a numerical model of the XPS foam, a series of uniaxial compression tests was performed. Three different foam densities, with specified compressive strength of 250, 400 and 700 kPa respectively, were tested. [41]

Specimens were cut from foam sheets with a specified thickness of 50mm, forming cubes approximately 50x50x50mm. A total of 5 cubes were cut for each of the three densities. To obtain accurate material data, the specimens were weighed, and the dimensions thoroughly measured. The density was calculated based on these measurements. These can be found in Table 3.4.

Uniaxial compressions tests were preformed in an Instron universal testing machine, with a 100 kN load cell. The specimens were oriented such that they were loaded through the thickness of the foam sheets. The load was applied as quasi-static displacements at approximately 0.05 mm/s. A DIC camera was used to capture the displacements, while the load cell logged the forces.

*Table 3.4: Measurements of the test specimens*

| ***Test Specimen*** | ***Weight [g]*** | ***Avg. Length [mm]*** | ***Avg. Width [mm]*** | ***Avg. Height [mm]*** | ***Measured Density [kg/m$^3$]*** |
|---|---|---|---|---|---|
| *XPS-250-1* | 4.20 | 50.07 | 49.84 | 51.15 | 32.897 |
| *XPS-250-2* | 4.32 | 49.96 | 49.87 | 51.59 | 33.609 |
| *XPS-250-3* | 4.24 | 49.90 | 49.81 | 51.54 | 33.094 |
| *XPS-250-4* | 4.16 | 50.03 | 49.85 | 50.93 | 32.751 |
| *XPS-250-5* | 4.40 | 49.98 | 49.88 | 51.54 | 34.246 |
| *XPS-400-1* | 4.96 | 50.36 | 49.88 | 53.00 | 37.256 |
| *XPS-400-2* | 4.90 | 49.85 | 50.04 | 53.01 | 37.063 |
| *XPS-400-3* | 4.90 | 50.00 | 50.06 | 53.01 | 36.932 |
| *XPS-400-4* | 5.02 | 50.00 | 50.01 | 52.87 | 37.972 |
| *XPS-400-5* | 5.10 | 50.01 | 50.20 | 52.43 | 38.749 |
| *XPS-700-1* | 6.34 | 50.25 | 50.27 | 50.05 | 50.140 |
| *XPS-700-2* | 6.26 | 50.21 | 50.21 | 49.56 | 50.106 |
| *XPS-700-3* | 6.38 | 50.23 | 50.19 | 50.21 | 50.399 |
| *XPS-700-4* | 6.40 | 50.26 | 50.32 | 50.29 | 50.323 |
| *XPS-700-5* | 6.36 | 50.26 | 50.21 | 50.20 | 50.194 |

An interesting observation was made by weighing the specimens both before and after compression. It was observed that the weight increased when the foam was compressed. This may indicate that the blowing agent used in production of the foam is a gas lighter than air.

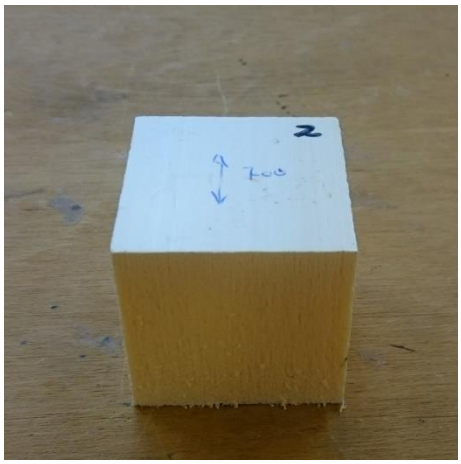

*a) Foam test specimen*

*b) Foam test specimen meshed in LS DYNA*

*Figure 3.2: Typical foam test specimen*

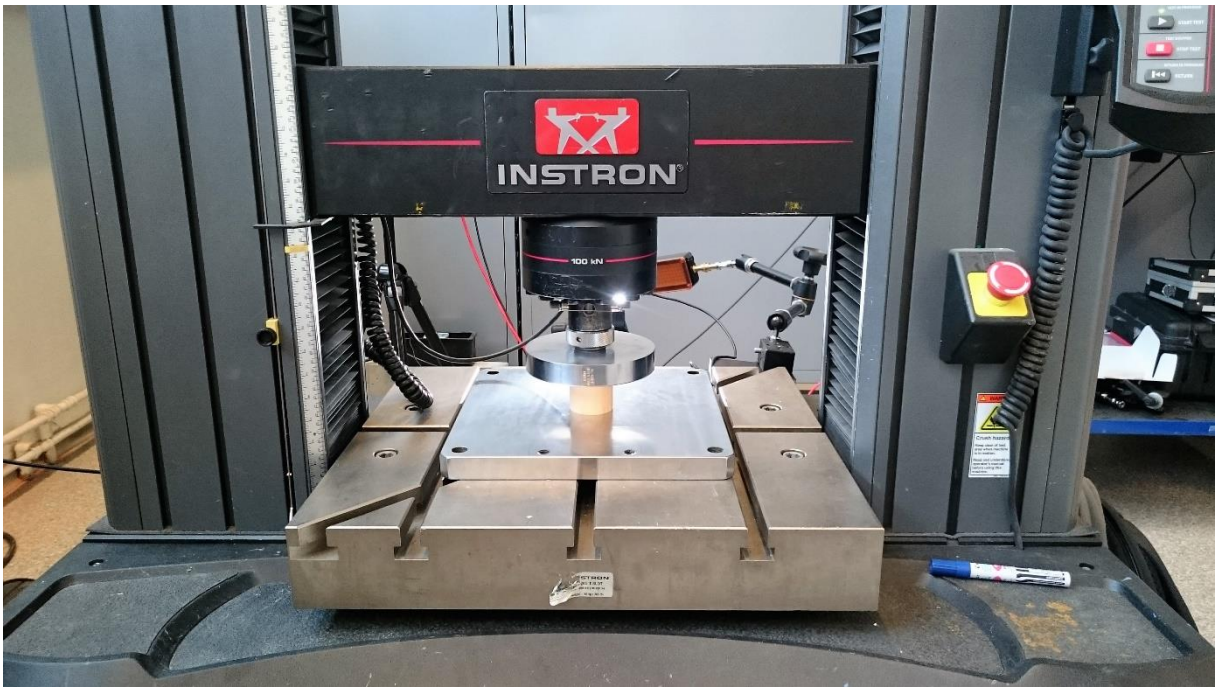


*Figure 3.3: Test specimen in the test rig*

### 3.2.3 Numerical model

The raw data gathered from the tests were processed with MATLAB [47] to obtain the stress-plastic strain relationship necessary for the material model. First, the engineering stresses and strains where calculated according to:

$$s = \frac{F}{A_0} \tag{3.13}$$

$$e = \frac{\Delta L}{L_0} \tag{3.14}$$

Where $F$ is the applied force, $A_0$ is the initial cross sectional area, $\Delta L$ is the measured elongation and $L_0$ is the initial height of the specimen.

The engineering strains were then converted to true strains:

$$\varepsilon = -\ln(1 - e) \tag{3.15}$$

Note that the engineering strain is defined positive for tension.

The Poisson's ratio is assumed to be zero, which results in the true stresses be equal the engineering stresses. Thus, the engineering stress was used without modification.

To get the plastic response of the material, it was necessary to eliminate the elastic response in the data. To do this the elastic stiffness was estimated. There is however, a lot of uncertainty when estimating the elastic stiffness based on experimental test, mainly due to the elastic response of the test rig. Thus, the estimated stiffness modulus, while being sufficiently accurate to the eliminate elastic response (of both the machine and the test material), were not considered accurate enough to describe the linear elastic behavior in the material model. It was therefore chosen to use the elastic modulus specified by Sundolitt [41] for this purpose.

Using the curve fitting toolbox in MATLAB [48], the hardening model was fitted to the derived data points by optimizing $\sigma_p$, $\gamma$, $\alpha_2$ and $\beta$. Figure 3.5 shows the results plotted together for each density. One set of representative material parameters were chosen for each of the three densities to use in the numerical study of the experiments. The chosen parameters are taken from the test specimens XPS-250-03, XPS-400-01 and XPS-700-03, and are summarized in Table 3.5, and plotted in Figure 3.6. These models were chosen as representative since they appear to exhibit the average behavior for each foam density.

*Table 3.5: Material parameters for Deshpande-Fleck material model*

| **Material** | **$\rho_f$ [kg/m$^3$]** | **E [MPa]** | **$\sigma_p$ [MPa]** | **$\gamma$ [MPa]** | **$\varepsilon_D$ [-]** | **$\alpha_2$ [MPa]** | **$\beta$ [-]** |
|---|---|---|---|---|---|---|---|
| XPS-250-03 | 33.09 | 9 | 0.255 | 0.794 | 3.448 | 28.080 | 5.439 |
| XPS-400-01 | 37.26 | 15.3 | 0.402 | 0.700 | 3.329 | 23.858 | 5.152 |
| XPS-700-03 | 50.40 | 31 | 0.745 | 0.156 | 3.027 | 25.322 | 4.464 |

The uniaxial compression were analyzed numerically in LS-DYNA to validate the material models. The foam specimen cubes where modeles with 1000 elements, and for simplicity the imposed displacements and boundary conditions were introduced directly on the nodes, i.e. and the analysis were modeled contact free. The analysis was stopped after 45 mm compression. Figure 3.7 shows a comparison of the force-displacement response between the compression tests and the LS-DYNA analysis.

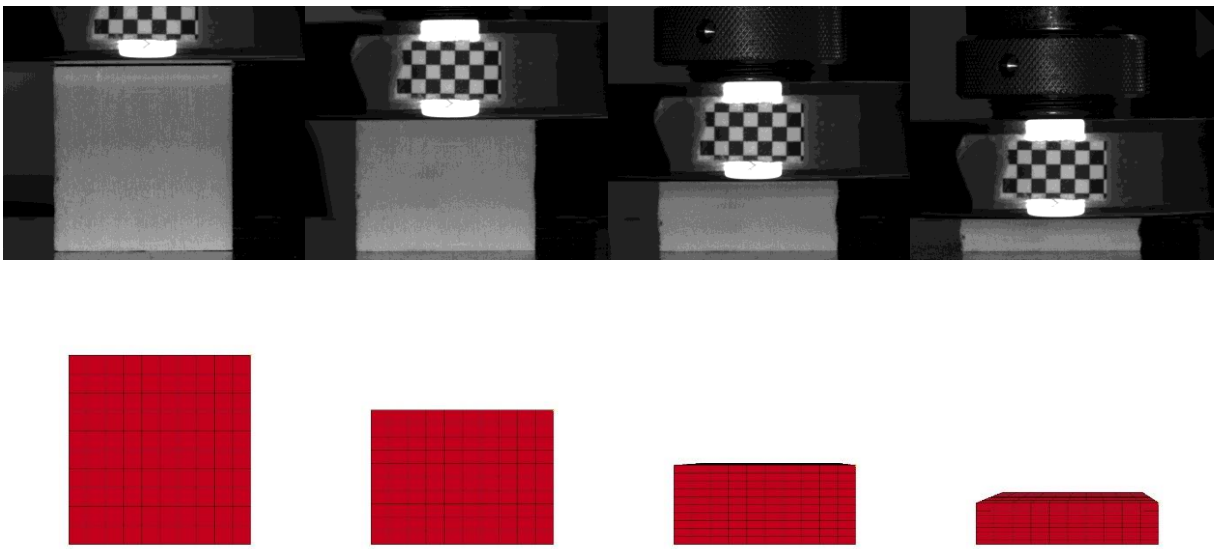

*Figure 3.4: Typical foam specimen during compression test compared to LS DYNA simulation*

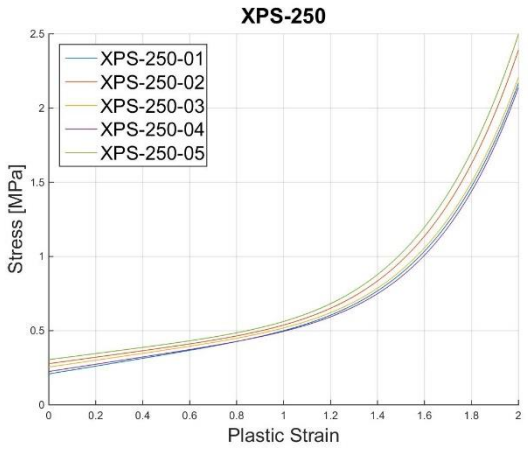


*a) Material models for XPS250*

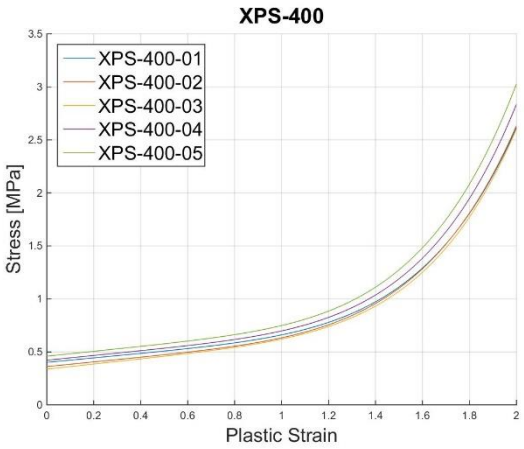


*b) Material models for XPS400*

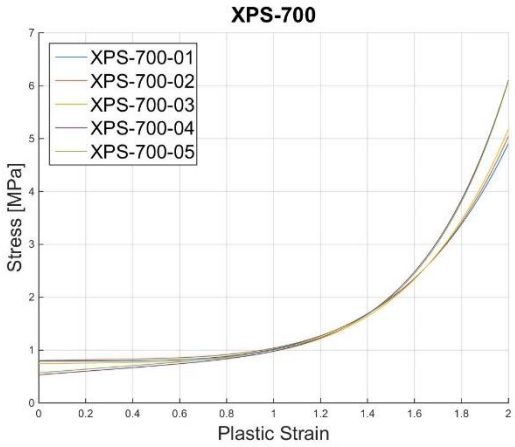


*c) Material models for XPS700*

*Figure 3.5: Calibrated material models for all square test specimens*

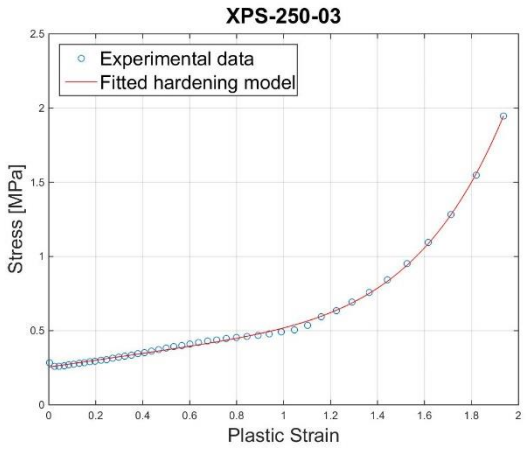


*a) Representative model for XPS250*

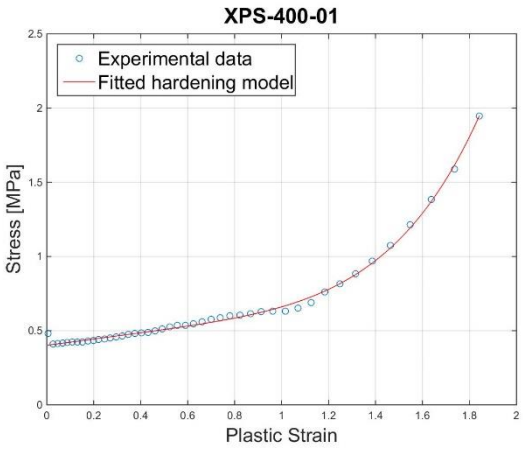


*b) Representative model for XPS400*

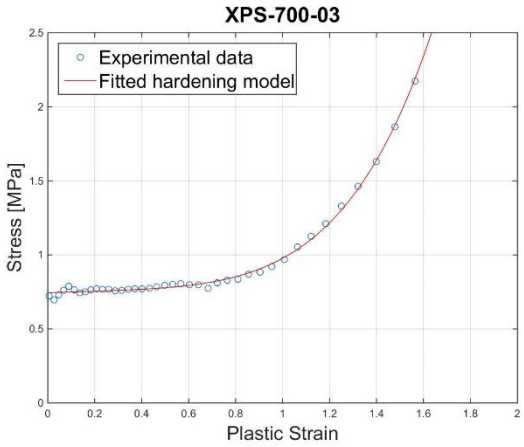


*c) Representative model for XPS700*

*Figure 3.6: Representative material models compared to the corresponding tests*

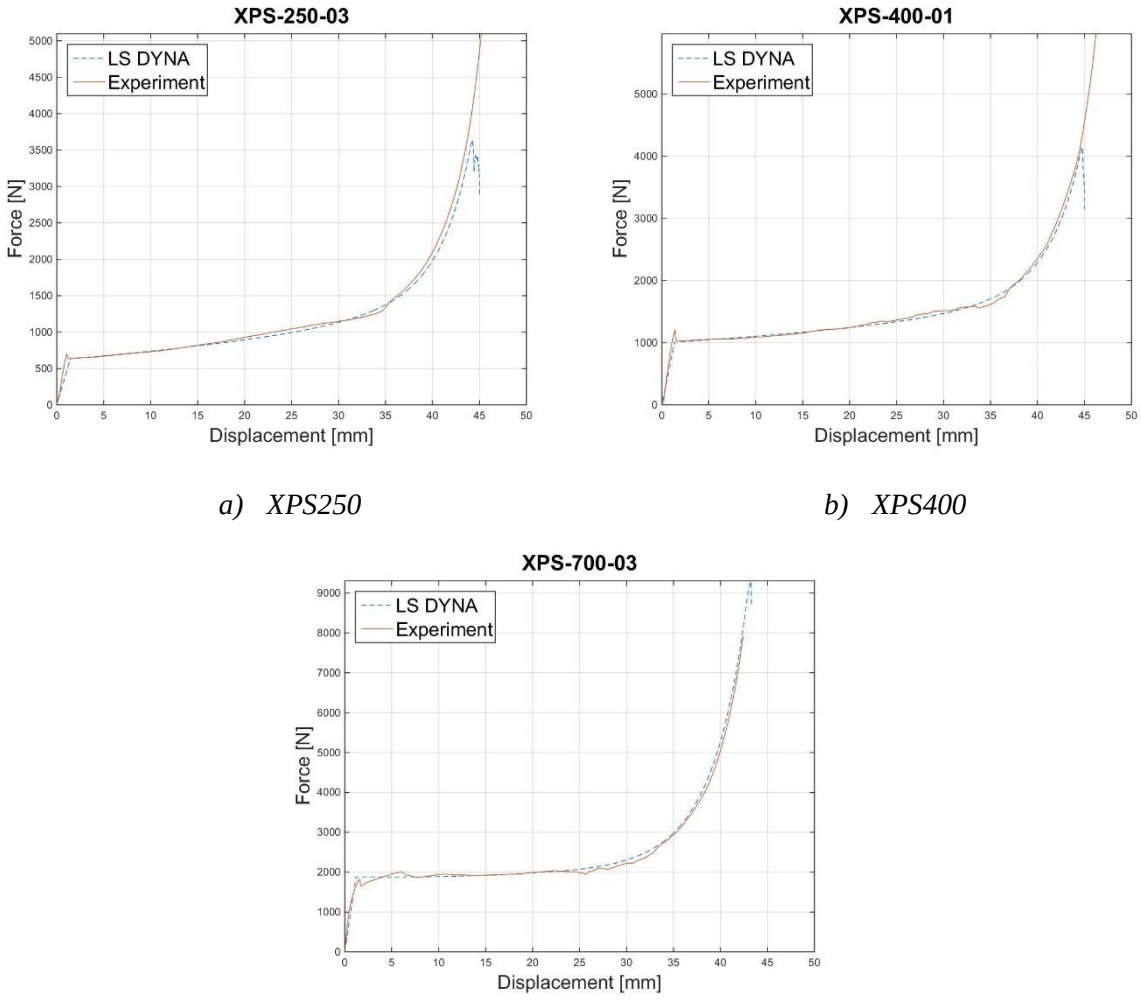


*a) XPS250*

*b) XPS400*

*c) XPS700*

*Figure 3.7: Comparison of the response between LS DYNA simulations and the experiments*

### 3.2.4 Density dependent model

A density dependent model was extrapolated from the material data found from the compression tests. By making the material parameters density dependent, it possible to study foam densities that were not tested. However, since the model is built on only a few quasi-static compression tests, this model is only used to study the sensitivity of the material model with respect to foam density, within the density range tested. The material model was constructed by fitting the power-law function (equation 3.12) stated above to the material parameters found for each compression test. The value of each material parameter was plotted against that specific specimen's density (Figure 3.8), and the curve fitting toolbox [48] in MATLAB was used to fit the equation constants. The constants for each material parameter

are given in Table 3.6. It should be noted that the density dependent model includes some additional material test.

Figure 3.9 shows a typical comparison between the density dependent material model, the directly fitted material model and the experimental data. Since the density dependent model is generic for all densities, some deviation from the experimental data can be expected. However the model fits with reasonable accuracy.

*Table 3.6: Calibrated constants for density dependent material model*

| | $\sigma_p$ | $\gamma$ | $\alpha_2$ | $\beta$ |
|---|---|---|---|---|
| $C_0$ | 0 | 1.410 | 19.91 | 0 |
| $C_1$ | 828.6 | -2009 | $5.141 \times 10^{-3}$ | 0.853 |
| $n$ | 2.335 | 2.497 | -2.251 | -0.549 |

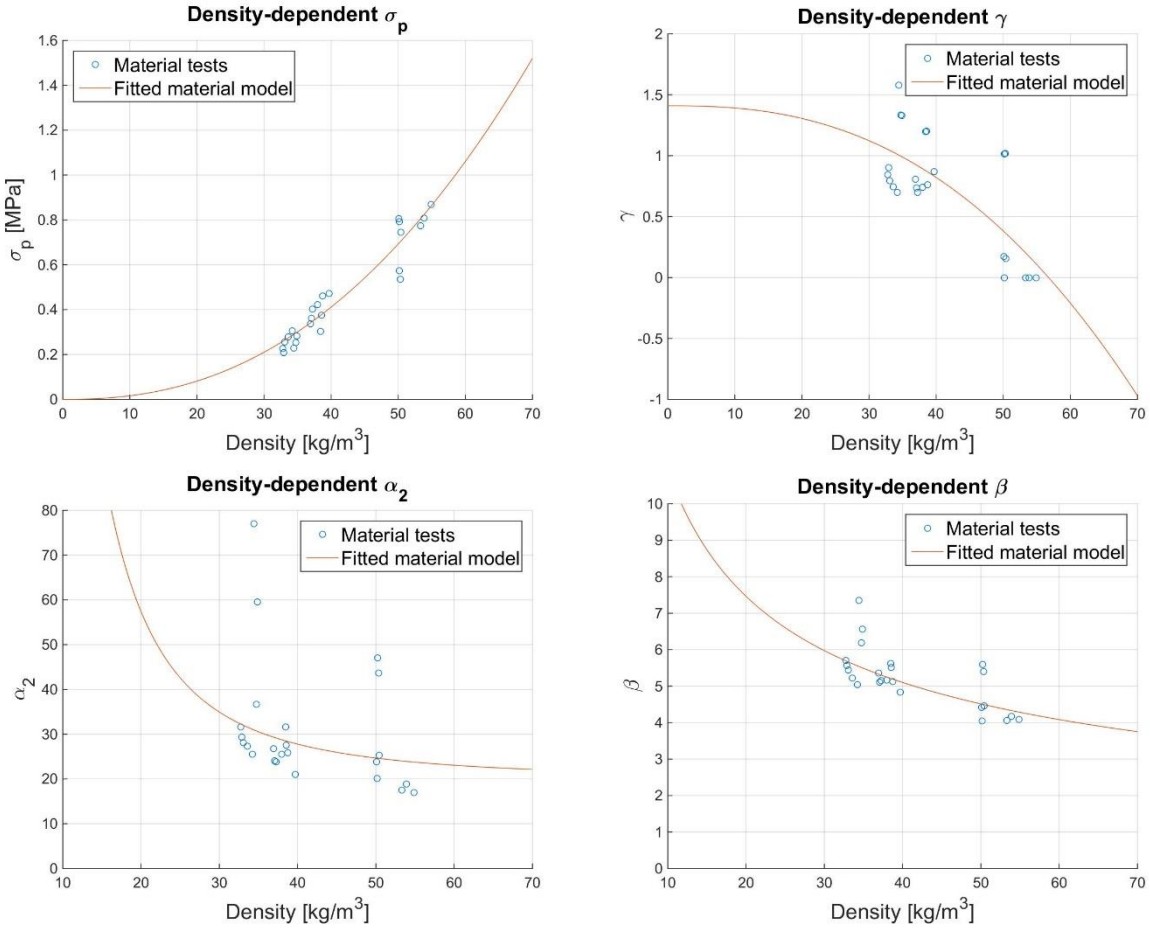


*Figure 3.8: Calibration of density dependent material model*

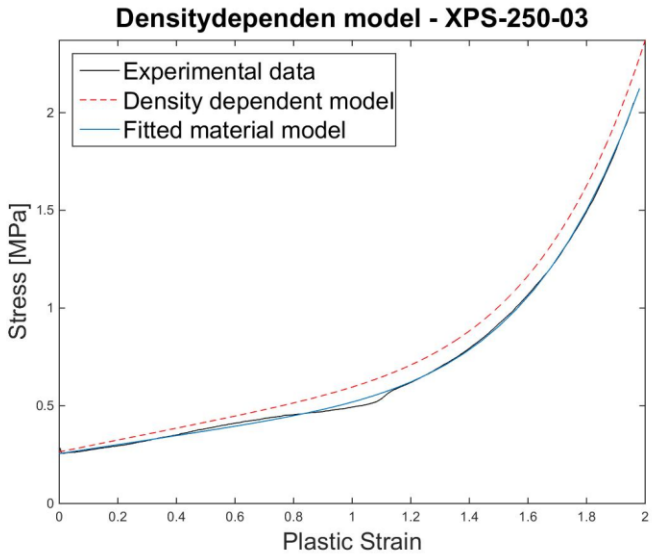


*Figure 3.7: Correlation between the density dependent and the fitted material model for a typical test*

# 4 EXPERIMENTAL PROGRAM

## 4.1 INTRODUCTION

The experimental program consist of two different type of experiments. Section 4.2 describes the experiments performed in the drop tower rig at SIMLab [49], while Section 4.3 concentrates on experiments performed in the SIMLab shock tube facility [50].

The drop tower rig was used to investigate the behavior of the polymer foam under low velocity impact loads. Using a dropped mass rig is a controlled and easily repeatable way to measure the dynamic response of the specimens. A series of drop experiments where performed on sandwich panels with steel skins and polymer foam cores of different density (XPS250, XPS400 and XPS700) both with and without a front-plate, at three different velocities. No bonding agent was used between the skins and the foam core. The steel skins were also tested without a foam core. An overview of the experiments performed is given in Table 4.1. An Instron CEAST 9350 drop tower impact system [34] was used for the experiments. The test specimens where impacted with a falling mass, and the force response was measured using a load cell in the rig. The primary goal of the experiments were to quantify the the energy absorption and the force response of the polymer foam, and to obtain a baseline for comparison with FE analyses.

The shock tube facility was used to recreate loading conditions similar to those that occur under explosive detonations. The shock tube offers a controlled alternative to detonation of explosives, which makes replicating the experiments easier. Only the lowest foam density, XPS-250, were studied. A total of five tests were performed. Three foam plates with a nominal thickness of 50mm, were tested as the core material in a sandwich structure. The panels were subjected to three different blast loads. Further, one foam plate were tested without a steel front plate (XPS250_35), and one test was done on the steel plates without a foam core (D600_60). No bonding agent was used between foam and the skins. An overview of the study is given in the Table 4.4, all values in the Table are nominal. The primary goals of the experiment was to observe the response of the polymer foam sandwich under blast load conditions, and to get a basis for comparison to numerical analyses.

## 4.2 DROP TOWER

A total of 22 test were performed in the drop tower rig. Foams with different densities were tested, both in a sandwich configuration and without a front plate at three different impact velocities. In addition three more test were performed with no foam core, for the same velocities as the previous tests. This test program was chosen to investigate the effect of the foam core densities and the interaction between the core material and the front plate. The test on the steel skins alone serve to give an indication on the contribution of the skins with respect to energy absorption. The experimental program is summarized in the Table 4.1.

*Table 4.1: Experimental program for the drop tower*

| *Test* | *Core Material* | *Thickness [mm]* | *Density [kg/m$^3$]* | *Front plate?* | *Impact Mass [kg]* | *Velocity [m/s]* |
|---|---|---|---|---|---|---|
| **XPS-250-049S** | XPS-250 | 50.7925 | 33.1218 | YES | 14.895 | 4.9 |
| **XPS-250-049** | XPS-250 | 50.8275 | 33.1138 | NO | 14.895 | 4.9 |
| **XPS-250-07S** | XPS-250 | 50.845 | 33.0753 | YES | 14.895 | 7 |
| **XPS-250-07** | XPS-250 | 50.8325 | 33.2001 | NO | 14.895 | 7 |
| **XPS-250-10S** | XPS-250 | 50.7225 | 33.1354 | YES | 14.895 | 10 |
| **XPS-250-10** | XPS-250 | 50.7625 | 33.1035 | NO | 14.895 | 10 |
| **XPS-400-049S** | XPS-400 | 52.855 | 37.2014 | YES | 14.895 | 4.9 |
| **XPS-400-049** | XPS-400 | 52.7225 | 37.4572 | NO | 14.895 | 4.9 |
| **XPS-400-07S** | XPS-400 | 52.75 | 37.2868 | YES | 14.895 | 7 |
| **XPS-400-07** | XPS-400 | 52.8 | 37.2001 | NO | 14.895 | 7 |
| **XPS-400-10S** | XPS-400 | 52.7475 | 37.2954 | YES | 14.895 | 10 |
| **XPS-400-10** | XPS-400 | 52.7675 | 37.2200 | NO | 14.895 | 10 |
| **XPS-700-049S2** | XPS-700 | 50.185 | 50.3507 | YES | 14.895 | 4.9 |
| **XPS-700-049** | XPS-700 | 50.1975 | 50.3869 | NO | 14.895 | 4.9 |
| **XPS-700-049S** | XPS-700 | 50.145 | 50.3644 | YES | 14.895 | 4.9 |
| **XPS-700-07** | XPS-700 | 50.065 | 50.3799 | NO | 14.895 | 7 |
| **XPS-700-07S** | XPS-700 | 50.4475 | 50.2014 | YES | 14.895 | 7 |
| **XPS-700-10** | XPS-700 | 50.355 | 50.2838 | NO | 14.895 | 10 |
| **XPS-700-10S** | XPS-700 | 50.4175 | 50.3487 | YES | 14.895 | 10 |
| **DOCOL600DL-049** | - | 0.8 x 2 | 7850 | - | 14.895 | 4.9 |
| **DOCOL600DL-07** | - | 0.8 x 2 | 7850 | - | 14.895 | 7 |
| **DOCOL600DL-10** | - | 0.8 x 2 | 7850 | - | 14.895 | 10 |

### 4.2.1 Test Set-up

Impact tests were performed on an Instron CEAST 9350 drop tower impact system [34]. The standard instrumented striker and striker-holder were used in conjunction with a large surface rounded impactor (see Figure 4.3 for the geometry). The striker and holder have a combined mass of 5.735 kg, and the impactor has a mass of 1.660 kg. This gave a total impacting mass of 7.395 kg. However, after performing two initial tests on the rig, it became apparent that the recoil of the impactor would be too violent. To keep the impactor from bouncing too high after impact, additional weights were added to achieve a total impacting mass of approximately 15 kg (14.895 kg).

The test rig uses a load-cell to measure the forces acting on the impactor during the experiment. In addition to the force measurements, two Phantom v1610 high-speed cameras were used to capture a stereovision image series of the back plate, suitable for DIC.

A thorough experimental study were performed by testing all three foam densities at 4.9, 7 and 10 m/s. Square foam specimens of dimension 400 mm x 400 mm x 50 mm were tested both as a sandwich structure, with steel plates on either side, and without a front plate. Tests were also performed on the steel skins alone, i.e. double steel plates. All the tests were performed without any bonding agent between the layers. The specimens were bolted to a circular frame with an inner diameter of 300 mm using 12 equidistant M12 bolts. For the tests performed with a front plate, the bolts were tightened to 2 Nm using a torque wrench, while the bolts were only tightened by hand, to keep the foam from deforming, when no front plate were used. An overview of the study is given in Table 4.1. The thickness and density given in the Table are based measurements.


*a) The drop tower test rig*

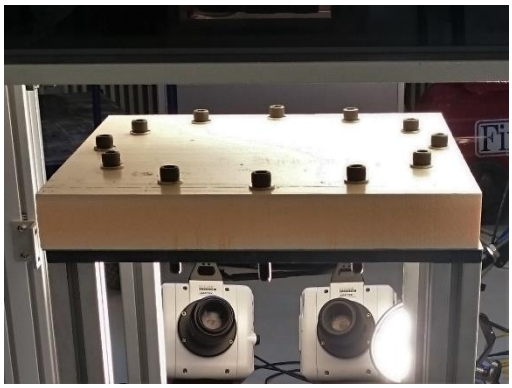

*b) Foam specimen without front plate bolted in place*

*c) Sandwich test specimen bolted in place*

*Figure 4.1: Test set up*

### 4.2.2 Data processing

The rig's load-cell logged the force-time history at a sampling frequency of 0.5 MHz (time step $\Delta t = 2 \times 10^{-6}$ s). This provides sufficient information to compute the velocity- and displacement-time history for the tests. An optical sensor in the rig measured the velocity of the impactor just before impact, it should be noted that the distance from the sensor to the specimen is significant enough that it is reasonable to expect the impact velocity to be slightly higher than the measured value. This has however been disregarded in the following. The incremental velocity change is calculated by numerical integration of the acceleration, which can be found from Newton's 2nd law. The current velocity is then calculated by an iterative process described by;

$$v_{n+1} = v_n - \left(\frac{F_{n+1} + F_n}{2m_p} - g\right)\Delta t, \tag{4.1}$$

where $v_{n+1}$ is the current velocity, $v_n$ is the previous velocity, $F_{n+1}$ is the current force, $F_n$ is the previous force, $m_p$ is the impacting mass, $g$ is the gravitational accelerations and $\Delta t$ is the time step.

Further, the displacements after impact can now be calculated by a similar iteration scheme based on the velocities;

$$u_{n+1} = u_n + \left(\frac{v_{n+1} + v_n}{2}\right)\Delta t, \tag{4.2}$$

where $u_{n+1}$ is the current displacement and $u_n$ is the previous displacement.

***Force correction***

The load-cell used to capture the forces in the drop-tower is placed behind the impactor. As a result of this, a considerable mass is located ahead of the load-cell. It is therefore necessary to derive a correlation between the forces measured by the load-cell, *P*, and the forces acting on the specimen. *F*. Figure 4.2 shows an illustration of the striker setup.

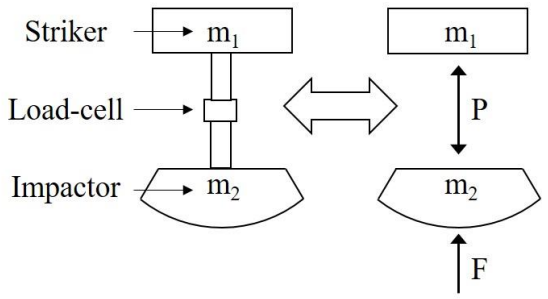


*Figure 4.2: Striker setup*

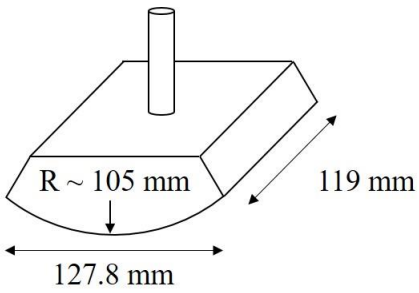


*Figure 4.3: Impactor geometry*

By using Newton's second law of motion. *P* and *F* can be expressed by:

$$P = m_1\ddot{x}_1 + m_1 g \tag{4.3}$$

$$F = P + m_2\ddot{x}_1 + m_2 g \tag{4.4}$$

Setting up the force equilibrium then results in:

$$F = \left(1 + \frac{m_2}{m_1}\right) P, \tag{4.5}$$

where $m_2$ is the mass of the impactor, $m_1$ is the rest of the impacting mass and $P$ is the forces measured by the load-cell.

### 4.2.3 Experimental results

As mentioned earlier, the main objective of these experiments was to learn more about the material properties under impulse loading. The main material property investigated is the energy absorption of the foam material. Further, the amount of compression of the foam is of great interest. Unfortunately, problems occurred when post processing the DIC measurements, so those results are absent. Ideally the test specimens should have been bisected and measured after the experiments, however that was not done in the current work.

Since the energy can not be measured directly during the tests, it is necessary to measure other physical parameters that can be used to derive the work i.e. the energy absorbed. In this case, the force-time history was captured by a load cell in the rig. The data captured during the experiments were processed using MATLAB [47] according to the procedure described in the previous section. The forces, velocities and displacements were used to calculate the impulse, and the work done by the test specimen i.e. the energy absorbed, for each experiment. The impulse is calculated by numerical integration of the force vs. time relationship, while the work is calculated by numerical integration of the force vs. displacement relationship. The results are listed in Table 4.2. To check for numerical errors that might have occurred during the data processing, the impulse and work were compared to values calculated by an analytical approximation. The impulse, *I*, was approximated as the linear momentum prior to impact, given by:

$$I = mv_0, \tag{4.6}$$

and the work, *W*, was approximated as the change in the kinetic energy of the impactor;

$$W = \frac{1}{2} m(v_0^2 - v_r^2) \tag{4.7}$$

Where $m$ is the impacting mass, $v_0$ is the initial velocity, and $v_r$ is the residual velocity. The approximate residual velocity of the impactor after impact (while bouncing of the component) was extracted from the data. Figure 4.4 shows the comparison of the two methods, and confirms the results as reasonable.

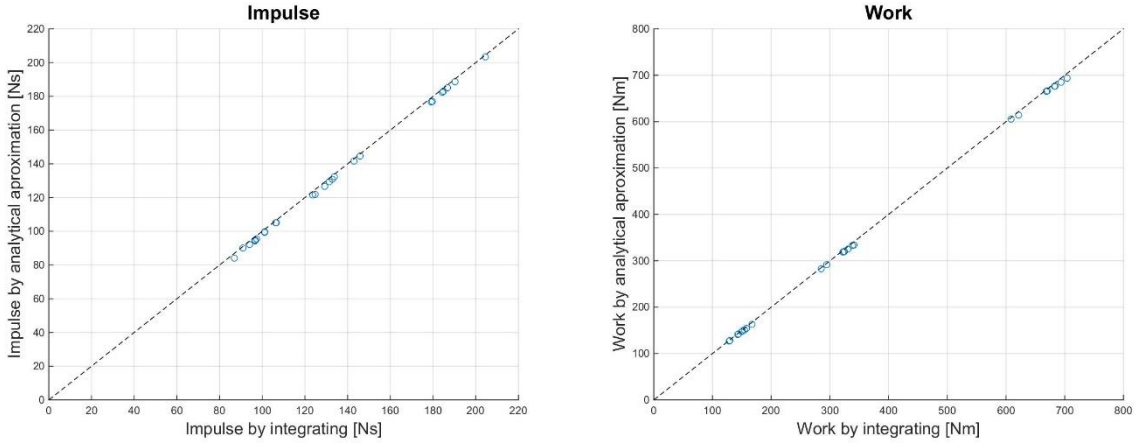


*a) Impulse* *b) Work*

*Figure 4.4: Comparison of calculation methodology for the work and impulse*

*Table 4.2: Summary of the experimental results with respect to absorbed energy (work) and impulse*

| Test | Front plate? | Measured density [kg/m$^3$] | Measured $v_0$ [m/s] | Impulse [Ns] | Work [Nm] |
|---|---|---|---|---|---|
| **XPS-250-049S** | YES | 33.12 | 4.75 | 96.63 | 150.54 |
| **XPS-250-049** | NO | 33.11 | 4.76 | 86.84 | 167.64 |
| **XPS-250-07S** | YES | 33.08 | 6.84 | 132.75 | 323.64 |
| **XPS-250-07** | NO | 33.20 | 6.83 | 124.74 | 340.81 |
| **XPS-250-10S** | YES | 33.14 | 9.84 | 184.91 | 682.39 |
| **XPS-250-10** | NO | 33.10 | 9.86 | 179.25 | 703.84 |
| **XPS-400-049S** | YES | 37.20 | 4.77 | 101.07 | 144.07 |
| **XPS-400-049** | NO | 37.46 | 4.76 | 96.59 | 153.99 |
| **XPS-400-07S** | YES | 37.29 | 6.85 | 133.82 | 321.92 |
| **XPS-400-07** | NO | 37.20 | 6.82 | 129.19 | 331.07 |
| **XPS-400-10S** | YES | 37.30 | 9.81 | 186.74 | 670.71 |
| **XPS-400-10** | NO | 37.22 | 9.81 | 179.71 | 693.36 |
| **XPS-700-049S2** | YES | 50.35 | 4.74 | 106.46 | 129.06 |
| **XPS-700-049** | NO | 50.39 | 4.73 | 97.36 | 150.31 |
| **XPS-700-049S** | YES | 50.36 | 4.75 | 106.35 | 128.49 |
| **XPS-700-07** | NO | 50.38 | 6.81 | 131.45 | 324.43 |

| | | | | | |
|---|---|---|---|---|---|
| **XPS-700-07S** | YES | 50.20 | 6.82 | 145.87 | 285.52 |
| **XPS-700-10** | NO | 50.28 | 9.86 | 184.32 | 683.02 |
| **XPS-700-10S** | YES | 50.35 | 9.83 | 190.23 | 669.23 |
| **DOCOL600DL-049** | - | - | 4.76 | 101.12 | 142.99 |
| **DOCOL600DL-07** | - | - | 6.81 | 143.11 | 294.22 |
| **DOCOL600DL-10** | - | - | 9.80 | 204.60 | 608.46 |

Figures 4.8-4.10 summarizes the results for each of the experiments. It should be noted that all the force measurements exhibit significant oscillations at what appear to be at a constant frequency. A possible explanation for these oscillations is that the impact causes a shockwave to propagate through the impactor. The wave would reflect of the ends and move up and down inside the impactor, resulting in oscillations in the force data. However, this hypothesis has not been confirmed, and the phenomenon has not been investigated in this study. The test XPS-700-049S (see Figure 4.10 a) shows oscillations uncharacteristic of the other experiments, the experiment was therefore repeated with a new specimen, and the data from the first test has not been used further.

Note that test “XPS-250-10”, i.e. XPS250 foam impacted without a front-plate at 10 m/s, exhibits a force history different from the other similar experiments. The measured force rises faster, and peaks at a higher value than the other experiments conducted at 10 m/s without a front-plate. This behavior is probably caused by the impactor punching through the foam, see the Figure bellow (Figure 4.5).

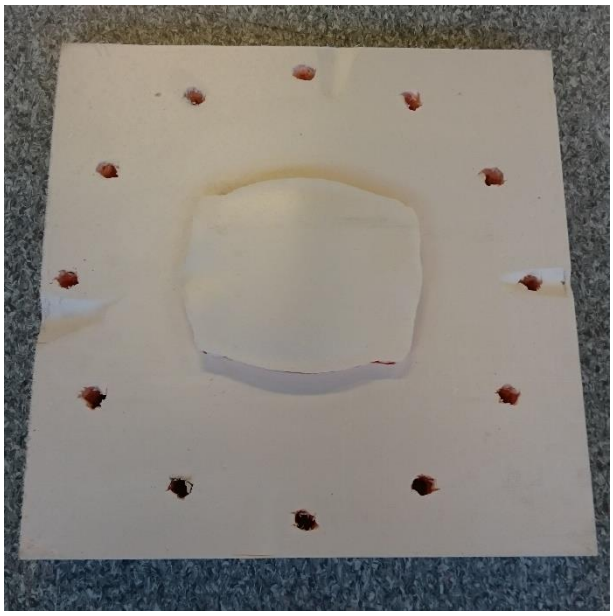

*Figure 4.5: Backside of foam specimen XPS-250-10*

It is interesting to compare the amount of energy absorbed by the specimens with respect to their core density. Such a comparison is shown in Figure 4.6 a-b. The results indicate that the amount of energy that is absorbed from the impact is independent of the foam density. However, when the energy absorption is compared against the experiments done without a foam core (see 4.6 c), it is clear that the steel skins dominate the energy absorption, especially at lower velocities. This fits well with visual observation of the foam core specimens after impact (see Figures 4.11-4.16). The specimens that experienced the lowest velocity impact exhibit little to non plastic deformations for all three foam densities. As the impact velocity was increased, the visible plastic deformations in the foam also increased. This indicating that more energy was absorbed by the foam, as suggested by the increasing distance between the "no foam core" line and the other lines in Figure 4.6 c. The amount of plastic deformation on the specimens gets lower as the density increases. This is as expected given the increase in stiffness and plateau stress in higher density foam.

Another interesting observation is that components with front plates appears to absorb nearly the same amount of energy as components without front plates, although the deformation characteristics are significantly different. The impact tests done without a front plate exhibits large plastic deformations surrounded by significant fractures, localized to the impacted area (see Figure 4.7). When a front plate is present, the loading is spread out on a larger area, and no fractures are visible.

The main findings from the drop tower experimental program can be summarized as follows:

- All the test shows oscillations in the force measurements – probably caused by stress waves
- The steel skins dominate the energy absorption for lower impact velocities
- The amount of absorbed energy appear to be independent of the foam density for low-velocity impacts
- Removing the front plate have no significant effect on the amount of energy absorbed although the failure modes change significantly

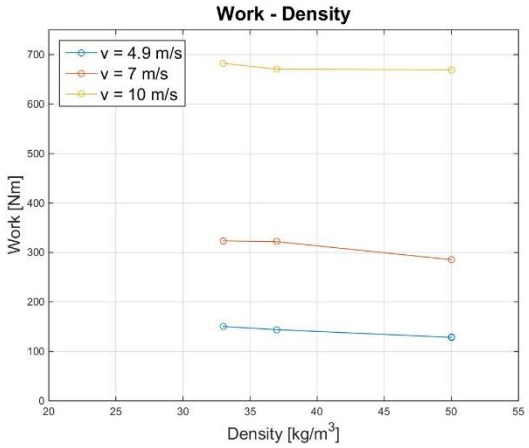


*a) With a front plate*

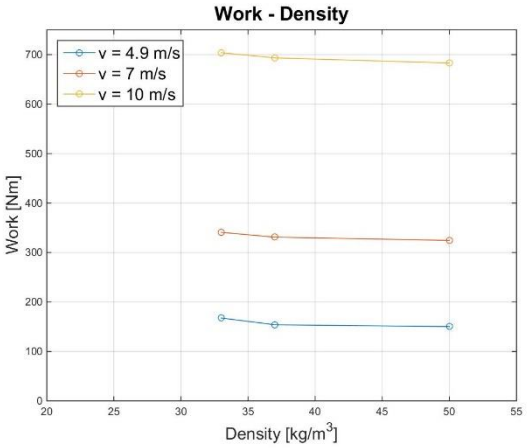


*b) Without a front plate*

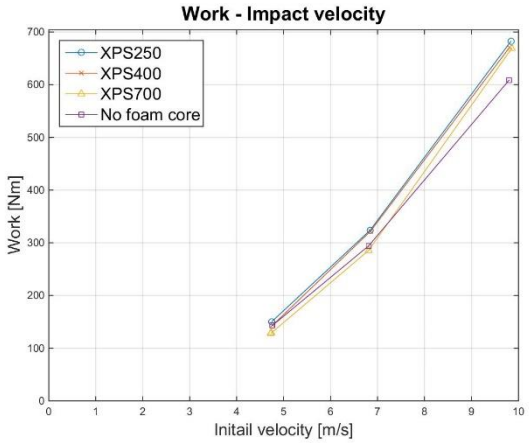


*c) With a front plate*

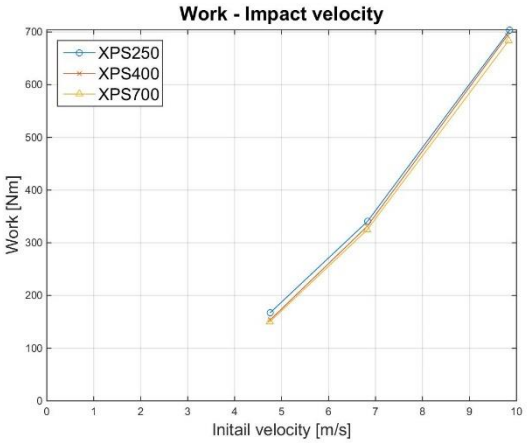


*d) Without a front plate*

*Figure 4.6: a)-b) Absorbed energy vs. foam density, c)-d) Absorbed energy vs. initial velocity*


*a) With a front plate (XPS-250-07S)*

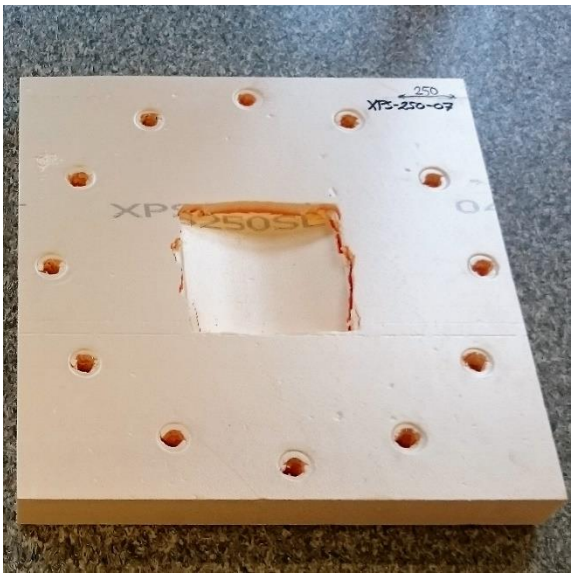

*b) Without a front plate (XPS-250-07)*

*Figure 4.7: XPS250 foam subjected to impacts at 7 m/s*

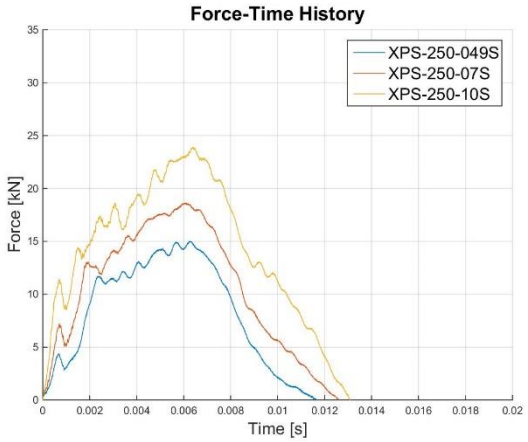


*a) Force vs. time for XPS250 with a front plate*

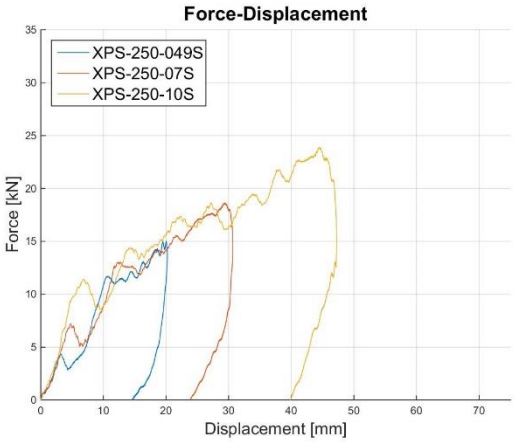


*b) Force vs. displacement for XPS250 with a front plate*

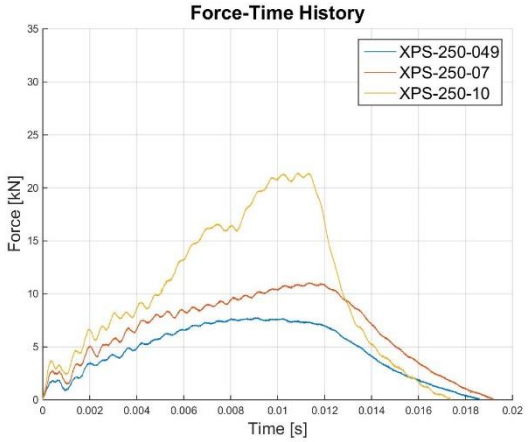


*c) Force vs. time for XPS250 without a front plate*

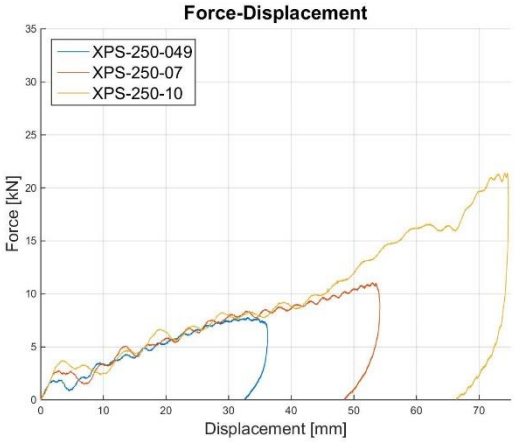


*d) Force vs. displacement for XPS250 without a front plate*

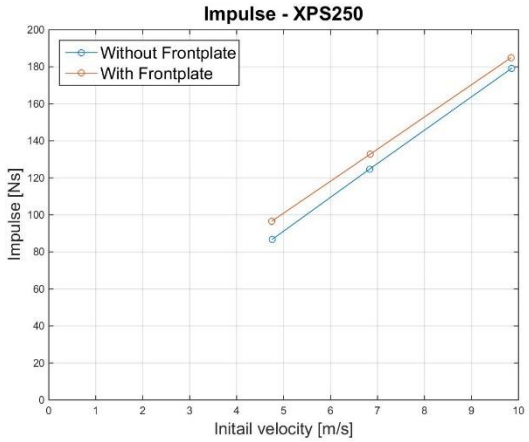


*e) Impulse for different initial velocities*

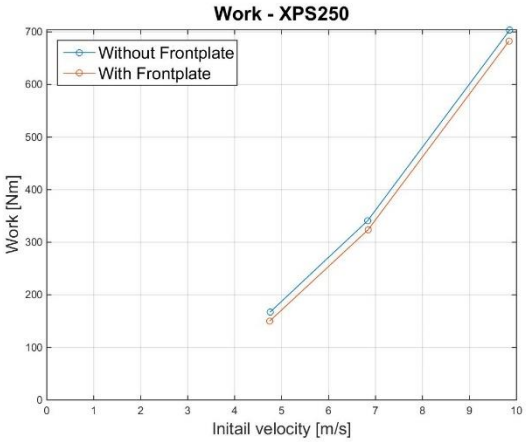


*f) Work done by the component for different initial velocities*

*Figure 4.8: Experimental results for XPS250*

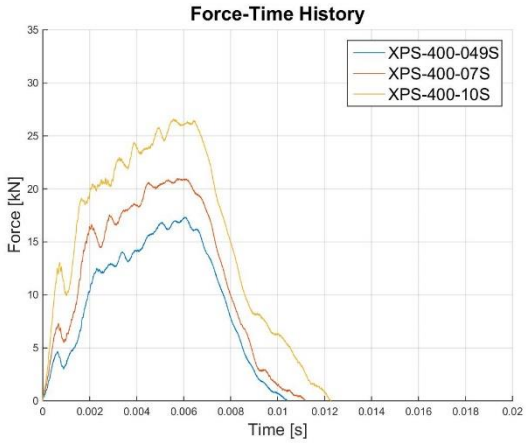


*a) Force vs. time for XPS400 with a front plate*

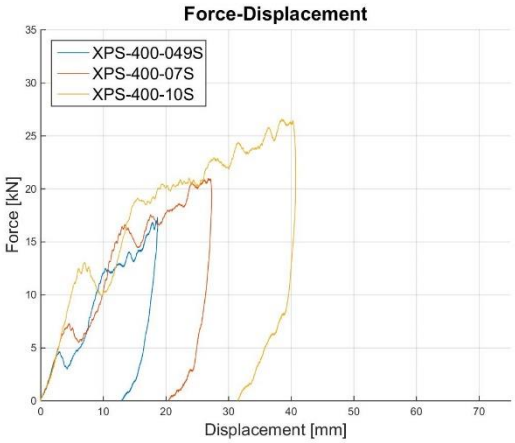


*b) Force vs. displacement for XPS400 with a front plate*

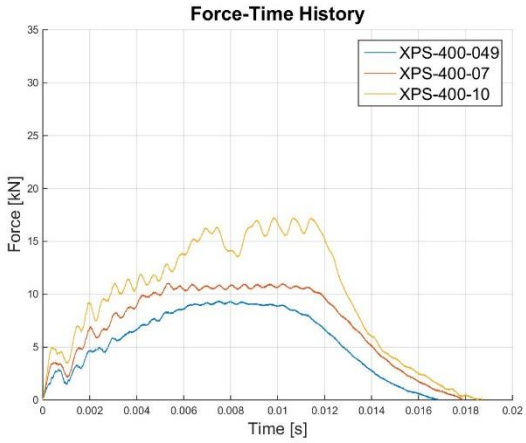


*c) Force vs. time for XPS400 without a front plate*

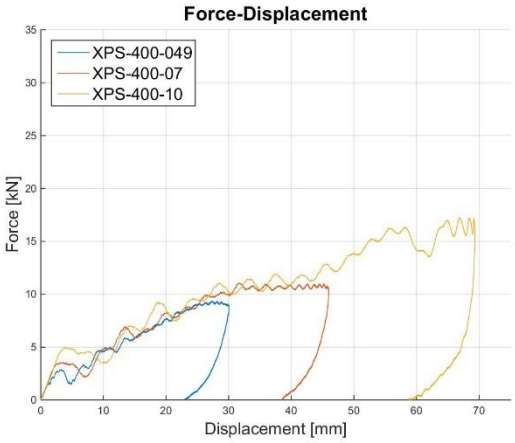


*d) Force vs. displacement for XPS400 without a front plate*

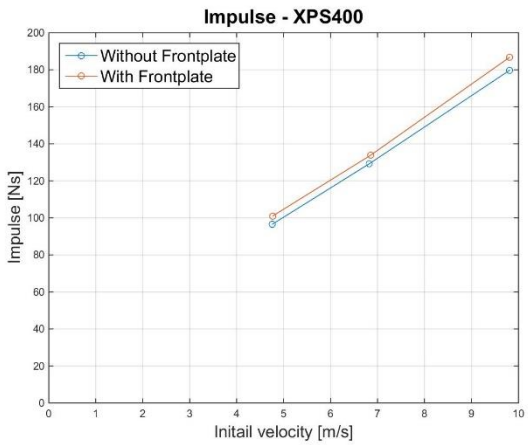


*e) Impulse for different initial velocities*

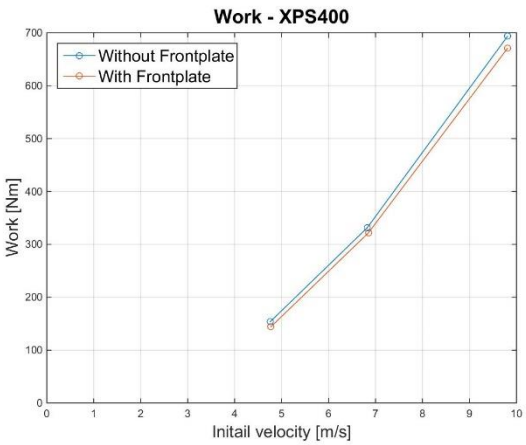


*f) Work done by the component for different initial velocities*

*Figure 4.9: Experimental results for XPS400*

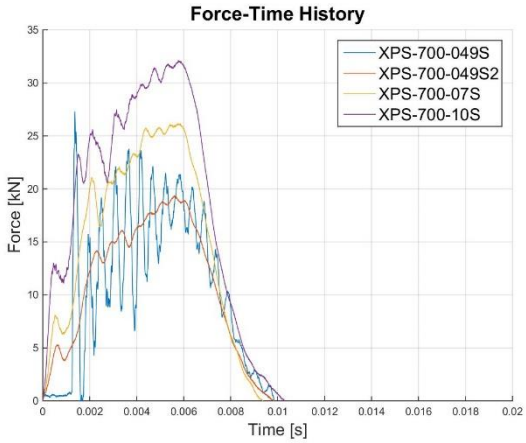


*a) Force vs. time for XPS700 with a front plate*

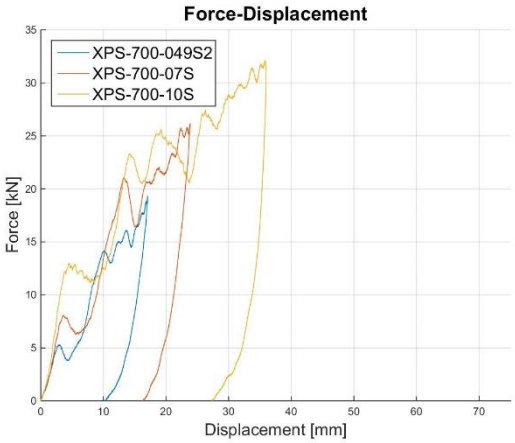


*b) Force vs. displacement for XPS700 with a front plate*

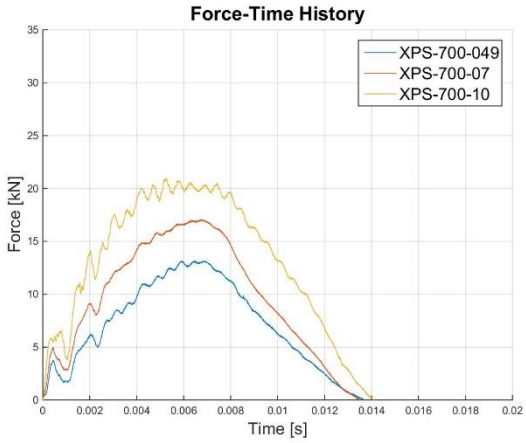


*c) Force vs. time for XPS700 without a front plate*

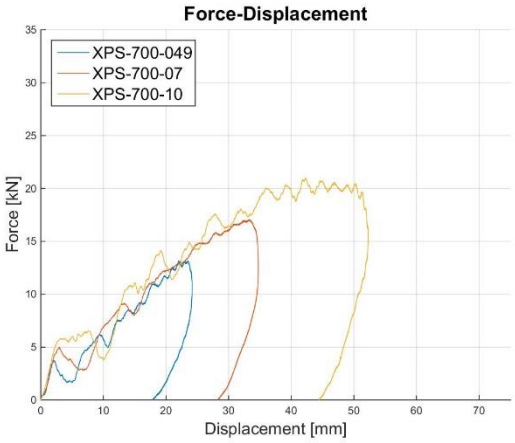


*d) Force vs. displacement for XPS700 without a front plate*

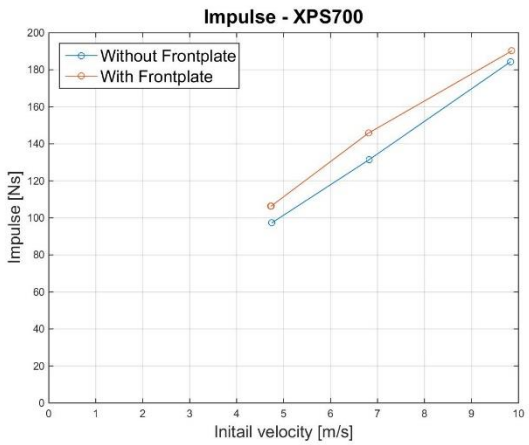


*e) Impulse for different initial velocities*

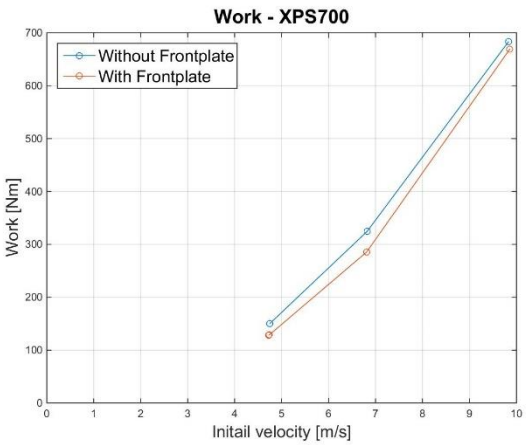


*f) Work done by the component for different initial velocities*

*Figure 4.10: Experimental results for XPS700*


*a) XPS-250* *b) XPS-400* *c) XPS-700*

*Figure 4.11: Impact at v = 4.9 m/s with a front-plate*

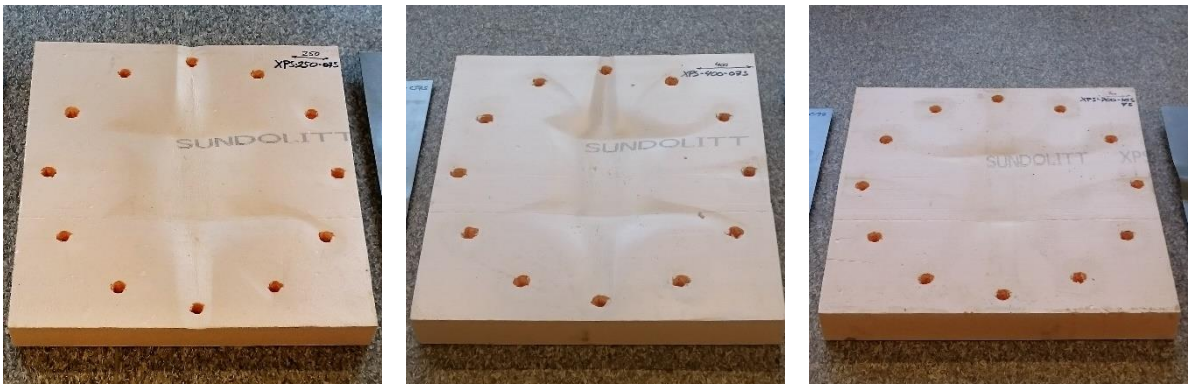


*a) XPS-250* *b) XPS-400* *c) XPS-700*

*Figure 4.12: Impact at v = 7.0 m/s with a front-plate*

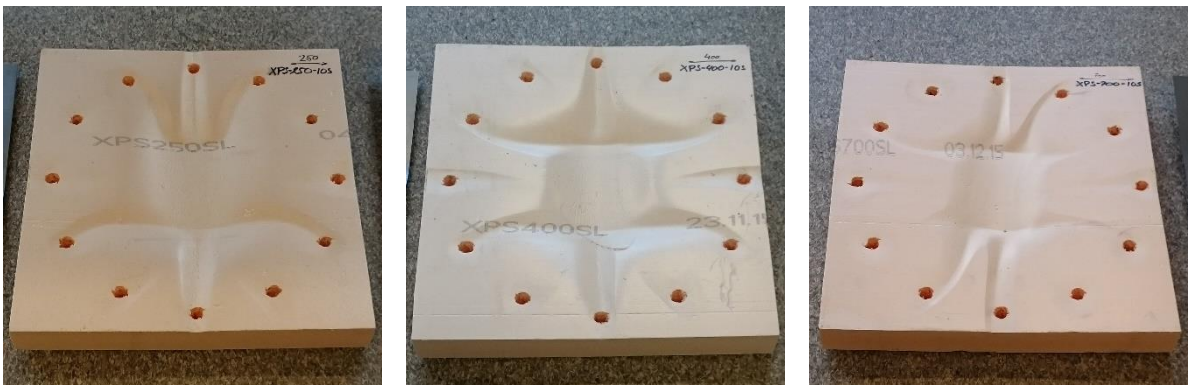


*a) XPS-250* *b) XPS-400* *c) XPS-700*

*Figure 4.13: Impact at v = 10.0 m/s with a front-plate*

*a) XPS-250* *b) XPS-400* *c) XPS-700*

*Figure 4.14: Impact at v = 4.9 m/s without a front-plate*

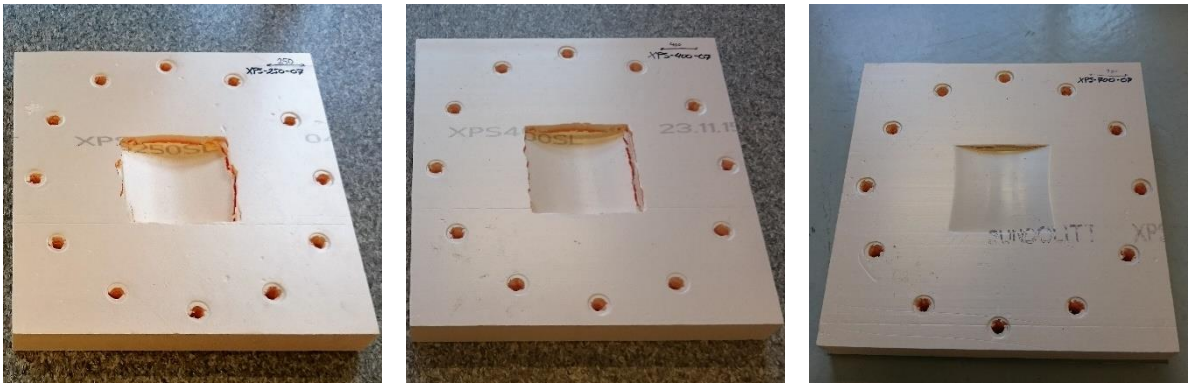

*a) XPS-250* *b) XPS-400* *c) XPS-700*

*Figure 4.15: Impact at v = 7.0 m/s without a front-plate*

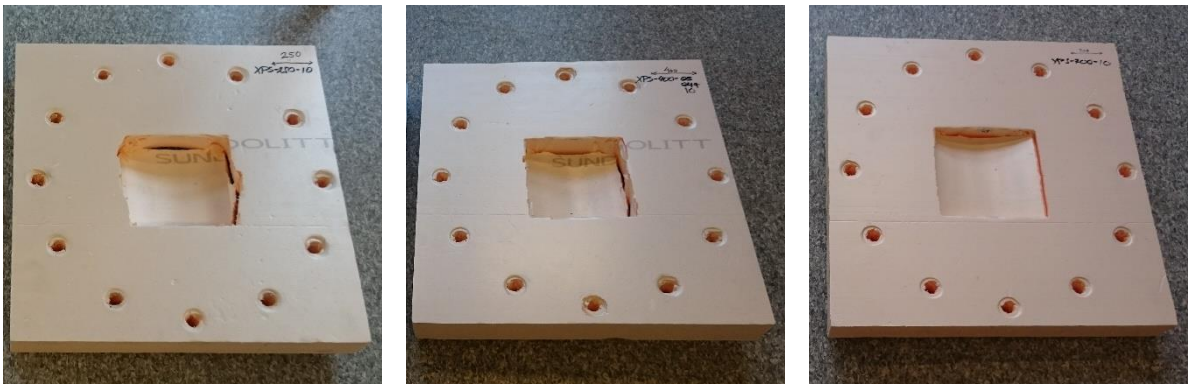

*a) XPS-250* *b) XPS-400* *c) XPS-700*

*Figure 4.16: Impact at v = 10.0 m/s without a front-plate*

## 4.3 SHOCK TUBE

Due to shock tube tests being more comprehensive than drop tower test, it was decided to limit the test program to only five tests and one foam density. It was the chosen to keep the foam density constant, and focus on different load magnitude. Therefore a sandwich configuration with XPS250 foam core were to three different load cases. Further, to study the effect of the front plate, one test was repeated with only a back plate. The skins were also tested without a foam core. The test program is summarized in Table 4.3.

*Table 4.3: Experimental program for the shock tube*

| *Name* | *Core material* | *Foam density [kg/m$^3$]* | *Front plate?* | *Driver Pressure* |
|---|---|---|---|---|
| **D600-60** | - | - | - | 60 |
| **XPS250S-35** | XPS-250 | 33 | YES | 35 |
| **XPS250S-60** | XPS-250 | 33 | YES | 60 |
| **XPS250S-75** | XPS-250 | 33 | YES | 75 |
| **XPS250-35** | XPS-250 | 33 | NO | 35 |

### 4.3.1 Test Set-up

The test specimens were pre drilled with 24 bolt holes as shown in Figure 4.18. To emulate fixed boundary condition, the plates were clamped to the end of the driven section using a clamping-plate and 12 bolts. When the specimens are clamped, only a 300 mm x 300 mm section is exposed to the shockwave. It should be noted that the compressibility of the foam limited the tautness of the bolts, as well as it made it challenging to tighten the bolts equally.

Pressure sensors placed along the driven section are used to measure the shockwave as it propagates down stream of the driver section. Two of the sensors (no. 409 and no. 410) are placed close to the test specimen. These two sensors are important in order to estimate the peak pressure acting on the test specimens. Two Phantom v1610 high-speed cameras were used to capture the structural response of the backside of the specimen. The cameras recording rate was set to 24kHz for all the experiments.

*Figure 4.16: Specimen bolted in place*

*Figure 4.17 Camera set up*

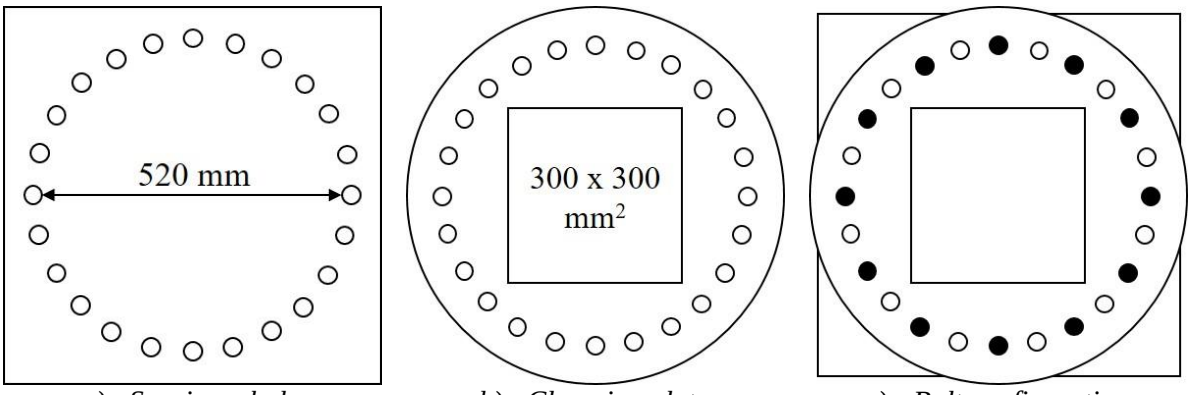


*a) Specimen hole configuration*

*b) Clamping plate*

*c) Bolt configuration*

*Figure 4.18 Clamping of the specimen*

### 4.3.2 Data Processing

Since there are no pressure sensors at the specimen during experiments, the pressure history needs to be estimated based on measurements from sensor 409 and 410, located in front of the test specimen. In order to do this, it is necessary to know when the pressure wave reaches the specimen. The time of impact with the specimen, $t_w$, is calculated from the known geometry of the sensor layout (se Figure 4.20). The time it takes the shockwave to propagate from sensor 409 to 410, $\Delta t$, can be found directly from the pressure data. Since the distance between the sensors are known, the incident wave velocity, $v_s$, can be approximated. Further,

if the wave velocity is assumed to be constant, the time it takes the wave to propagate the known distance from sensor 410 to the specimen can be calculated.

To estimate the reflected peak pressure, it is necessary to fit the pressure data to an analytical expression and extrapolate the fit to the time $t_w$. This is typically done using the modified Friedlander equation (eq. 2.1). The duration of the positive phase, $t_+$, can be taken directly from the data, while the reflected peak pressure, $P_r$, and the decay coefficient, $b$, is found by curve fitting, using MATLAB [47]. However, one of the limitations of using a shock tube is that a high driver pressure can cause secondary and tertiary reflections during the positive phase (see Figure 2.8). This introduces a problem when it comes to fitting the test data to the Friedlander equation. In the current work, the peak reflected overpressure, $P_r$, was found by fitting the Friedlander equation to the experimental data before the secondary reflections occurred. The decay coefficient, $b$, was then found such that the specific impulse based on the Friedlander equation (eq. 2.2) matched the specific impulse calculated from the measured pressure history of sensor 410. This approach was selected to give a conservative estimate of the reflected peak pressure.

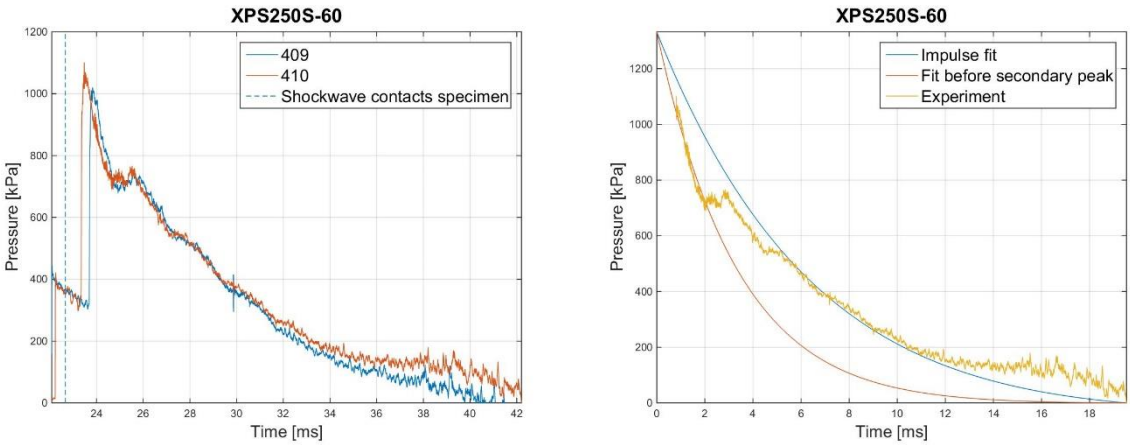


a) *Positive phase of the measured pressure history*

b) *Friedlander fit and extrapolation to the pressure history*

*Figure 4.19 Identification of the Friedlander parameters for a typical test*

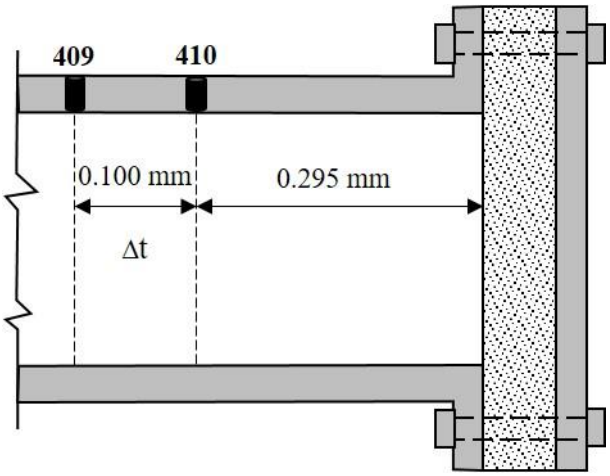


*Figure 4.20 Layout of sensor 409 and 410*

### 4.3.3 Experimental results

The results from the shock tube experiments are given in the form of a Friedlander equation (eq 2.1) fitted to the pressure history acting on the specimen, and the deflection of the back plate. Ideally the test specimens should have been bisected and measured after the experiments so that the compression of the foam could be compared to the numerical analyses explained in chapter 5. However that was not done in the current work. The results from the Friedlander fitting and the maximum displacement of the back-plate is given in the table below (Table 4.4).

*Table 4.4: Experimental results*

| Name | Driver Pressure [bar] | $Pr$ [kPa] | $b$ [-] | $t_+$ [ms] | $i_+$ [kPa x ms] | $u_{max}$ [mm] |
|---|---|---|---|---|---|---|
| **D600-60** | 60 | 1362 | 1.272 | 48.8 | 15436.7 | 26.8 |
| **XPS250S-35** | 35 | 1100 | 1.653 | 15.8 | 3617.0 | 24.5 |
| **XPS250S-60** | 60 | 1332 | 2.190 | 19.5 | 4250.2 | 29.8 |
| **XPS250S-75** | 75 | 1767 | 2.591 | 18.0 | 4123.5 | 37.2 |
| **XPS250-35** | 35 | 935 | 1.460 | 20.8 | 6147.3 | 37.9 |

The image series of the experiments, captured by the high-speed cameras, shows the response of the back plate of the sandwich component. By post processing these images with the 3D DIC software Ecorr [35], it was possible to extract the displacement fields. The results are

illustrated by a series of three plots, plotted at three different time steps, for each experiment (Figures 4.22 – 4.26). At each time step the following is plotted:

a) A 3D contour plot of the deflection (taken from Ecorr), the color bar is in mm
b) The synchronized pressure and displacement history, where the pressure is captured by sensor 410 and the displacement is taken from the node exhibiting the maximum displacement
c) The displacement over the cross section

The time steps where chosen such that they give a snapshot at three different stages of the deformation history. The first time step shows the plate as it has just started deforming, while the third time step shows the plate as it reaches a maximum displacement. The second time step is an intermediate stage between these two.

To protect the camera windows in the dump tank, a sheet of plexiglass is attach in front of the windows using magnets. In some of the experiments (XPS250S_60 and XPS250_75), pressure leakage into the dump tank caused the plexiglass to flex during the experiments. This resulted in a warping of the images captured, which caused the DIC analysis to diverge and thereby giving incomplete results. This can be seen in Figure 4.24 b) and Figure 4.25 b), where the displacement curve is cut off. However, this is of no major concern as the first part of the DIC analyses, where the deformation occurs, is unaffected.

Both a sandwich component and two steel skins alone (no foam core) were tested with a driver pressure of 60 bar. It is quite interesting to compare the results from these two experiments (D600_60 and XPS250_60). The component with a foam core exhibits a larger maximum displacement of the back-plate than the component without foam. Further, if we compare the 3D contour plots and the cross section plots at maximum deflection (Figure 4.22 a and Figure4.24 a), it is clear that the component with a foam core exhibits a wider and more extensive displacement field. These findings indicate that the FSI (Fluid Structure Interaction) effects change significantly when a foam core is present.

With a driver pressure of 35 bar, the sandwich was tested both with and without a front-plate (XPS250S_35 and XPS250_35 respectively). As expected, the deformation are significantly higher when no front-plate is present.

It should be noted that all the components survived the experiments i.e. stayed in one piece within the loaded area, and exhibited no penetrations. There were no fracturing observed in

the middle section of the foam specimens with the exception of specimen XPS250_35 i.e. the experiment without a front-plate (Figure 4.21 a). This fracture probably occurred as the specimen was sucked into the driven section during the negative phase. Fractures of varying extent was however observed outside the bolts on all the experiments (see Figure 4.21).

The main findings in the experimental program can by summarized by the following:

- A foam core appears to increase the deformation of the back-plate
- Fracturing of the foam is limited to the boundary condition, no fractures visible within the loaded section
- Significant plastic deformation in the foam indicate significant energy absorption

*a) No front plate a 35 bar driver pressure*

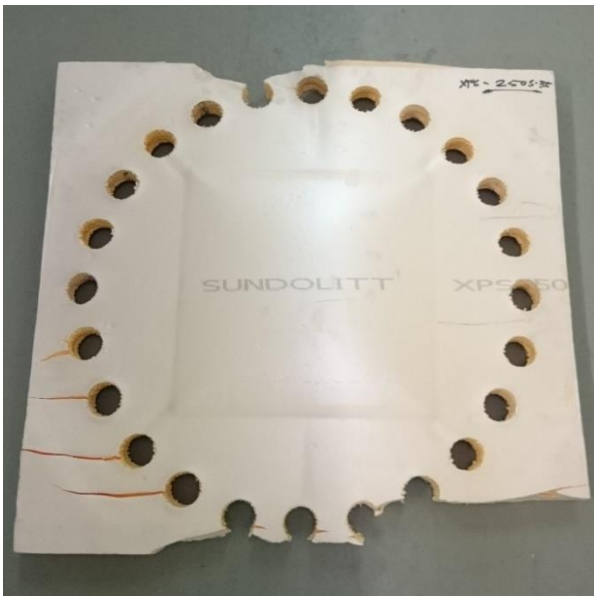


*b) Sandwich at 35 bar driver pressure*

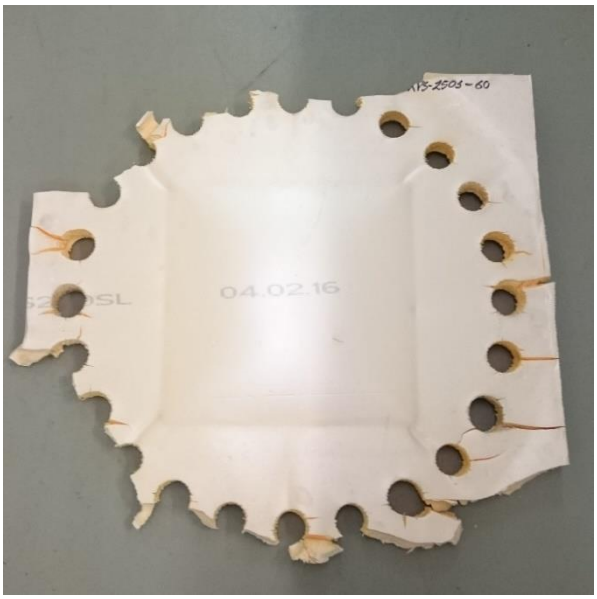


*c) Sandwich at 60 bar driver pressure*

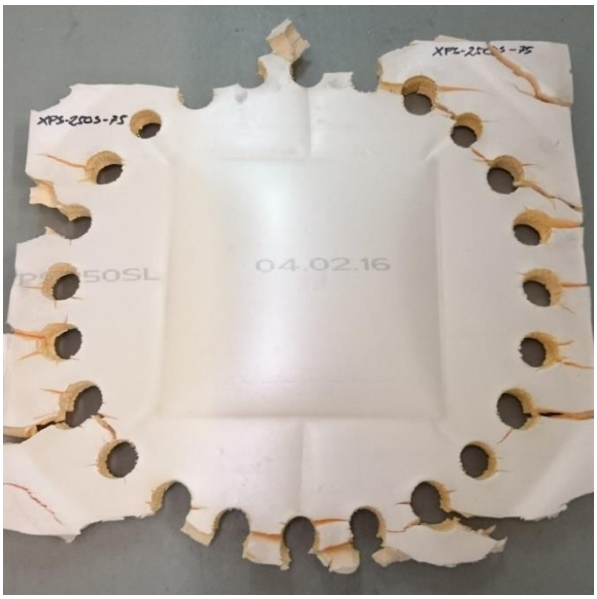


*d) Sandwich at 75 bar driver pressure*

*Figure 4.21: Foam after deformation in the shock tube*

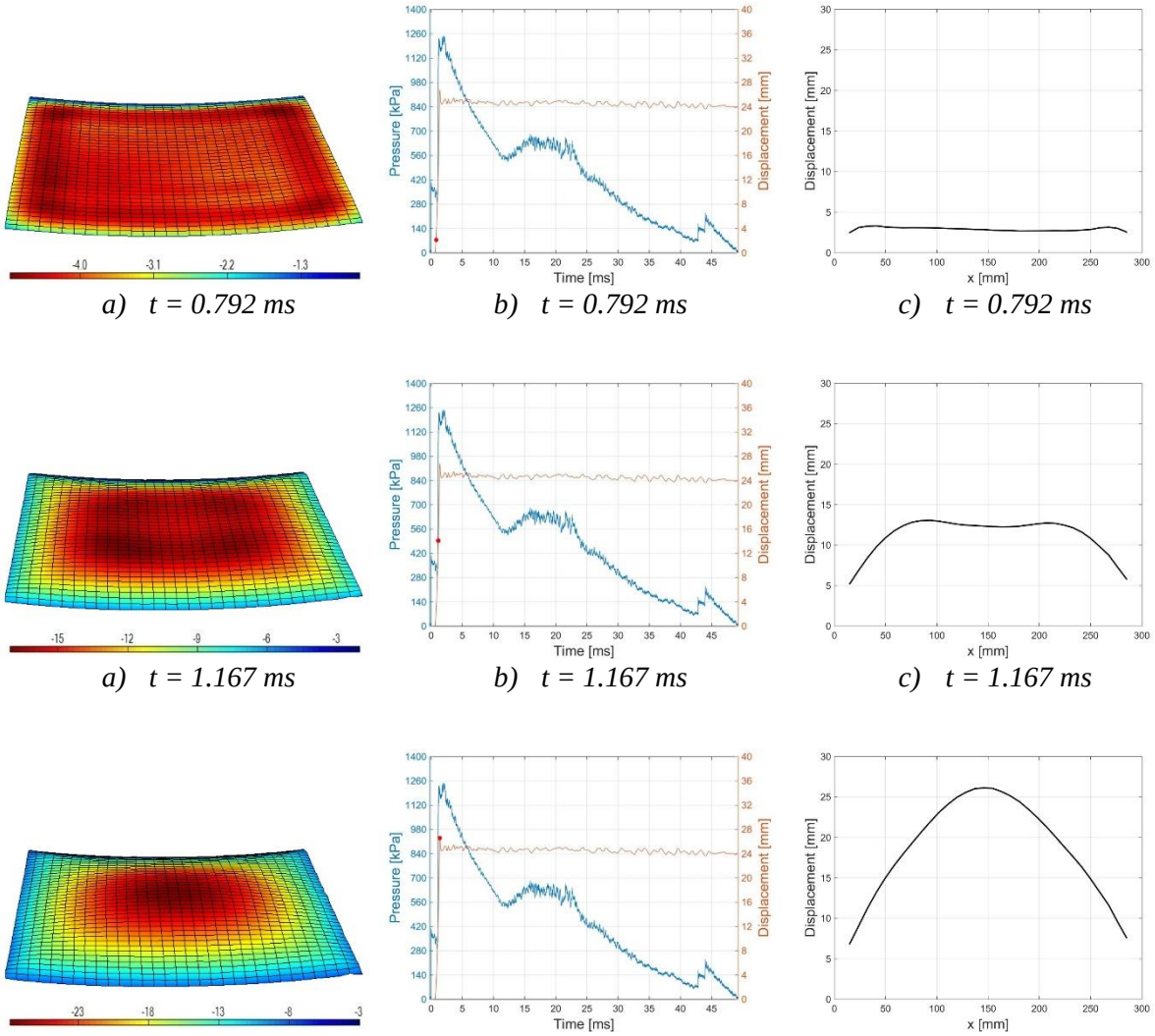


*a) t = 0.792 ms* *b) t = 0.792 ms* *c) t = 0.792 ms*

*a) t = 1.167 ms* *b) t = 1.167 ms* *c) t = 1.167 ms*

*a) t = 1.417 ms* *b) t = 1.417 ms* *c) t = 1.417 ms*

*Figure 4.22: Back-plate response of D600_60*

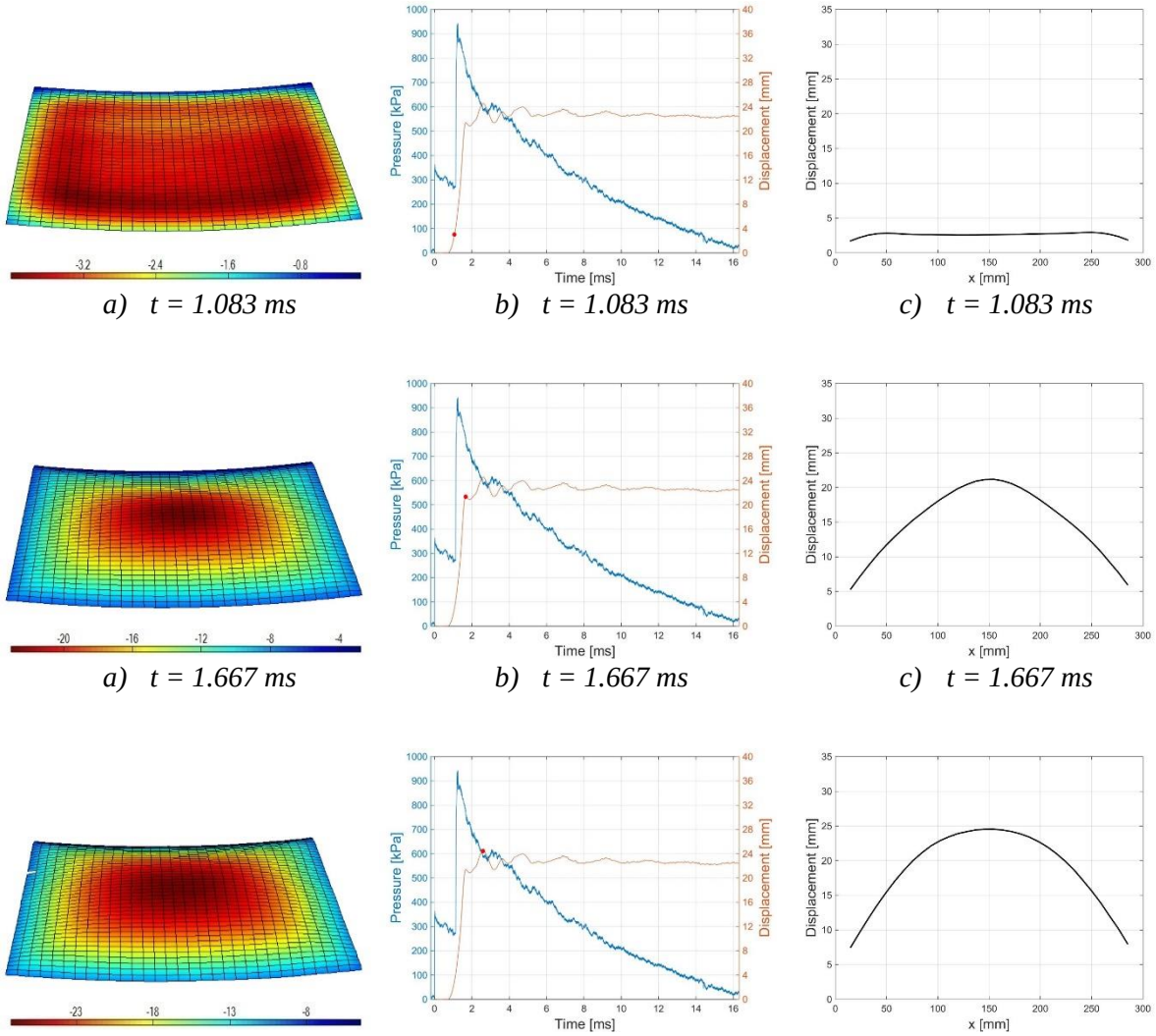


*a) t = 1.083 ms* *b) t = 1.083 ms* *c) t = 1.083 ms*

*a) t = 1.667 ms* *b) t = 1.667 ms* *c) t = 1.667 ms*

*a) t = 2.625 ms* *b) t = 2.625 ms* *c) t = 2.625 ms*

*Figure 4.23: Back-plate response of XPS250S_35*

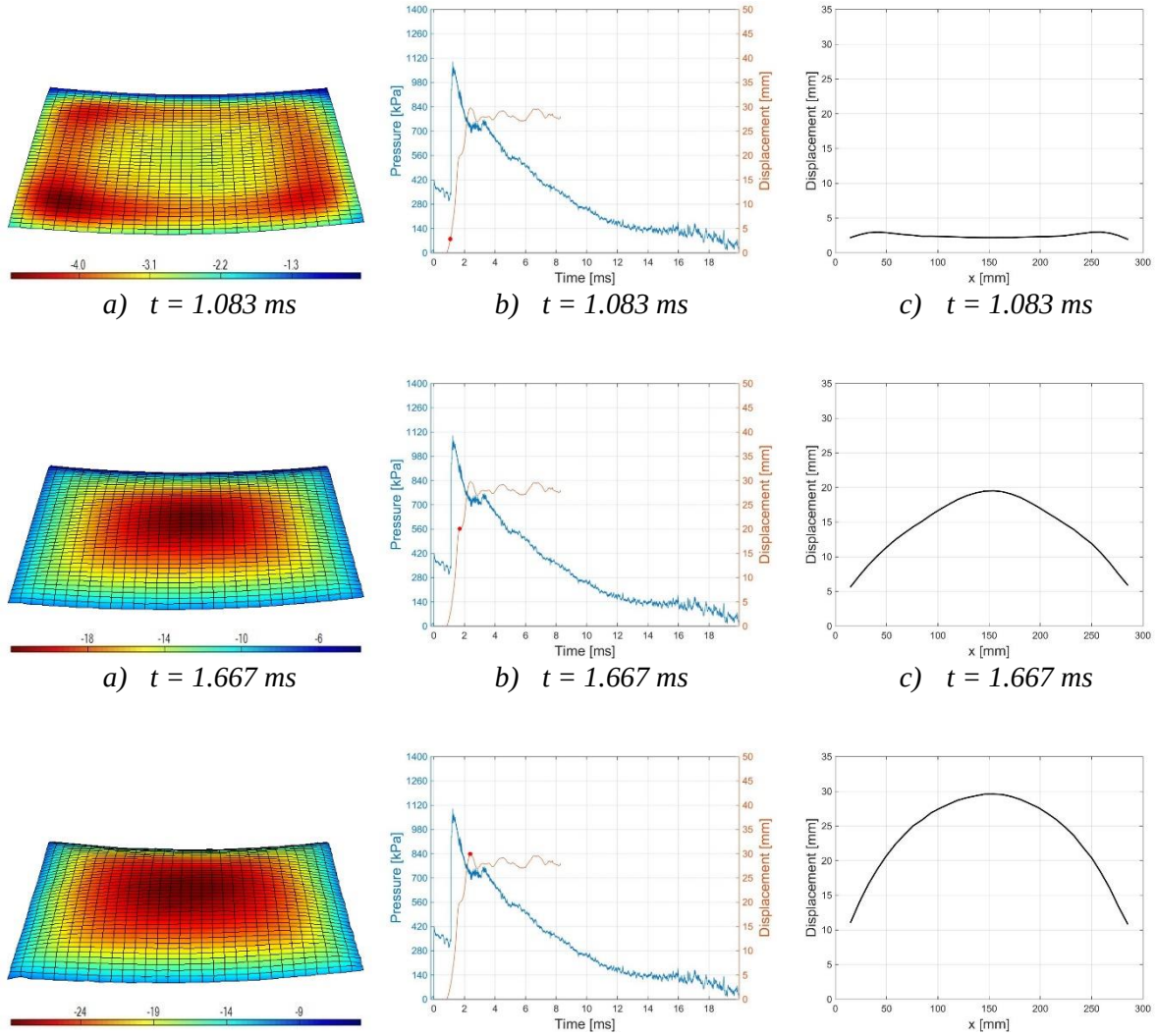


*a) t = 1.083 ms* *b) t = 1.083 ms* *c) t = 1.083 ms*

*a) t = 1.667 ms* *b) t = 1.667 ms* *c) t = 1.667 ms*

*a) t = 2.417 ms* *b) t = 2.417 ms* *c) t = 2.417 ms*

*Figure 4.24: Back-plate response of XPS250S_60*

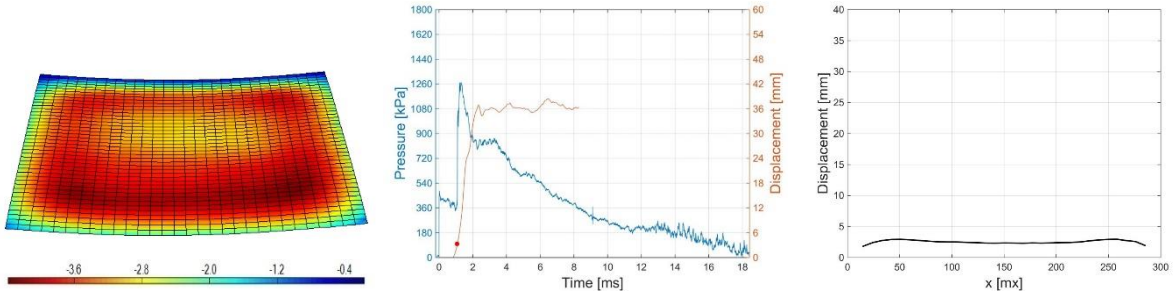


*a) t = 1.083 ms* *b) t = 1.083 ms* *c) t = 1.083 ms*

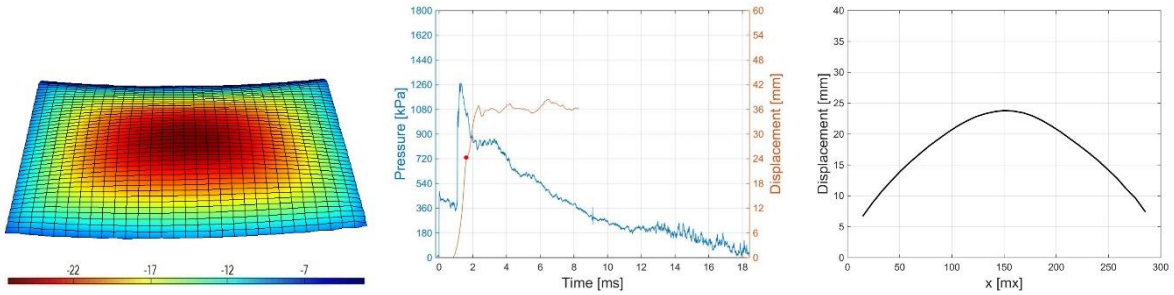


*a) t = 1.667 ms* *b) t = 1.667 ms* *c) t = 1.667 ms*

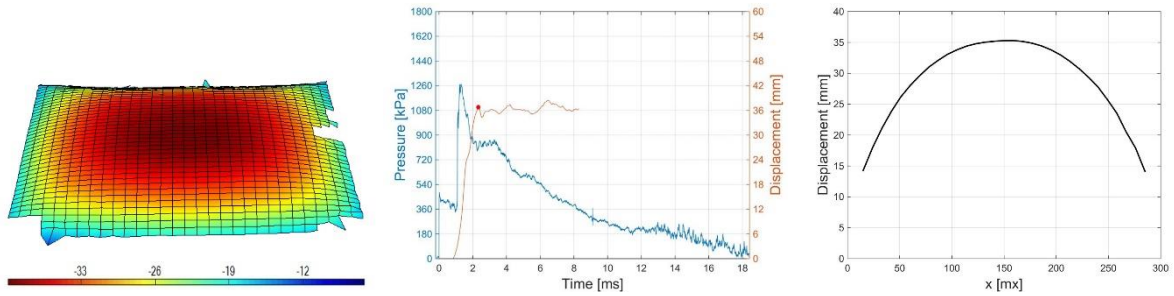


*a) t = 2.334 ms* *b) t = 2.334 ms* *c) t = 2.334 ms*

*Figure 4.25: Back-plate response of XPS250S_75*

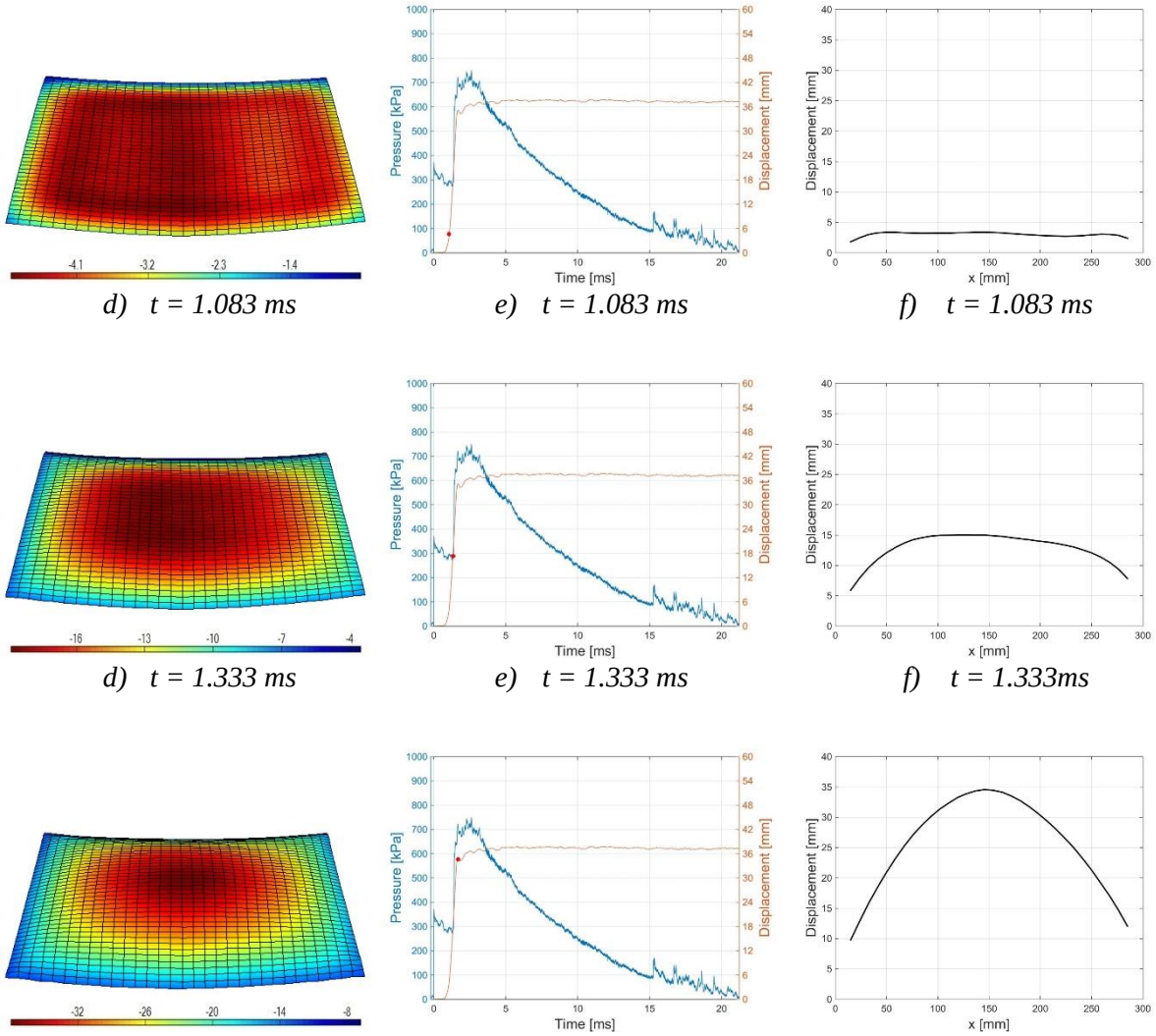


*d) t = 1.083 ms* *e) t = 1.083 ms* *f) t = 1.083 ms*

*d) t = 1.333 ms* *e) t = 1.333 ms* *f) t = 1.333ms*

*d) t = 1.833 ms* *e) t = 1.833 ms* *f) t = 1.833 ms*

*Figure 4.26: Back-plate response of XPS250_35*

# 5 NUMERICAL STUDY

## 5.1 INTRODUCTION

Performing a numerical study in addition to experiments introduces several advantages. For one thing, numerical studies are far more cost effective than physical experiments. Further, numerical simulations makes it is easier to perform a comprehensive parametric study in witch specific and localized effects can be studied. Normally experimental work is limited to small scale testing, while numerical simulations can be applied in full scale. To gain confidence in the results that are found numerically, it is important to validate the models with experimental data. For complex problems, a numerical study might also help to validate the experimental data gathered.

To further study the response of the sandwich configuration, and to evaluate the models assumed for the material, both the drop tower and the shock tube experiments was modelled numerically using the commercially available explicit FE code LS DYNA [51]. All the analyses presented was performed on the computational cluster "Snurre" available through the department of structural engineering at NTNU. In the following sections the numerical study is outlined.

## 5.2 DROP TOWER

The experiments performed on the sandwich configuration in the drop tower rig, were simulated numerically in LS DYNA. The numerical results were then compared to the experimental results. A tailor made model (basis model) of the test set up was used in the analyses. A penalty based surface to surface contact algorithm is used for all the models, and friction has not been properly accounted for i.e. static and dynamic coefficient of friction is set to 0.1 for all contact formulations. The sensitivity of the model and the analysis input parameters has not been studied with the exception of a sensitivity study of the foam density and the foam thickness. The analysis model has not been calibrated to the experimental results, and all results presented in the current work is based on the basis model. Typical parameters that could be applied to optimize the model are; boundary conditions, friction,

mesh size and element type, strain-rate sensitive material model and variation of material properties throughout the test specimen.

### 5.2.1 Model and approach

Due to double symmetry, only a quarter of the tested plates were modelled. The boundary conditions in the experiment were simulated by rigid parts and elastic steel bolts. The impactor, also modelled as a quarter of the real size, was modelled by shell elements with rigid material properties. Some of the sharp corners were rounded to prevent numerical problems. Since only the part of the striker rig that impacts the specimen was modelled, the mass of the rest of the rig needed to be accounted for. This was done by increasing the density of the impactor. All of the analyses are based on nominal values for the geometry e.g. thickness of both the foam and the steel skins. Loading was applied similarly as in the experiments, i.e. by giving the impactor an initial velocity. To investigate the steel skins alone, the model was modified by removing the foam core and shortening the bolts. Both models are shown in Figure 5.1. Figure 5.2 – 5.3 shows the typical behavior of the numerical models during simulations.

The 0.8 mm thick Docol600DL steel plates was modelled by four-node Lagrangian shell elements and the Belytschko-Tsay element formulation was utilized [52]. The elements have five integration points through the thickness. The applied material model for the steel plates is based on the modified Johnsen-Cook material model, material *107 in LS DYNA, using the material parameters given in chapter 3.

The foam core is modelled with eight-node three-dimensional constant stress solid elements. 20 elements are used through the thickness of the foam. The foam material is represented with the Deshpande-Fleck material model, material *154 in LS DYNA, using the material parameters derived in chapter 3, and analytical derivation is activated in the analyses. Since the physical experiments on the sandwich components exhibited no visual fracture, no fracture criterion is introduced to the material model.

Impact problems are generally complex and difficult to predict numerically. The analysis results are very sensitive to some of the input parameters and some minor change in the input parameters might change the results significantly. Due to the complexity of such numerical simulations, there are several potential sources for uncertainties and error. However, these

have not been further addressed and investigated in the current work. A summary of uncertainties and possible error sources are listed below:

- Nominal geometry is used in the models
- Sharp edges on the impactor has been rounded
- There might be local variations in the foam material parameters due to mass production of the foam
- There is a thin plastic film on the surface of the foam that has been disregarded
- Friction is not properly accounted for – friction coefficient = 0.1 for all contact
- Strain-rate sensitivity of the foam material parameters
- The representation of the boundary conditions
- Complex contact interaction between a soft and stiff material
- The geometry is modelled as perfect i.e. no geometric irregularity

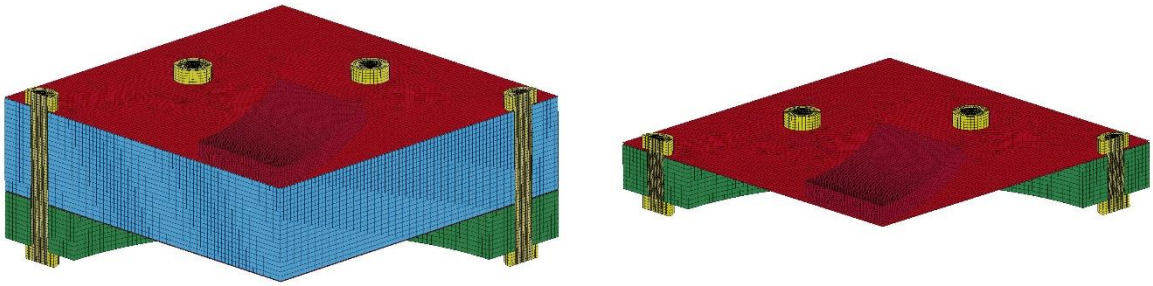

*a) Model of foam sandwich* *b) Model of steel skins alone*

*Figure 5.1: LS DYNA models of the drop tower experiments*

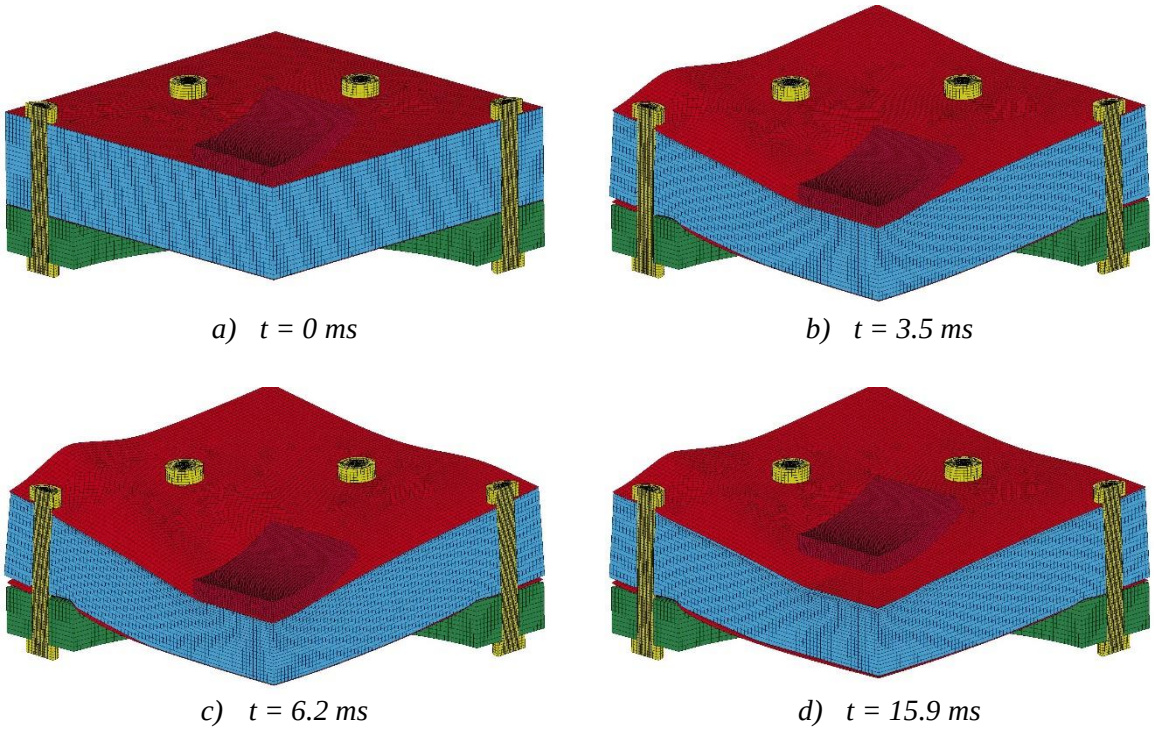

*a) t = 0 ms* *b) t = 3.5 ms*

*c) t = 6.2 ms* *d) t = 15.9 ms*

*Figure 5.2: Typical numerical simulation of foam sandwich in the drop tower*

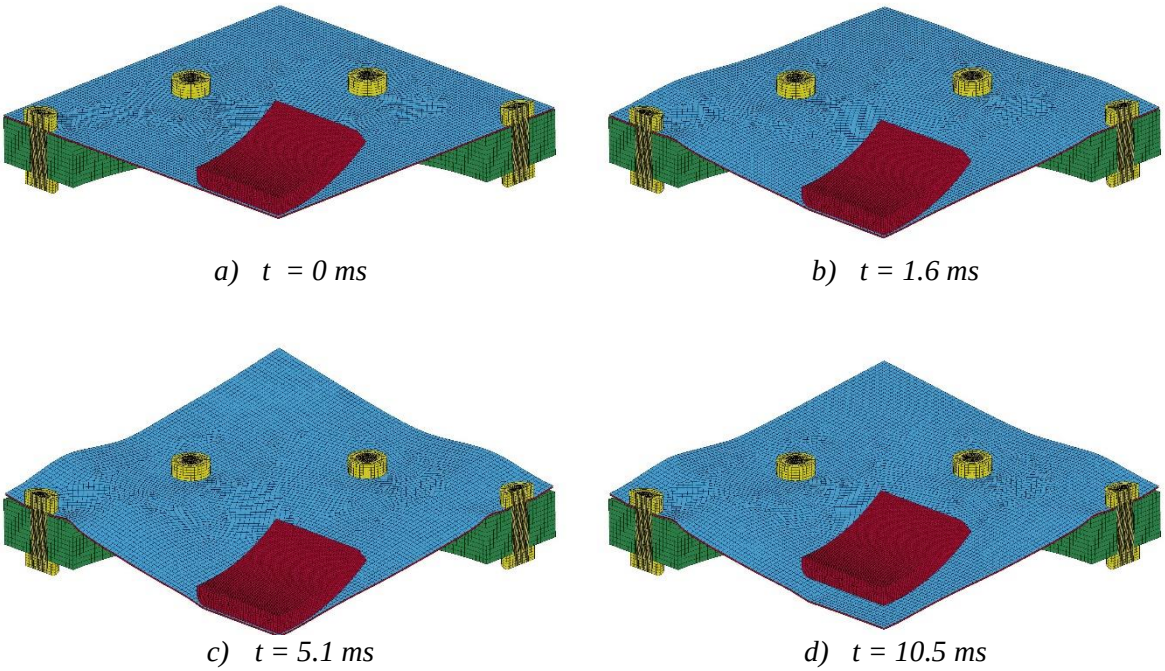

*a) t = 0 ms* *b) t = 1.6 ms*

*c) t = 5.1 ms* *d) t = 10.5 ms*

*Figure 5.3: Typical numerical simulation of only skins in the drop tower*

### 5.2.2 Numerical results

The sandwich experiments were recreated with numerical simulations using the corresponding nominal input parameters from the experiments. Hence, all the experiments have a corresponding numerical simulation. The velocity used in the simulations is the same as the one used as input parameter in the experimental test rig. Due to the location of the sensor that measures the velocity prior to impact, it is reasonable to expect the actual impact velocity to be slightly higher than the measured value. This fits well with the measured values consequently being slightly lower than the input velocity. The numerical results are extracted from the analyses in a similar manner as in the experiments i.e. the forces acting on the impactor, the displacement of the impactor and the change in kinetic energy of the impactor (absorbed energy).

It is not feasible to compare all details in the numerical analysis to the experimental results. Therefore only some main results are compared e.g. force-time history and displacement-time history as well as the impulse and absorbed energy. The comparisons of the impulse and absorbed energy are shown in Figures 5.4 - 5.6, while the force-time and displacement-time history are compared in Figures 5.7 - 5.10. The main observations are as follows:

***Steel skins without foam between:***

From the force-time and displacement-time plots in Figure 5.7, the difference between the numerical analyses and the experimental data appear to be significant, where only the first 2.5 ms is coinciding while the rest of the results differ significantly. Even though the work (absorbed energy) and the impulse is comparable in magnitude, see Figure 5.4 d, the peak forces are significantly higher and the time duration of the contact is significantly shorter in the numerical analyses. The reason for the observed differences is probably a combination of several factors, but it is expected that the modelling of the boundary conditions (too stiff in the numerical model), the lack of imperfections in the plates and the friction between the plates and between the impactor and plates, plays a significant role. Further, inaccuracy in the steel model may have influenced the results. It should be noted that the steel model material parameters are based on work by Holmen et al. [53], in which they performed perforation test on the same steel plates used for the skins in the current work. They observed higher peak forces in the numerical analyses compared to the experiments as well.

***Sandwich configuration:***

The calculated maximum displacement, impulse and work fits reasonably well with the test results for all velocities (within approx. ± 10%), see Figure 5.4 a-c. The peak force fits reasonably well for the lowest velocity impacts but differs significantly with increased velocity. The main reason for this could be that the material model used in the analysis does not include strain-rate dependency and the friction is not correctly modelled. It is also noted that the correlation between experiment and numerical analysis gets better for when the foam density is increased.

Considering the complexity of the problem, the overall observation is that the numerical simulation is able to predict the test results with reasonable accuracy. As mentioned earlier, no proper calibration of the numerical model has been performed. It is expected that much better agreement between the numerical simulation and the experimental results is possible to obtain by including proper contact formulation (friction) and by including strain-rate dependency in the foam material model.

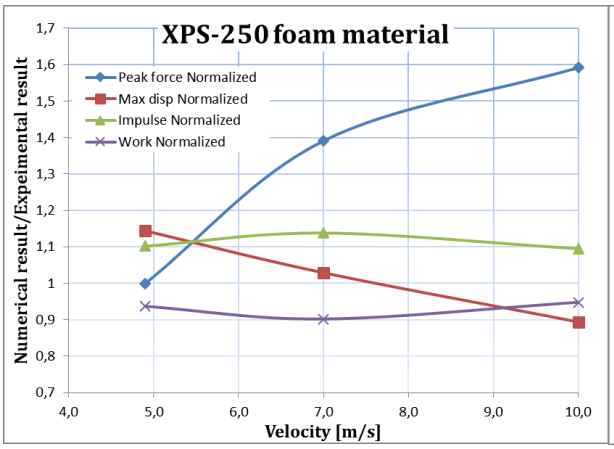


a) *Normalized results for XPS250 sandwich*

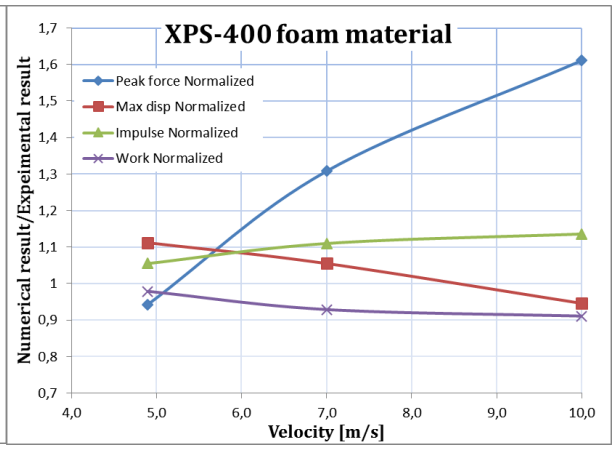


b) *Normalized results for XPS400 sandwich*

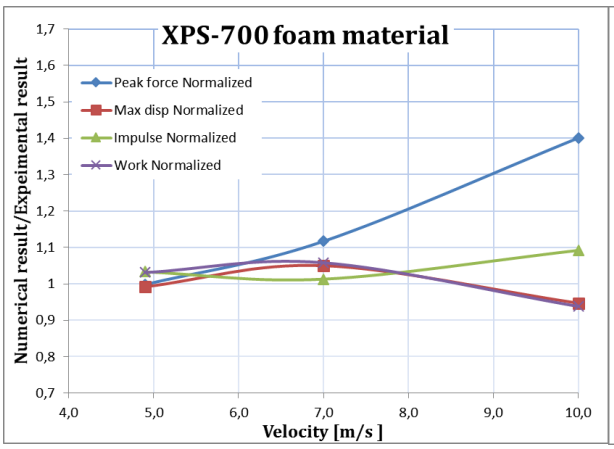


c) *Normalized results for XPS700 sandwich*

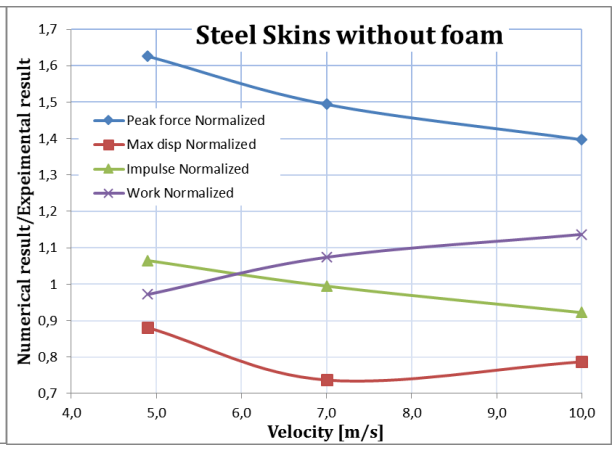


d) *Normalized results for the steel skins*

*Figure 5.4: Comparison of numerical and experimental results*

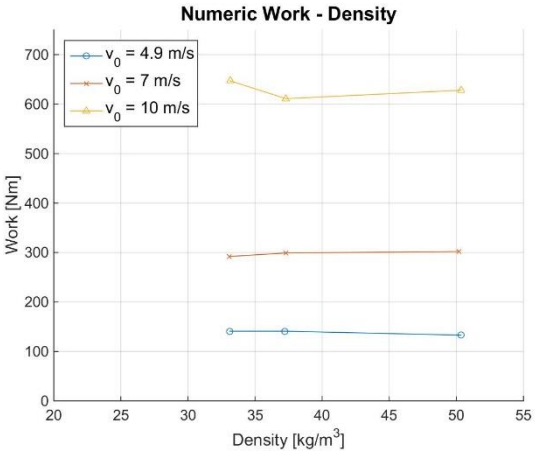


*a) Numerical energy absorption - density*

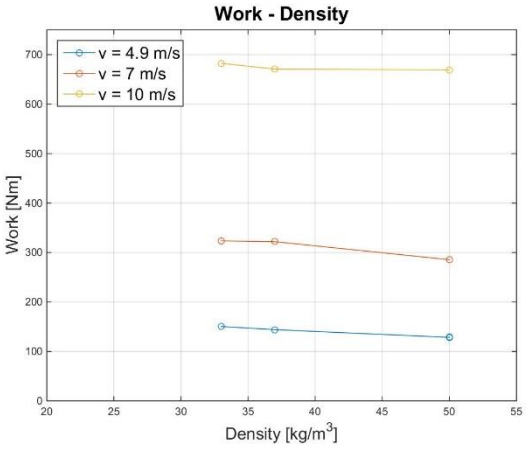


*b) Experimental energy absorption - density*

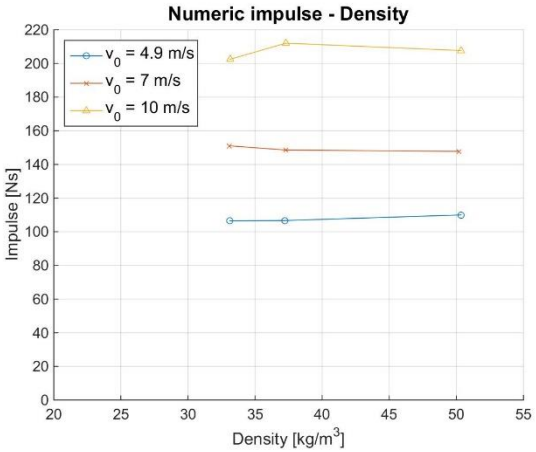


*c) Numerical impulse – foam density*

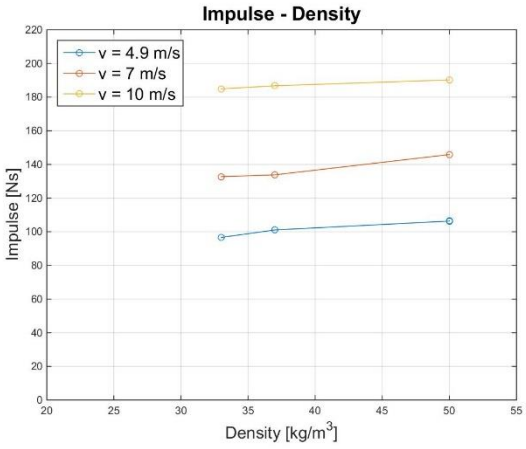


*d) Experimental impulse – foam density*

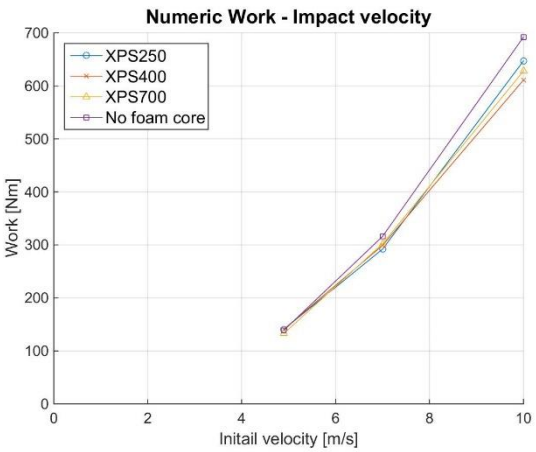


*e) Numerical energy absorption – impact velocity*

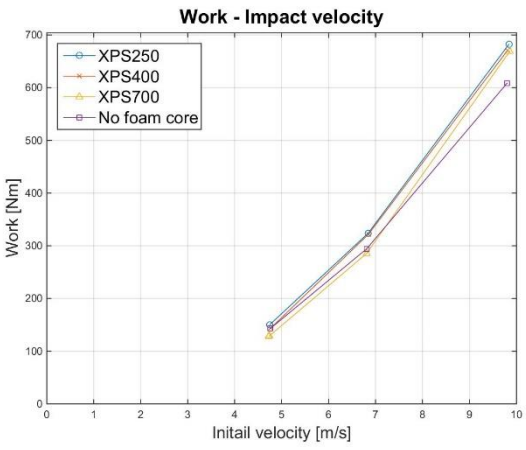


*f) Experimental energy absorption – impact velocity*

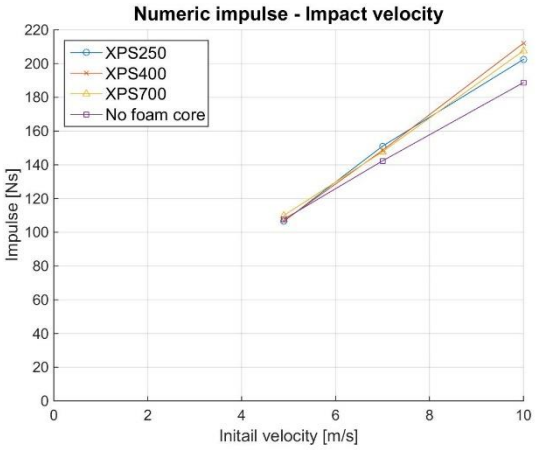


*g) Numerical impulse – impact velocity*

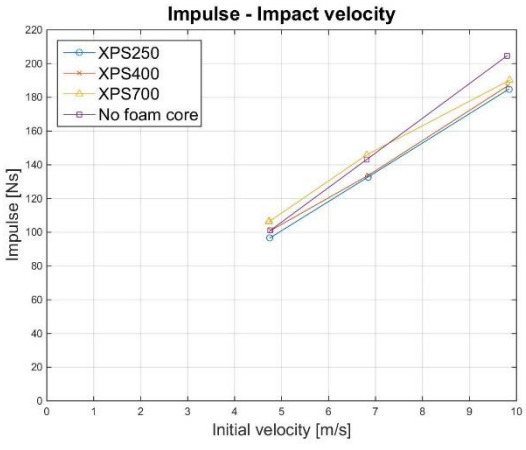


*h) Experimental impulse – impact velocity*

*Figure 5.5: Comparison between the experimental data and the numerical simulations with respect to absorbed energy (Work) and impulse*

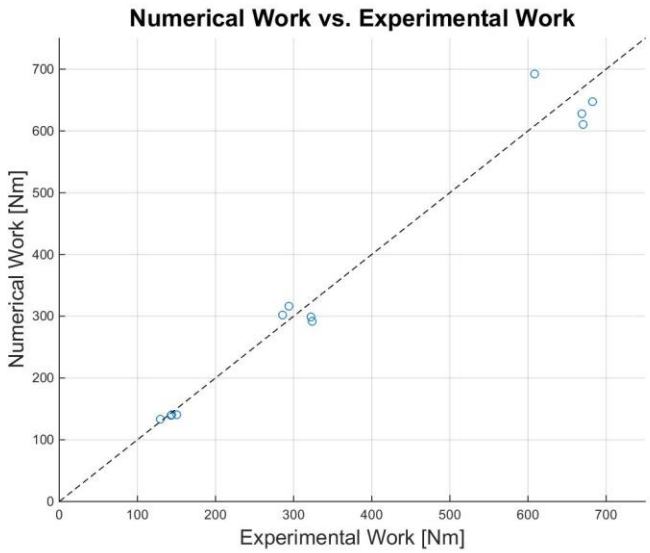


*Figure 5.6: Numerical energy absorption plotted against experimental energy absorption*

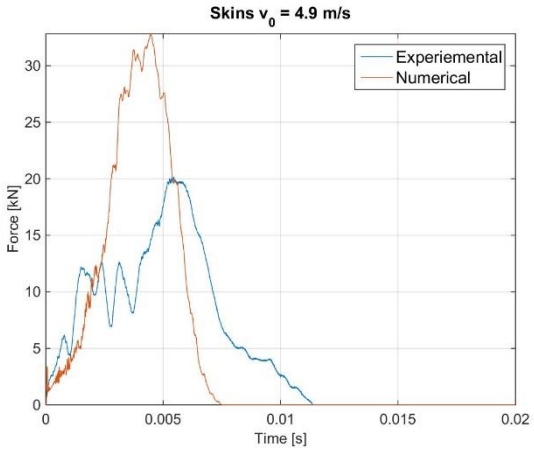


*a) Force vs. time at $v_0$ = 4.9 m/s*

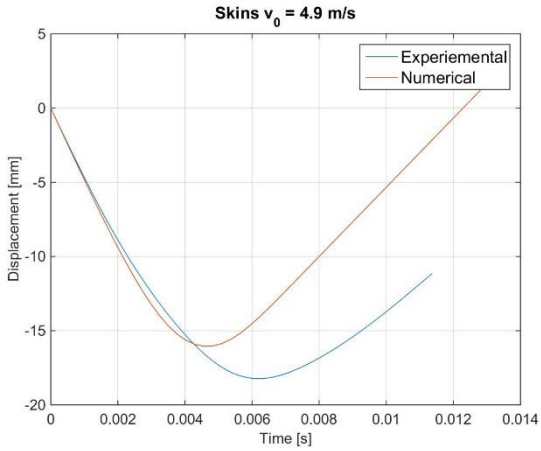


*b) Displacement vs. time at $v_0$ = 4.9 m/s*

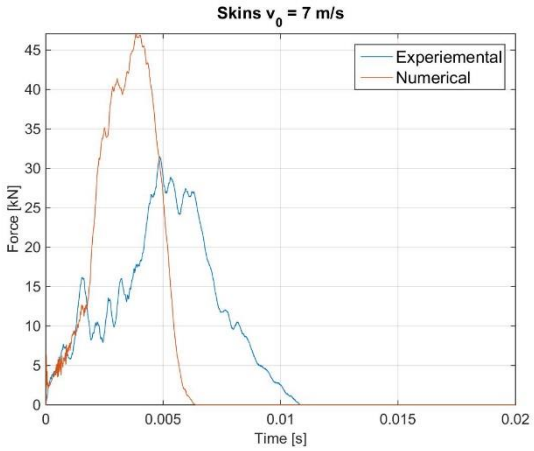


*c) Force vs. time at $v_0$ = 7 m/s*

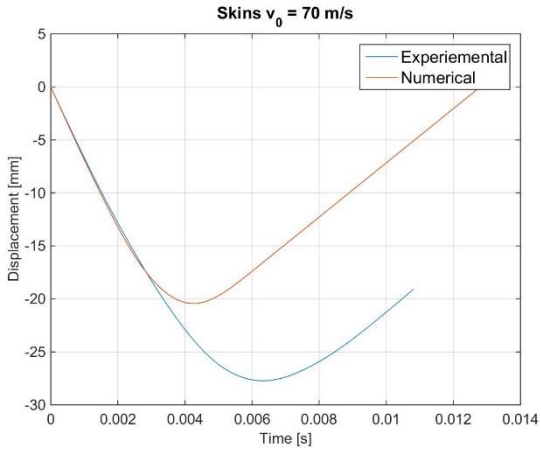


*d) Displacement vs. time at $v_0$ = 7 m/s*

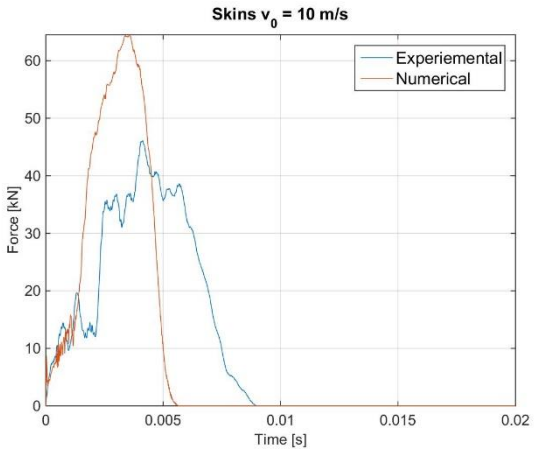


*e) Force vs. time at $v_0$ = 10 m/s*

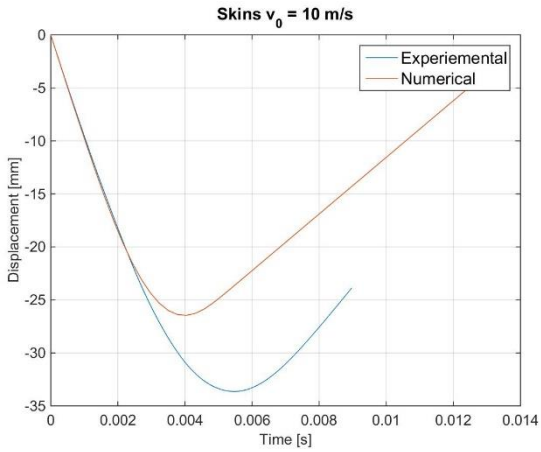


*f) Displacement vs. time at $v_0$ = 10 m/s*

*Figure 5.7: Comparison between the numerical and experimental response of the steel skins alone*

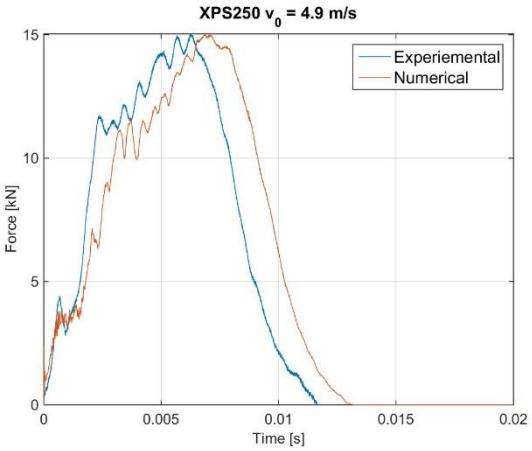


*a) Force vs. time at $v_0$ = 4.9 m/s*

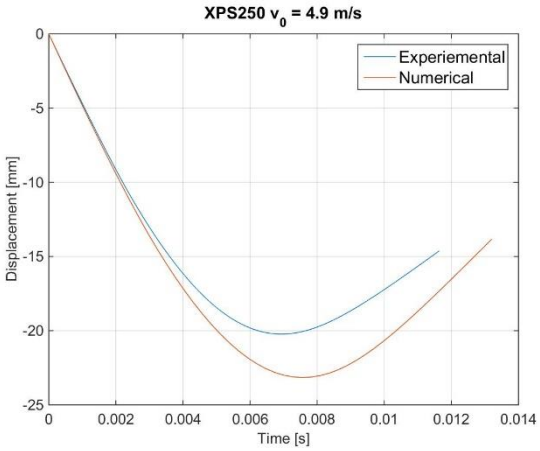


*b) Displacement vs. time at $v_0$ = 4.9 m/s*

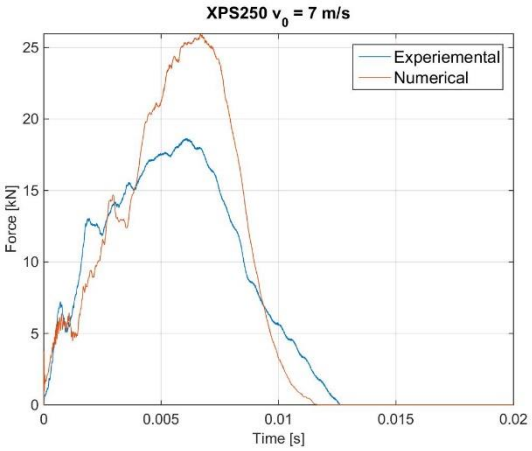


*c) Force vs. time at $v_0$ = 7 m/s*

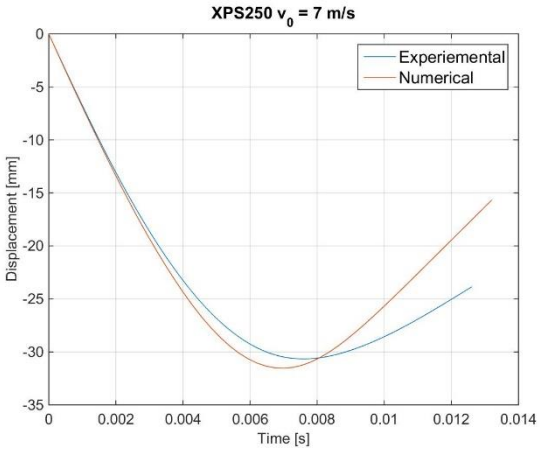


*d) Displacement vs. time at $v_0$ = 7 m/s*

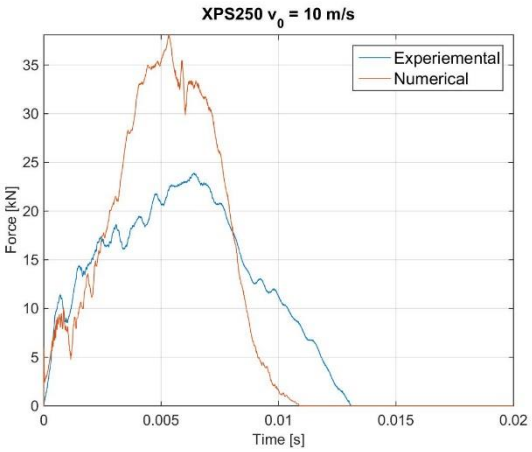


*e) Force vs. time at $v_0$ = 10 m/s*

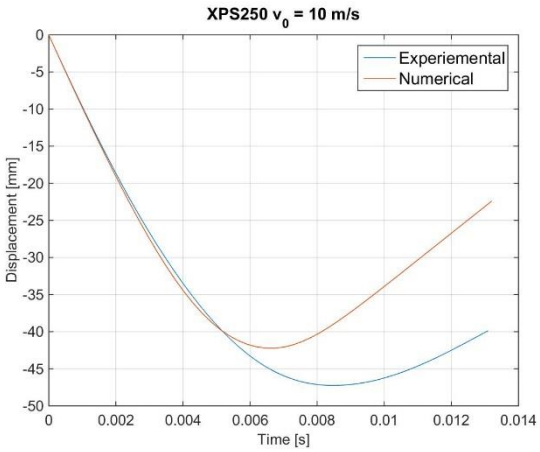


*f) Displacement vs. time at $v_0$ = 10 m/s*

*Figure 5.8: Comparison between the numerical and experimental response of the XPS250 sandwich*

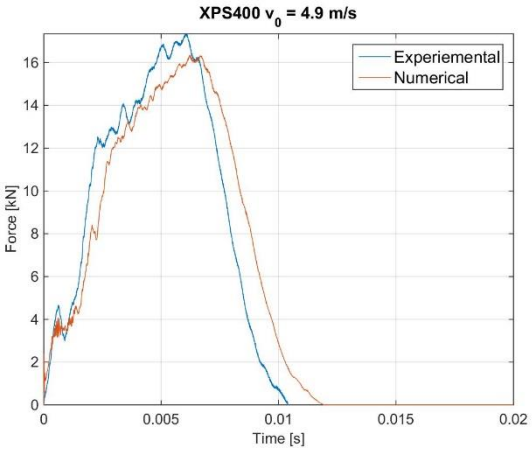


*a) Force vs. time at $v_0$ = 4.9 m/s*

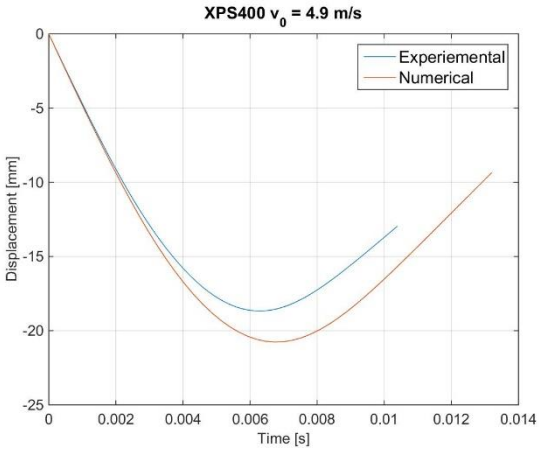


*b) Displacement vs. time at $v_0$ = 4.9 m/s*

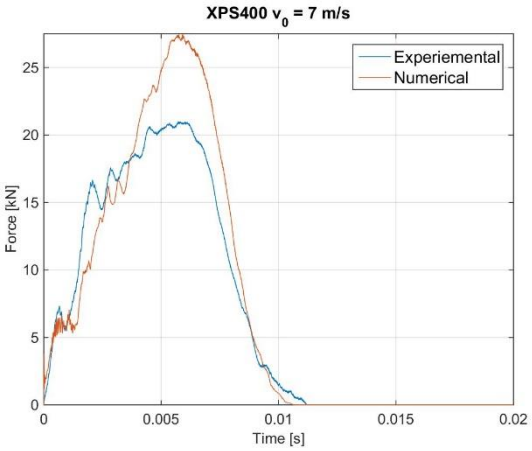


*c) Force vs. time at $v_0$ = 7 m/s*

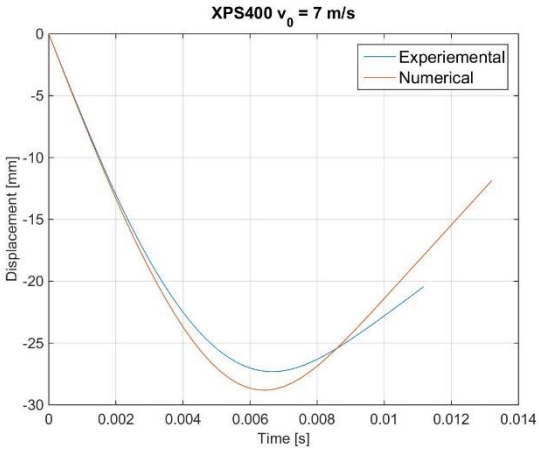


*d) Displacement vs. time at $v_0$ = 7 m/s*

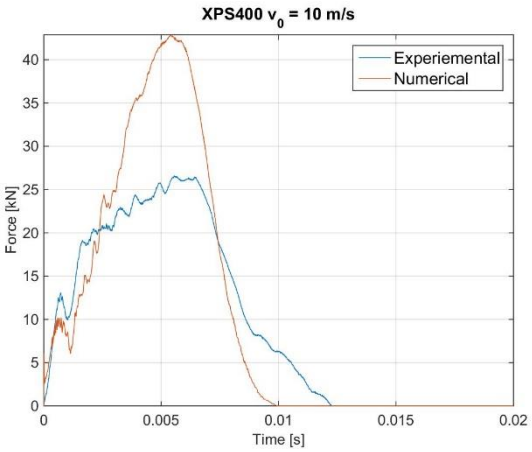


*e) Force vs. time at $v_0$ = 10 m/s*

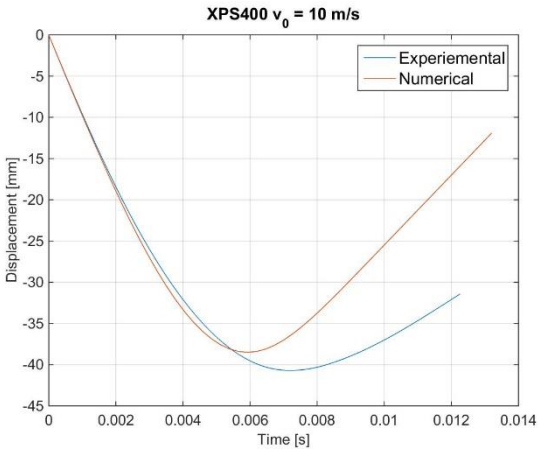


*f) Displacement vs. time at $v_0$ = 10 m/s*

*Figure 5.9: Comparison between the numerical and experimental response of the XPS400 sandwich*

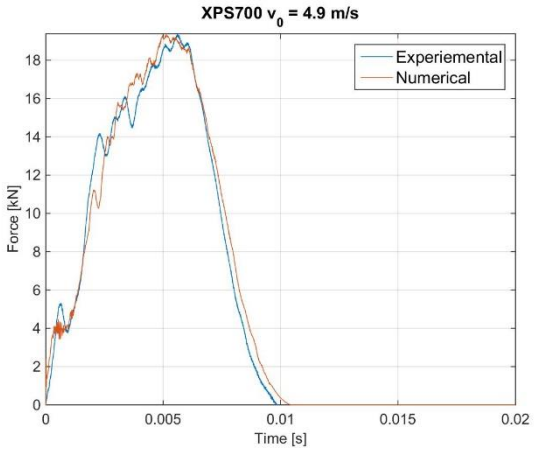


*a) Force vs. time at $v_0$ = 4.9 m/s*

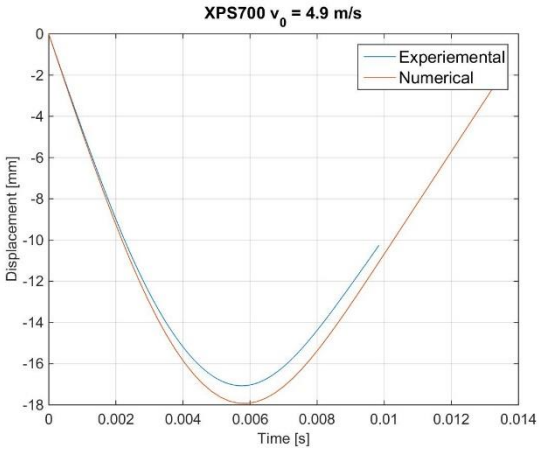


*b) Displacement vs. time at $v_0$ = 4.9 m/s*

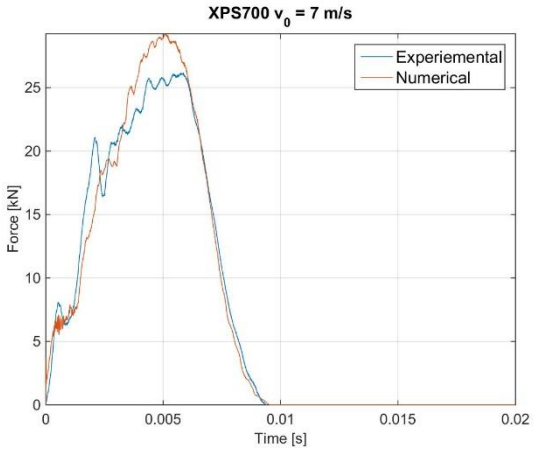


*c) Force vs. time at $v_0$ = 7 m/s*

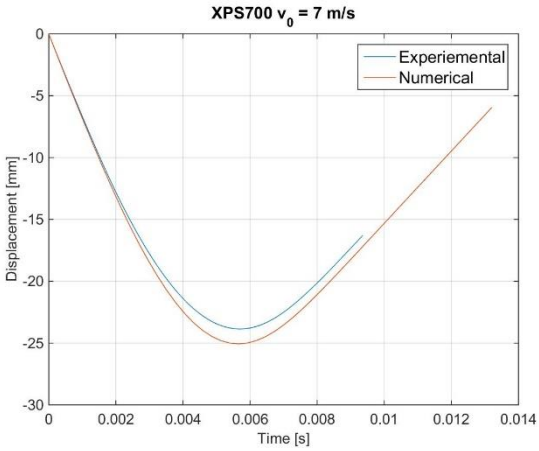


*d) Displacement vs. time at $v_0$ = 7 m/s*

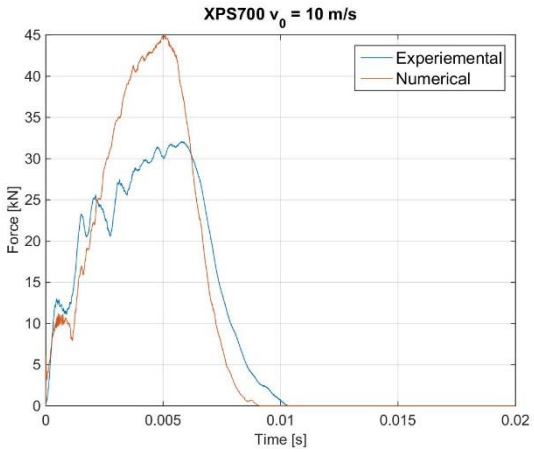


*e) Force vs. time at $v_0$ = 10 m/s*

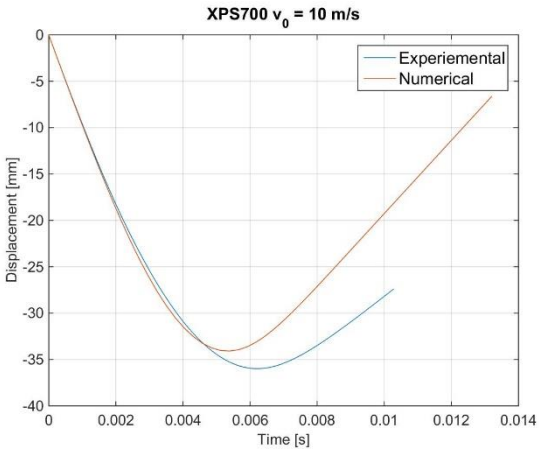


*f) Displacement vs. time at $v_0$ = 10 m/s*

*Figure 5.10: Comparison between the numerical and experimental response of the XPS700 sandwich*

### 5.2.3 Parametric study

Parametric studies on the effects of the foam thickness and the foam density, on the absorbed energy is outlined in the following.

***Foam core thickness***

In order to study the effect of foam core thickness three different thicknesses for the same core density (XPS250) are compared. The results are shown in Figure 5.11-5.12. As can be seen, the core thickness appear to have minor effects on the energy absorption of the sandwich. However, it is observed that the absorbed energy decreases with an increase in foam thickness, the reason for this behavior is currently not known.

A further comparison of the force-time and displacement-time histories indicates that a higher foam thickness results in larger deformations at the impact point, but also lower peak forces. Based on these observations, it's believed that when the foam thickness is increased the flexible back plate is less activated during impacts, partly due to the increase in the bending stiffness of the sandwich.

These findings might indicate that increasing the foam thickness does not necessarily improve the performance of the sandwich structures with respect to impact loading. A more detailed study is warranted.

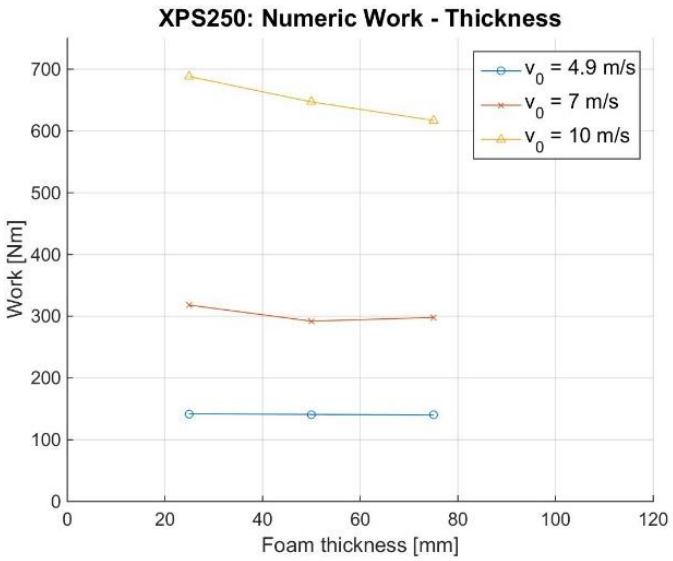


*Figure 5.11: Absorbed energy vs thickness*

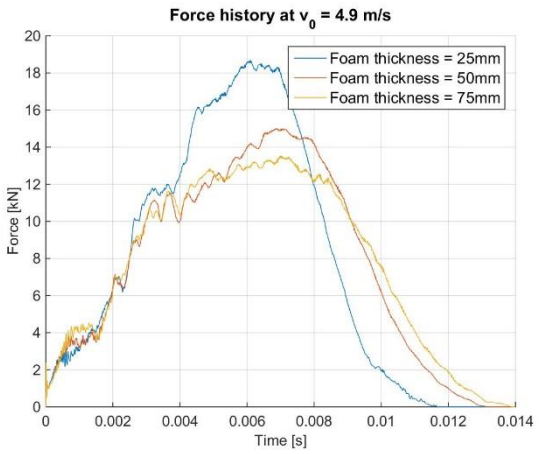


*a)*

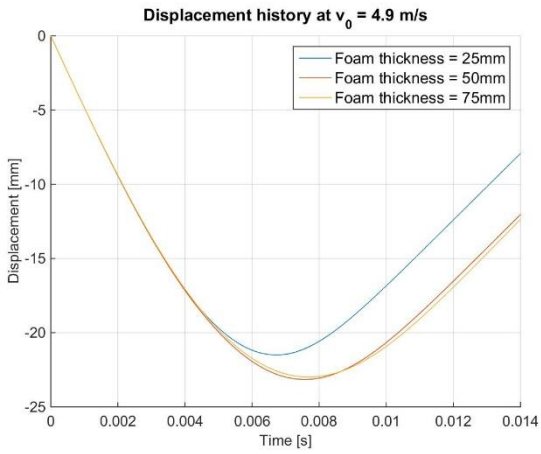


*b)*

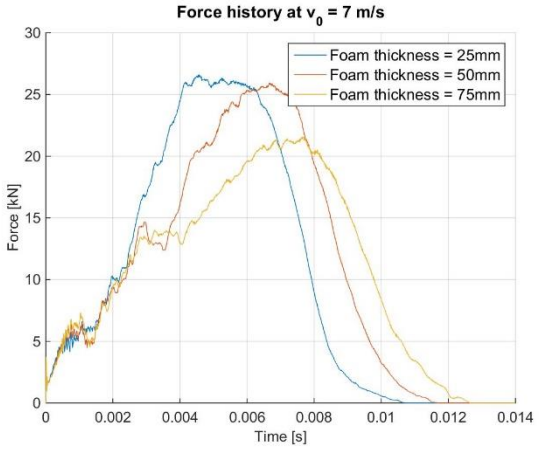


*c)*

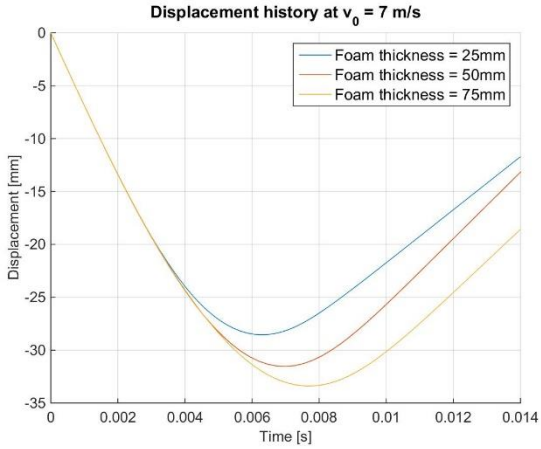


*d)*

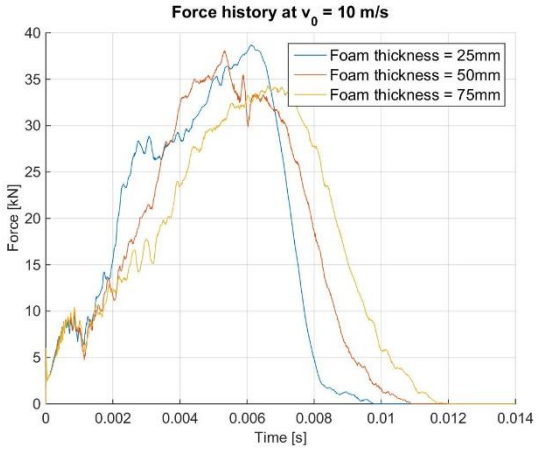


*e)*

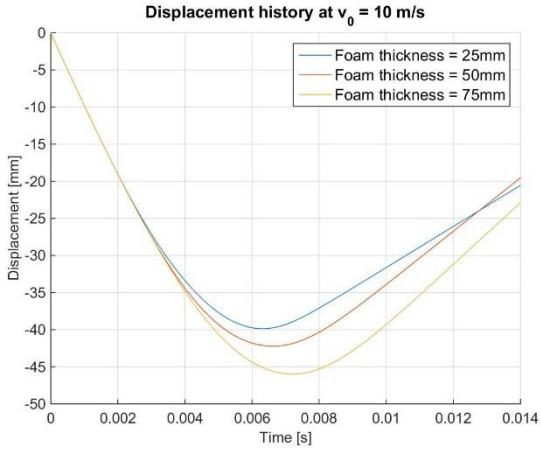


*f)*

*Figure 5.12: Sensitivity study wrt. foam thickness*

***Foam core density***

Sundolitt XPS is a mass produced commercially available foam material, it is therefore reasonable to expect variation in the material properties throughout the foam. These variations are probably highly influenced by the local density of the foam. It is therefore interesting to study the ramifications of small variations in foam density. A small study into the density sensitivity of the model was therefore performed.

The density sensitivity was studied numerically by comparing three simulations with slight variations in the global foam density. XPS400 was chosen for the sensitivity study since it was the intermediate foam density tested. For these simulations, the material was represented with the density dependent material model derived in chapter 3. To new sets of material parameters were created by increasing and decreasing the material density by 10 %. Figure 5.13 illustrates the three different material models.

The forces acting on the impactor, and the displacement of the impactor are compared in Figure 5.14. Although some changes in the response can be observed, the results suggest that the model is relative in-sensitive to minor changes (±10%) in the foam density, see Figure 5.15.

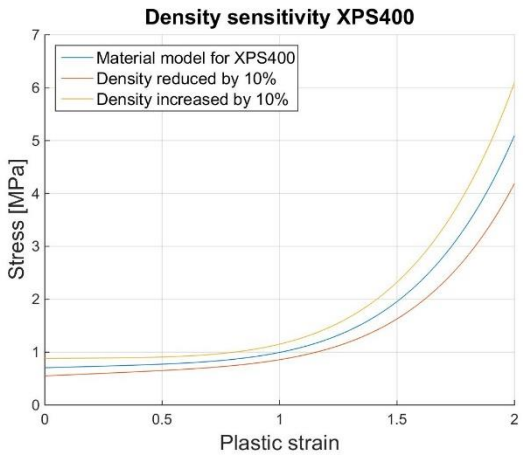


*Figure 5.13: Density sensitivity of the material model*

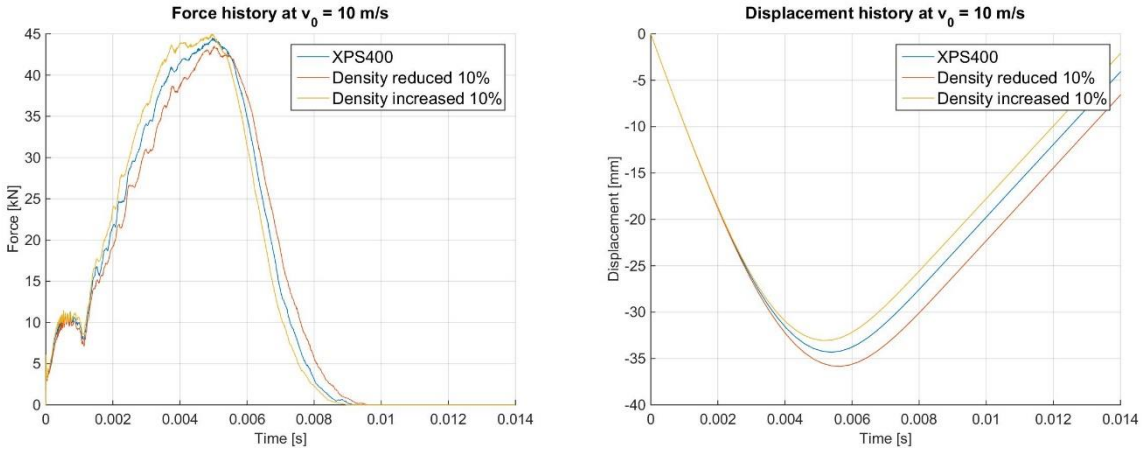


*a) Force time history* *b) Displacement time history*

*Figure 5.14: Sensitivity study wrt. variations in foam density – force and displacement time history*

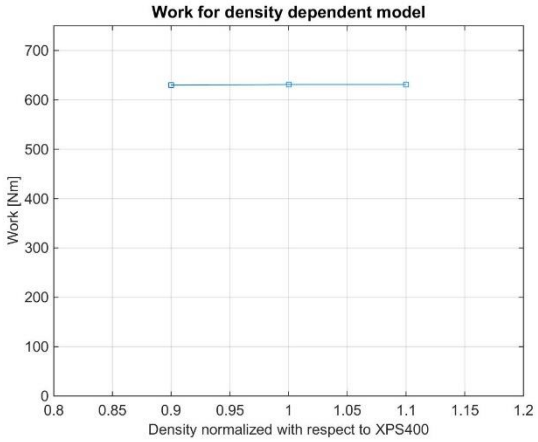


*Figure 5.15: Sensitivity study wrt. variations in foam density – Absorbed energy*

## 5.3 SHOCK TUBE

The experiments performed in shock-tube facility at SIMLab, on the sandwich configuration and the steel skins alone, were simulated numerically in LS DYNA. The numerical results were then compared to the experimental results. A tailor made model (basis model) of the test set up was used in the analyses. A penalty based surface to surface contact algorithm is used for all the models, and friction has not been properly accounted for i.e. static and dynamic coefficient of friction is set to 0.1 for all contact formulations. The analysis model has not been calibrated to the experimental results, and all results presented in the current work is based on the basis model. Typical parameters that could be applied to optimize the model are; boundary conditions, friction, mesh size and element type, strain-rate sensitive material model and variation of material properties throughout the test specimen.

The analysis of XPS250 at the highest driver pressure (75 bar) resulted in a negative volume error in the foam elements, and consequently caused LS DYNA to abort the analysis, i.e. no numerical results to compare to the experiment at 75 bar driver pressure. The experiments performed without a front-plate was not modeled numerically. Thus, only three experiments (D600-60, XPS250S-35 and XPS250S-60) are compared to the corresponding numerical results.

A small numerical study into the effects of changing the foam core density was also performed. The foams XPS400 and XPS700 were analyzed under the same loading conditions as the XPS250 foam. The analysis of XPS400 at the highest driver pressure (75 bar) resulted in the same numerical error as the analysis of XPS250 at the same pressure.

### 5.3.1 Model and approach

The shock tube experiments was modelled with the specimen clamped in between two rigid plates using elastic bolts. The loading was introduced directly as pressure directly on the inner steel skin. The Friedlander equation was used to represent the pressure history. The model is shown in Figure 5.16.

The 0.8 mm thick Docol600DL steel plates was modelled by four-node Lagrangian shell elements and the Belytschko-Tsay element formulation was utilized [52]. The elements have five integration points through the thickness, and the Gauss quadrature rule is used to solve the equations. The applied material model for the steel platees is based on the modified Johnsen-Cook material model, material *107 in LS DYNA, using the material parameters given in chapter 3.

The foam core is modelled with eight-node three-dimensional constant stress solid elements. 20 elements are used through the thickness of the foam. The foam material is represented with the Deshpande-Fleck material model, material *154 in LS DYNA, using the material parameters derived in chapter 3, and analytical derivation is activated in the analyses. No fracture criterion is used in the material model.

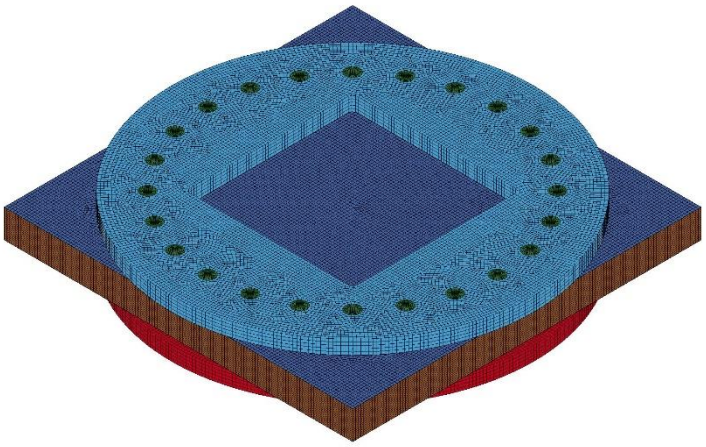

*Figure 5.16: LS DYNA model of the shock tube*

### 5.3.2 Numerical results

The experiments were recreated with numerical simulations using the corresponding nominal input parameters from the experiments. As mentioned earlier, the experiment performed without a front plate was not modelled, and the analyses at the highest driver pressure failed. Thus, only three analyses (XPS250S_35, XPS250S_60 and D600_60) are compared to the corresponding experiments. The comparisons are shown in Figure 5.17-5.19 and Table 5.1.

*Table 5.1: Comparison between numerical and experimental results*

| Test | Driver pressure [bar] | $P_r$ [kPa] | Experimental $u_{max}$ [mm] | Numerical $u_{max}$ [mm] |
|---|---|---|---|---|
| **D600-60** | 60 | 1362 | 26,8 | 35,2 |
| **XPS250S-35** | 35 | 1100 | 24,5 | 18,90 |
| **XPS250S-60** | 60 | 1332 | 29,8 | 25,40 |
| **XPS250S-75** | 75 | 1767 | 37,2 | - |
| **XPS250-35** | 35 | 935 | 37,9 | - |

The results from the shock tube experiments are limited to the displacements of the back plate of the test specimen and a pressure history inside the shock tube. Only the displacements are relevant for comparison.

Note that in general the numerical analyses over-predicts the compression of the foam compared to observations during the test (unfortunately not measured or documented during the testing). This can possibly be explained by the lack of strain rate dependency in the foam material model.

Further, as can be seen in Figures 5.17-5.19 (note that the color bars are not the same for the experimental and numerical results), the numerical model under-predicts the deformation significantly for all the experiments on a sandwich configuration, while it over -predicts the response of the steel skins alone. The displacements fields is somewhat different in the numerical results compared to the experimental results, especially with respect to the gradient of the deformation. However, the numerical model appears to predict the correct shape of the displacement-time history for the mid-point, although the magnitude is different. Note that the experimental displacement-time history in Figure 5.18 e) gets distorted after approximately 5 ms due to interference in the DIC images.

A possible explanation to the observed differences between the experimental and numerical results, is that the clamping frame is modelled as analytically rigid, which might result in higher fixity in the numerical simulations. Further, similar to in the drop tower comparison, a combination of several factor might influence the results i.e. the lack of imperfections in the plates and the friction modeling, inaccuracy in the steel model and the strain rate sensitivity of the foam material.

Since the numerical results exhibit a similar pattern as the experimental results, it is believed that the numerical model can deliver accurate results after a proper calibration.

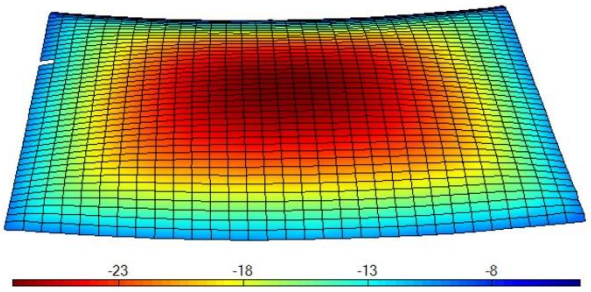


*a) Experimental displacement contour plot (DIC)*

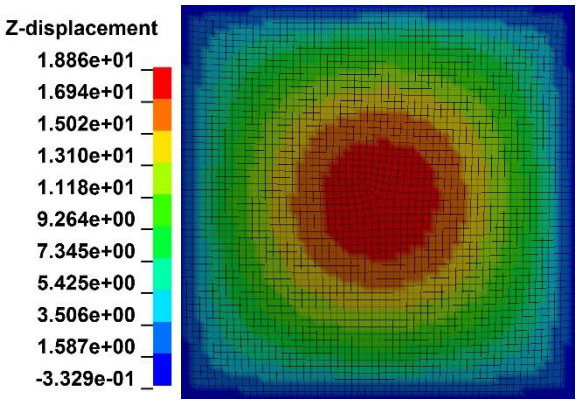


*b) Numerical displacement contour plot from LS DYNA*

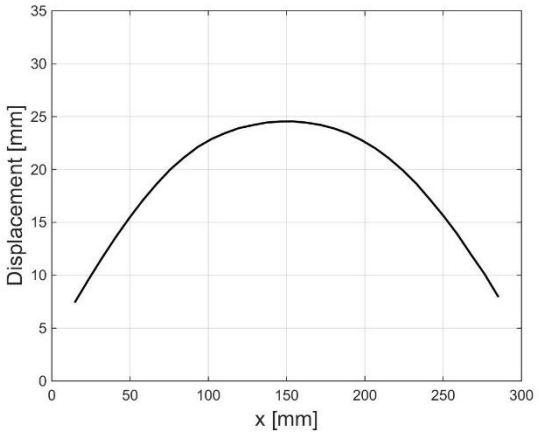


*c) Experimental cross section displacement of back plate*

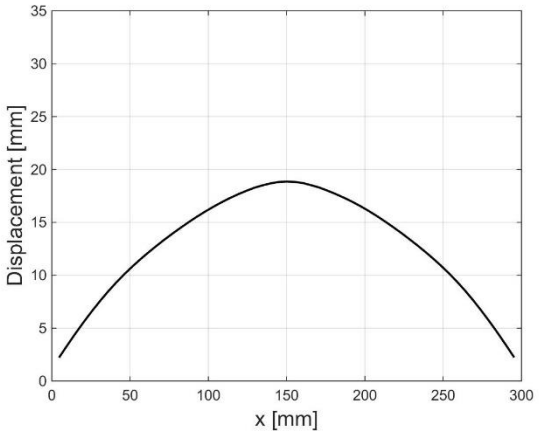


*d) Numerical cross section displacement of back plate*

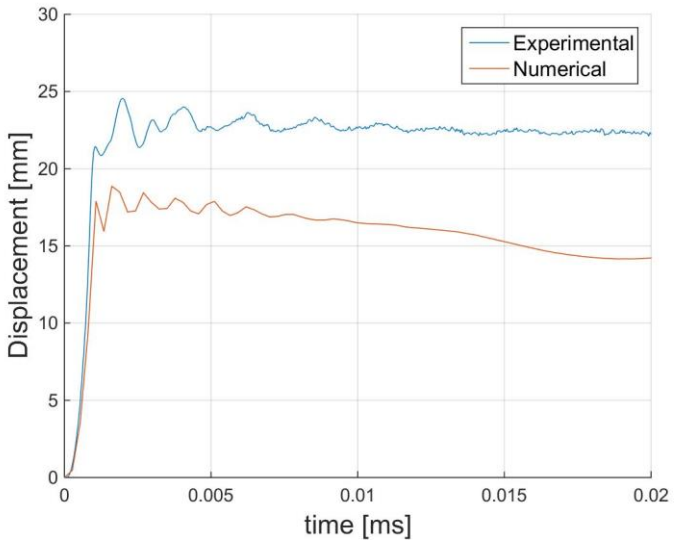


*e) Mid-point displacement history of the back plate*

*Figure 5.17: Comparison of the numerical and experimental results at max displacement for XPS250 at 35 bar driver pressure*

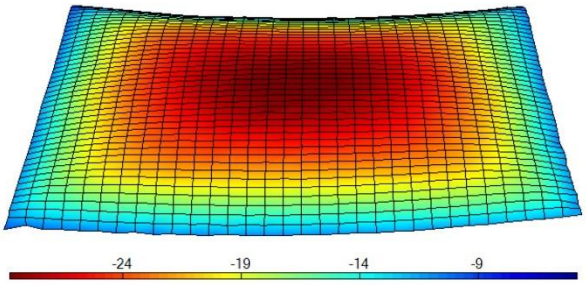


*a) Experimental displacement contour plot (DIC)*

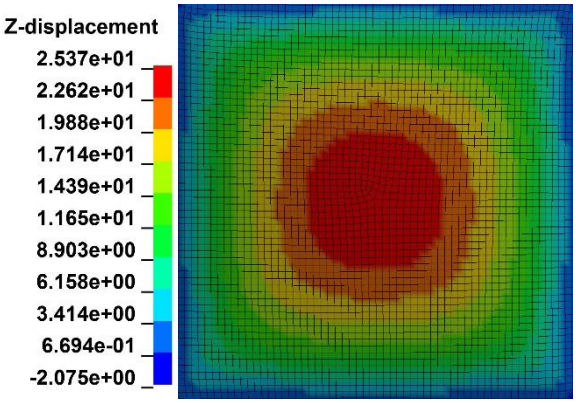


*b) Numerical displacement contour plot from LS DYNA*

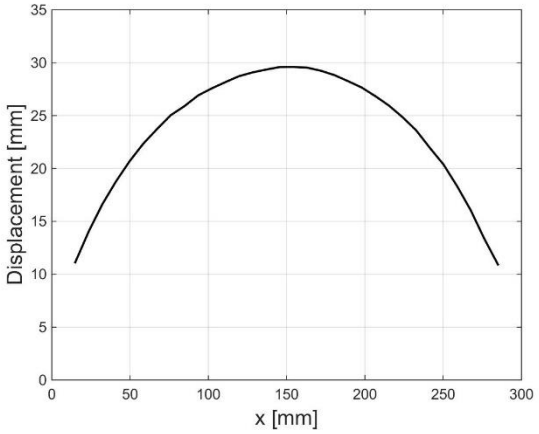


*c) Experimental cross section displacement of back plate*

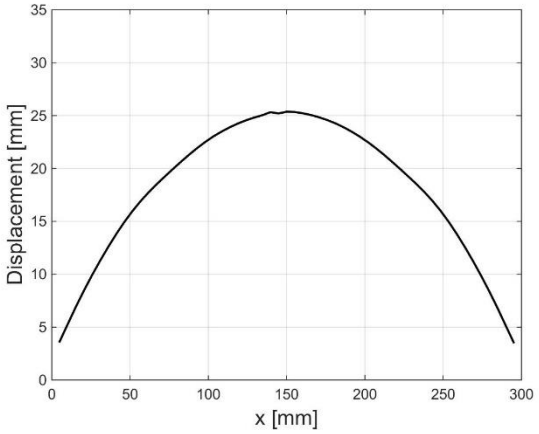


*d) Numerical cross section displacement of back plate*

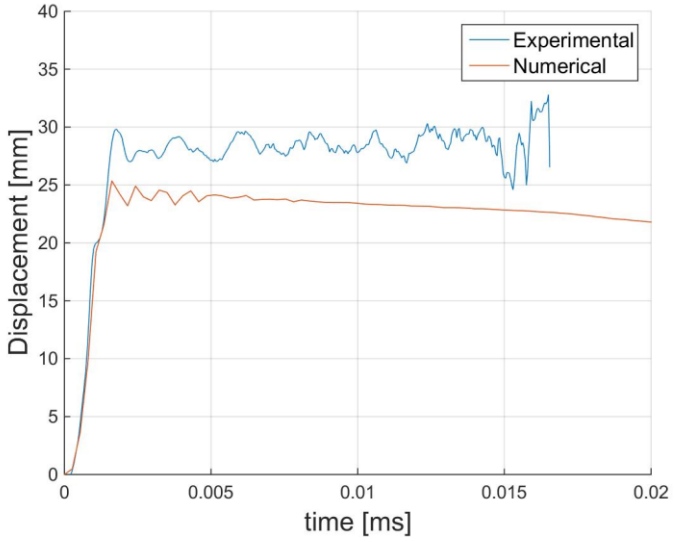


*e) Mid-point displacement history of the back plate*

*Figure 5.18: Comparison of the numerical and experimental results at max displacement for XPS250 at 60 bar driver pressure*

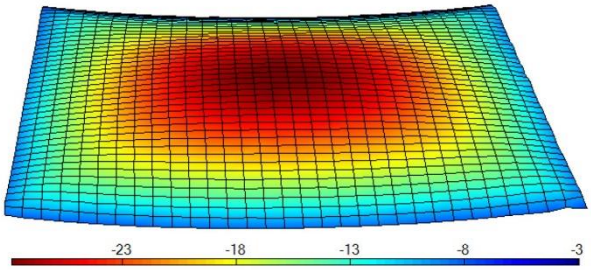


*a) Experimental displacement contour plot (DIC)*

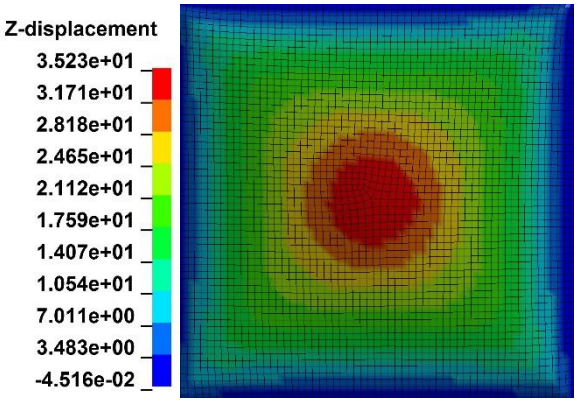


*b) Numerical displacement contour plot from LS DYNA*

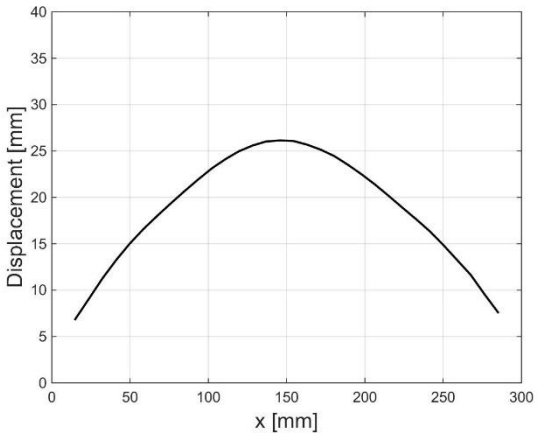


*c) Experimental cross section displacement of back plate*

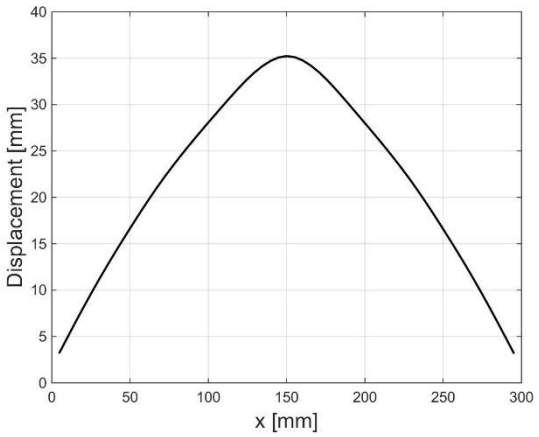


*d) Numerical cross section displacement of back plate*

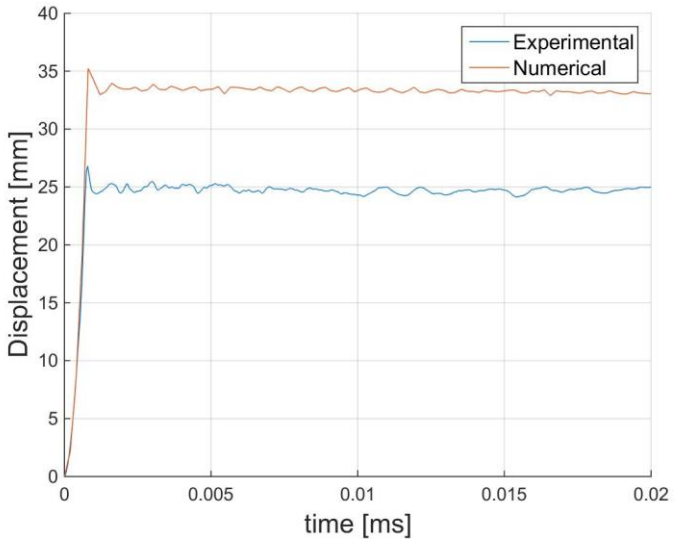


*e) Mid-point displacement history of the back plate*

*Figure 5.19: Comparison of the numerical and experimental results at max displacement for Skins only at 60 bar driver pressure*

### 5.3.3 Parametric study

Since only one foam density (XPS250) was tested experimentally in the shock tube, the other two densities (XPS400 and XPS700) were investigated numerically, using the constructed model described in Section 5.3.1. Both densities were subjected to the same loading conditions that were used in the experiments i.e. 35, 60 and 75 bar driver pressure. Figure 5.20 summarizes the results of the parametric study. Figures 5.21 – 5.23 shows the displacement time history for the mid-point deflection, the plastic strain and the deformation of the cross section at maximum displacement. Note that only the analysis of XPS700 converged for 75 bar driver pressure. An overview of the parametric study is given in Table 5.2.

*Table 5.2: Overview of the parametric study & the main results*

| Test | Density [kg/m$^3$] | Driver pressure [bar] | *Pr* [kPa] | $u_{max}$ [mm] | Absorbed energy [Nm] |
|---|---|---|---|---|---|
| **250S_35** | 33 | 35 | 1100 | 18,9 | 4030 |
| **250S_60** | 33 | 60 | 1332 | 25,4 | 5560 |
| **250S_75** | 33 | 75 | 1767 | - | - |
| **400S_35** | 37 | 35 | 1100 | 19,6 | 3190 |
| **400S_60** | 37 | 60 | 1332 | 21,6 | 4920 |
| **400S_75** | 37 | 75 | 1767 | - | - |
| **700_35** | 50 | 35 | 1100 | 22,4 | 1370 |
| **700_60** | 50 | 60 | 1332 | 24,6 | 2470 |
| **700_75** | 50 | 75 | 1767 | 27 | 5900 |

Figure 5.20 a) shows a clear dependency (nearly linear) between the foam density and the amount of absorbed energy. Where lower densities are able to absorb more energy than higher densities i.e. the absorbed energy decreases significantly with increased core densities. Even though there appears to be a significant tendency with regard to the absorbed energy, Figure 5.20 b) shows that the maximum displacement for all the analyses are of similar magnitude (approximately 20-25 mm). However, if we compare the amount of maximum plastic stain (e.g. see Figure 5.21) for different foam densities, it is shown that there is a large difference in the level of plastic strain (more than a factor of 2), therefore the above findings depends on the validity of the material model over wide strain range.

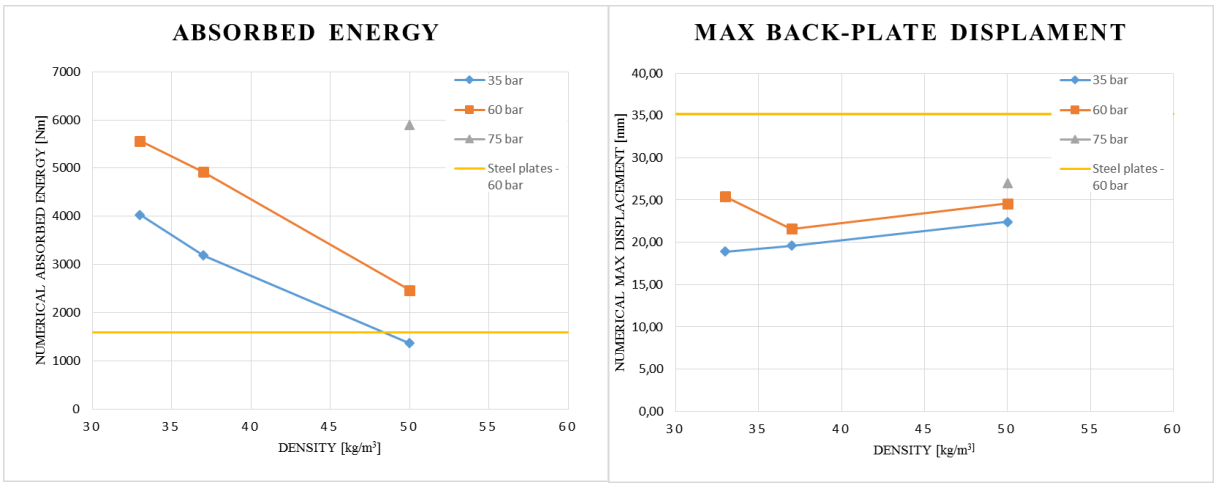


*a) Absorbed energy*

*b) Maximum displacement of the back plate*

*Figure 5.20: Absorbed energy and maximum deflection as a function of increased density for different blast pressures*

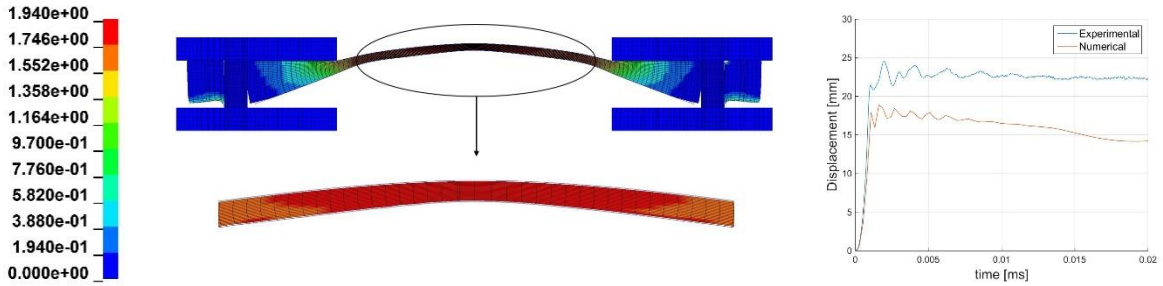


*a) Plastic strain for XPS250 at 35 bar*

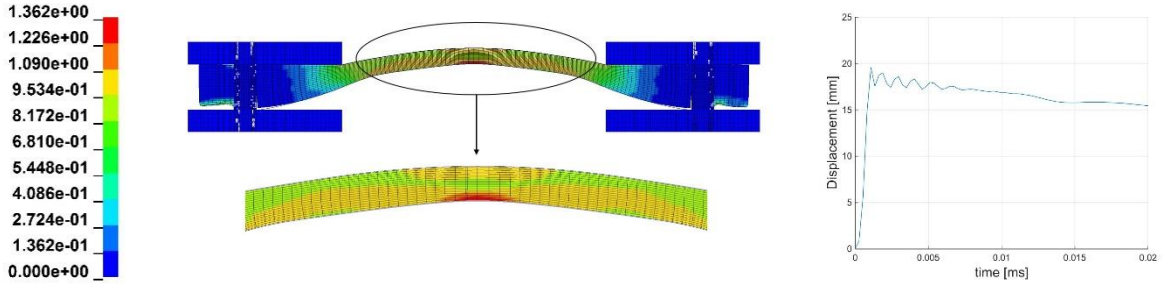


*b) Plastic strain for XPS400 at 35 bar*

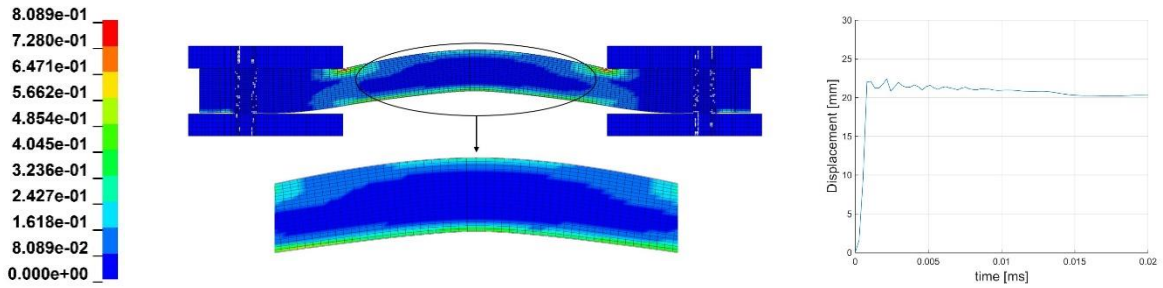


*c) Plastic strain for XPS700 at 35 bar*

*Figure 5.21: Effective plastic strain at maximum displacement for 35 bar driver pressure - shown for the specimens cross section*

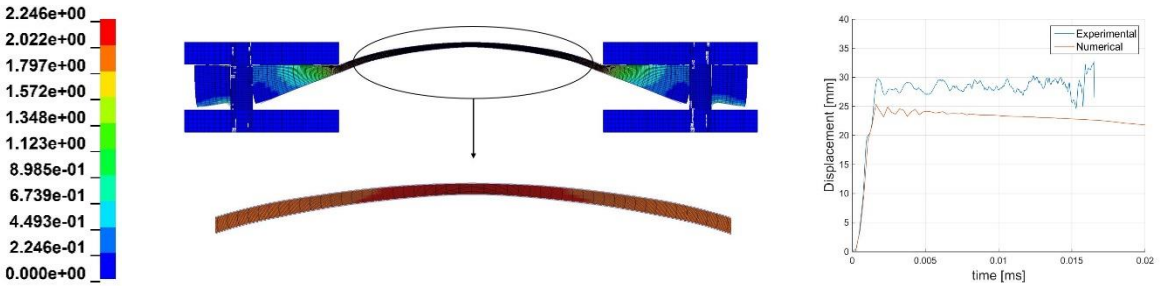


*a) Plastic strain for XPS250 at 60 bar*

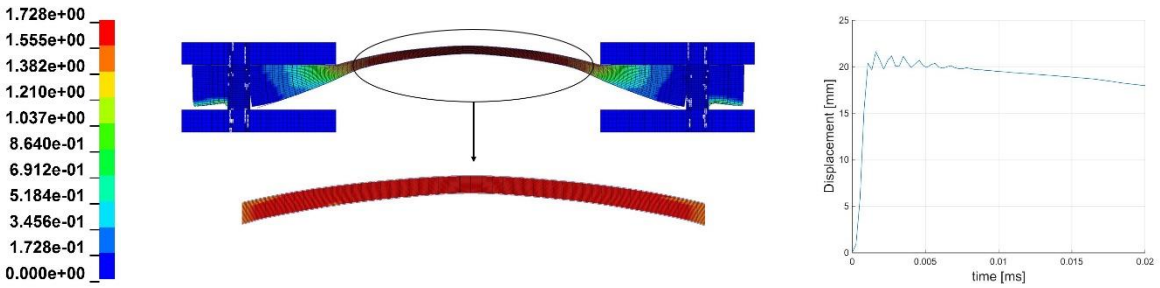


*b) Plastic strain for XPS400 at 60 bar*

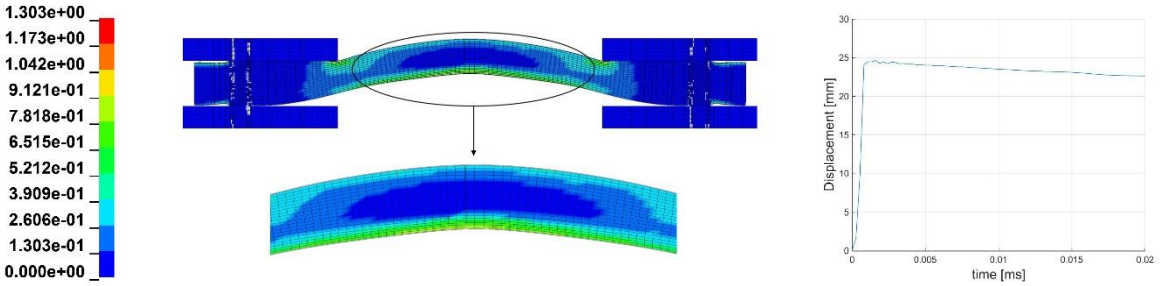


*c) Plastic strain for XPS700 at 60 bar*

*Figure 5.22: Effective plastic strain at maximum displacement for 60 bar driver pressure - shown for the specimens cross section*

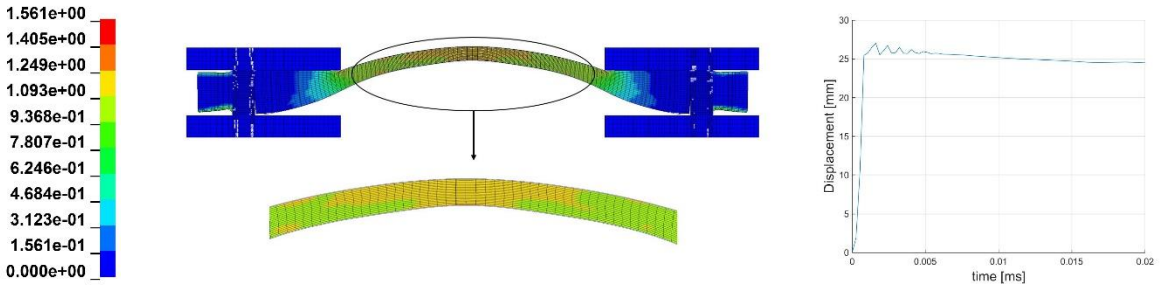


*a) Plastic strain for XPS700 at 75 bar*

*Figure 5.23: Effective plastic strain at maximum displacement for 60 bar driver pressure – shown for the specimens cross section*

# 6 DISCUSSION & CONCLUDING REMARKS

The main objective of the present work was to investigate how the polymer foam (XPS) behaves under dynamic impact and blast loading, and evaluate the performance of this type of foam under these load conditions. Further, it was studied to which extent the response can be predicted using computational tools. This was done by performing a number of laboratory tests and numerical studies. Impact and blast experiments were performed on sandwich panels with polymer foam cores and steel skins. The experiments were used to investigate the response of such a sandwich configurations. Focus was on the energy absorption of the sandwich. The dynamic impact tests were performed in a drop tower rig while the blast loading tests where preformed in a shock tube. Quasi static compression tests were performed on the polymer foam in order to derive a numerical material model. Almost all the experimental tests were modelled and analyzed by FE analysis using the commercial software tool LS-DYNA. The numerical models of the experiments were not calibrated to the experimental data but were based on rough assumptions and engineering judgment. Thus, the numerical results serve more as a proof of concept with regard to the numerical modelling. Nevertheless, the numerical results were compared to the experiments in order to validate to which extent the response could be predicted numerically using a basic numerical model. The main finding from the impact and blast study are listed below.

**The main findings for the impact study:**

- The steel skins dominate the energy absorption for lower impact velocities, this is show both experimentally and numerically.
- The amount of absorbed energy appear to be independent of the foam density for low-velocity impacts, this is supported both by experimental and numerical results.
- The numerical simulations of the sandwich configuration do not accurately predict the peak forces from the experiments, but the energy absorption, impulse and displacement are predicted with acceptable accuracy.
- The numerical simulations of the steel skins alone do not accurately predict the peak forces or the displacements, but the absorbed energy and impulse are predicted with acceptable accuracy.
- Numerical analyses indicate that the response of the sandwich configuration is somewhat independent of the foam thickness. However, for higher impact velocities

there is a tendency towards a reduction in the amount of absorbed energy with increased thickness.

**The main findings for the blast study:**

- Experimental results indicate that having a foam core increase the deformation of the back-plate.
- The numerical analyses over-predicts the compression of the foam.
- The numerical analyses under-predicts the deformation of the sandwich panels, but over-predicts the deformation of the steel skins alone.
- Numerical analyses indicate that increasing the foam density reduces the energy absorption significantly (near linear relationship).

Considering the complexity of the problems analyzed, the overall observation is that the numerical simulation is in many cases able to predict the test results with reasonable accuracy. As mentioned earlier, no proper calibration of the numerical model has been performed. It is expected that much better agreement between the numerical simulation and the experimental results is possible to obtain by including proper contact formulation (friction), more detailed modeling of the boundary conditions and by including strain-rate dependency in the foam material model.

Based on the results found both experimentally and numerically, XPS foam is believed to perform well as an energy absorbent in a flexible sandwich configuration, for both low-velocity dynamic impacts and blast loads. The absorbed energy of the test specimens appear to be independent of the foam density when subjected to low-velocity dynamic impact. But the blast study indicate that the energy absorption is greatly dependent on the density of the foam core, where low density results in higher energy absorption. It is further believed that the sandwich panels will exhibit a similar dependency on the thickness of the foam, although this has not been proven empirically.

The findings indicate that the blast protection performance of the studied sandwich panels greatly depend on the design parameters, e.g. foam core density. The observed trends suggests that it is beneficial to use a foam with as low density as possible. It is however important to use a foam that has a sufficiently high yield strength since the amount of energy that can be

absorbed depends on the area under the stress strain curve. It is therefore important to have realistic design criterions in order to optimize the protective design. A thorough case by case optimization of the design parameters could yield a very effective blast resistant design.

# 7 FURTHER WORK

The work present in this thesis is based on several assumptions, and several aspects has not been considered. In order to gain better knowledge and higher confidence with respect to numerical predictions of polymer foams subjected to blast loads, some further investigations are warranted. The following lists some suggestions.

- Do a proper calibration of the numerical model with respect to experimental results
- Perform more comprehensive material tests on both the foam and steel to derive a more detailed material model
- Do a comprehensive sensitivity study of the numerical model e.g. mesh density, element type, contact formulation and boundary conditions
- Study the effect of a fracture criterion in the numerical foam model
- Study the strain rate dependency of the foam
- Test the foam against a stiff surface

# 8 REFERENCES


[1] "Rapport fra 22. juli-kommisjonen," NOU 2012: 14, 2012.

[2] "Sundolitt XPS standard plater," Sundolitt, [Online]. Available: http://www.sundolitt.no/sundolitt/produkter/sundolitt-xps-standard. [Accessed 2 May 2016].

[3] "Granata material intelligence - Materials charts," [Online]. Available: http://www.grantadesign.com/download/pdf/teaching_resource_books/2-Materials-Charts-2010.pdf. [Accessed 08 June 2016].

[4] T. Børvik, A. G. Hanssen, Langseth and L. M. and Olovsson, "Response of structures to planar blast loads – A finite element engineering approach," *Computers and Structures,* no. 87, pp. 507-520, 2009.

[5] M. Larcher and F. Casadei, "Explosions in complex geometries – A comparison of several approaches," *International Journal of Protective Structures,* no. 1(2), pp. 169-165, 2010.

[6] S. H. Alsayed, H. M. Elsanadedy, Z. M. Al-Zaheri, Y. A. Al-Salloum and H. Abbas, "Blast response of GFRP - strengthened infill masonry walls," *Construction and Building Materials,* no. 115, p. 438–451, 2016.

[7] J. Xu, C. Wu, X. Hengbo, Y. Su, Z. X. Li, Q. Fang, H. Hao, Z. Liu, Y. Zhang and J. Li, "Behaviour of ultra high performance fibre reinforced concrete columns subjected to blast loading," *Engineering Structures,* no. 118, pp. 97-107, 2016.

[8] A. Schenker, I. Anteby, E. Nizri, B. Ostraich, Y. Kivity, O. Sadot, O. Haham, R. Michaelis, E. Gal and G. Ben-Dor, "Foam-protected reinforced concrete structures under impact: Experimental and numerical studies," *Journal of Structural Engineering,* no. 131(8), pp. 1233-1242, 2005.

[9] A. G. Hanssen, L. Enstock and M. Langseth, "Close-range blast loading of aluminium foam panels," *International Journal of Impact Engineering,* no. 27, pp. 593-618, 2002.

[10] N. Kambouchev, L. Noels and R. Radovitzky, "Numerical simulation of fluid-structure interaction between air blast waves and free-standing plates," *Computers & Structures,* no. 85(11-14), pp. 923-931, 2007.

[11] X. Li, P. Zhang, Z. Wang, G. Wu and L. Zhao, "Dynamic behavior of aluminum honeycomb sandwich panels under air blast: Experiment and numerical analysis," *Composite Structures,* no. 108, pp. 1001-1008, 2014.

[12] L. Zhang, R. Hebert, J. T. Wright, A. Shukla and J.-H. Kim, "Dynamic response of corrugated sandwich steel plates with graded cores," *International Journal of Impact Engineering,* no. 65, pp. 185-194, 2014.

[13] Ł. Mazurkiewicz, J.Małachowski and P. Baranowski, "Optimization of protective panel for critical supporting elements," *Composite Structures,* no. 134, pp. 493-505, 2015.

[14] M. Aleyaasinn, J. J. Harrigan and S. R. Reid, "Air-blast response of cellular material with a face plate: An analytical–numerical approach," *International Journal of Mechanical Sciences,* no. 91, pp. 64-70, 2015.

[15] H. Zhao, H. Yu, Y. Yuan and H. Zhu, "Blast mitigation effect of the foamed cement-base sacrificial cladding for tunnel structures," *Construction and Building Materials,* no. 94, pp. 710-718, 2015.

[16] D. Radford, G. McShane, V. Deshpande and N. Fleck, "The response of clamped sandwich plates with metallic foam cores to simulated blast loading," *International Journal of Solids and Structures,* no. 43, pp. 2243-2259, 2005.

[17] M. Z. Hassan, Z. W. Guan, W. J. Cantwell, G. S. . Langdon and G. N. Nurick, "The influence of core density on the blast resistance of foam-based sandwich structures," *International Journal of Impact Engineering,* no. 50, pp. 9-16, 2012.

[18] G. Langdon, C. v. Klemperer, B. Rowland and G. Nurick, "The response of sandwich structures with composite face sheets and polymer foam cores to air-blast loading: Preliminary experiments," *Engineering Structures,* no. 36, pp. 104-112, 2012.

[19] G. Langdon, D. Karagiozova, C. Klemperer, G. Nurick, A. Ozinsky and E. Pickering, "The air-blast response of sandwich panels with composite face sheets and polymer foam cores: Experiments and predictions," *International Journal of Impact Engineering,* no. 54, pp. 64-62, 2013.

[20] M. Sadighi and S. J. Salami, "An investigation on low-velocity impact response of elastomeric & crushable foams," *Central European Journal of Engineering,* no. 2, pp. 627-637, 2012.

[21] I. M. Daniel, J. M. Cho and B. T. Werner, "Characterization and modeling of stain-rate-dependent behavior of polymeric foams," *Composites Part A: Applied Science and Manufacturing,* no. 45, pp. 70-78, 2013.

[22] A. Yonezu, K. Hirayama, H. Kishida and X. Chen, "Characterization of the compressive deformation behavior with strain rate effect of low-density polymeric foams," *Polymer Testing,* no. 50, pp. 1-8, 2016.

[23] D. Whisler and H. Kim, "Experimental and simulated high strain dynamic loading of polyurethane foam," *Polymer Testing,* no. 41, pp. 219-230, 2015.

[24] V. S. Deshpande and N. A. Fleck, "Multi-axial yield behaviour of polymer foams," *Acta Materialia,* no. 49, pp. 1859-1866, 2001.

[25] A. Taherkhani, M. Sadighi, A. S. Vanini and M. Z. Mahmoudabadi, "An experimental study of high-velocity impact on elastic–plastic crushable polyurethane foams," *Aerospace Science and Technology,* no. 50, pp. 245-255, 2016.

[26] S. Vaitkus, S. Vėjelis and A. Kairytė, "Analysis of Extruded Polystyrene Short-Term Compression Dependence on Exposure Time," *Materials Science (MEDŽIAGOTYRA),* no. 19, pp. 471-474, 2013.

[27] F. Ramsteiner, N. Fell and S. Forster, "Testing the deformation behaviour of polymer foams," *Polymer Testing,* no. 20, pp. 661-670, 2001.

[28] "Docol 600DL," SSAB, [Online]. Available: http://www.ssab.com/Products/Brands/Docol/Products/Docol-600DL. [Accessed 12 April 2016].

[29] N. Milles, Polymer Foams Handbook - Engineering and Biomechanics Applications and Design Guide, Elsevier Science & Technology, 2007.

[30] T. Ngo, P. Mendis, A. Gupta and J. Ramsay, "Blast Loading and Blast Effects on Structures, An Overview," *Electronic Journal of Structural Engineering,* no. 7, pp. 76-91, 2007.

[31] V. Aune, T. Børvik and M. Langseth, Lecture notes in TKT4128 Impact mechanics - An introduction to Blast Mechanics (Draft), Trondheim: Department of Structural Engineering, Norwegian University of Science and Technology, 2015.

[32] V. Aune, E. Fagerholt, M. Langseth and T. Børvik, A Shock Tube Facility to Generate Blast Loading on Structures (Work in progress), Department of Structural Engineering, Norwegian University of Science and Technology, 2016.

[33] S. Downes, A. Knott and I. Robinson, "Towards a shock tube method for the dynamic calibration of pressure sensors," *Philosophical Transactions of the Royal Society A,* no. 372(2023), 2014.

[34] "CEAST 9350 Drop Tower Impact System," [Online]. Available: http://www.instron.se/sv-se/products/testing-systems/impact-systems/drop-weight-testers/9350-drop-tower. [Accessed 01 April 2016].

[35] E. Fagerholt, "ECorr 4.0 docuentation," 2016. [Online]. Available: http://folk.ntnu.no/egilf/ecorr/doc/index.html.

[36] T. Børvik, O. S. Hopperstad, T. Berstad and M. Langseth, "A computational model of viscoplasticity and ductile damage for impact and penetration," *European Journal of Mechanics - A/Solids,* no. 20(5), pp. 685-712, 2001.

[37] G. R. Johnson and W. H. Cook, "A constitutive model and data for metals subjected to large strains, high strain rates and high temperatures," *Proceedings of Seventh International Symposium on Ballistics,* 1983.

[38] J. Lemaitre and J.-L. Chaboche, Mechanics of Solid Materials, Cambridge University Press , 1990.

[39] M. G. Cockcroft and D. J. Latham, "Ductility and the Workability of Metals," *Journal Institute of Metals,* no. 96, pp. 33-39, 1968.

[40] V. Aune, E. Fagerholt, K. O. Hauge, M. Langseth and T. Børvik, "Experimental study on the response of thin aluminium and steel plates subjected to airblast loading," *International Journal of Impact Engineering,* no. 90, pp. 106-121, 2016.

[41] "Brochure on Sundolitt XPS," [Online]. Available: http://www.sundolitt.no/upload_images/CE9FA1ED03684229BFF8CE4A5B4EC5E5.pdf. [Accessed 18 April 2016].

[42] A. Reyes, O. S. Hopperstad, T. Berstad, A. G. Hanssen and M. Langseth, "Constitutive modeling of aluminium foam icluding fracture and statistical variation of density," *European Journal of Mechanics A/Solids,* no. 22, pp. 815-835, 2003.

[43] H. Schreyer, Q. Zuo and A. Maji, "Anisotropic Plasticity Model for Foams and Honeycombs," *Journal of Engineering Mechanics,* no. 120(9), pp. 1913-1930, 1994.

[44] R. E. Miller, "A continuum plasticity model for the constitutive and indentation behaviour of foamed metals," *International Journal of Mechanical Sciences,* no. 42(4), pp. 729-754, 2000.

[45] V. S. Deshpande and N. A. Fleck, "Isotropic constitutive models for metallic foams," *Journal of the Mechanics and Physics of Solids,* no. 48(6-7), pp. 1253-1283, 2000.

[46] A. G. Hanssen, O. S. Hopperstad, M. Langseth and H. Ilstad, "Validation of constitutive models applicable to aluminium foams," *International Journal of Mechanical Sciences,* no. 44(2), pp. 359-406, 2002.

[47] MATLAB R2014b, Natick, Massachusetts: MathWorks, 2014.

[48] "Curve fitting toolbox," Mathworks Inc, [Online]. Available: http://se.mathworks.com/products/curvefitting/. [Accessed 24 March 2016].

[49] "Droptower impact system at SIMLab," [Online]. Available: http://www.ntnu.edu/simlab/droptower-impact-system. [Accessed 25 May 2016].

[50] "SIMLab shock tube facility," [Online]. Available: http://www.ntnu.edu/simlab/shock-tube. [Accessed 25 May 2016].

[51] LS-DYNA R8.0.0, Livermore, CA: Livermore Software Technology Corporation, 2015.

[52] LS-DYNA Theory manual (r:7635), LIVERMORE SOFTWARE TECHNOLOGY CORPORATION (LSTC), 2016.

[53] J. K. Holmen, O. S. Hopperstad and T. Børvik, "Low-velocity impact on multi-layered dual-phase steel plates," *International Journal of Impact Engineering,* no. 78, pp. 161-177, 2015.